IOP Publishing Phys. Med. Biol. 65 (2020) 24TR06 https://doi.org/10.1088/1361-6560/abca00

Physics in Medicine & Biology

IPEM Institute of Physics and Engineering in Medicine

RECEIVED
31 March 2020

REVISED
14 September 2020

ACCEPTED FOR PUBLICATION
12 November 2020

PUBLISHED
21 December 2020

TOPICAL REVIEW

Elastography imaging: the 30 year perspective

J Ormachea and K J Parker

Department of Electrical and Computer Engineering, University of Rochester, 724 Computer Studies Building, Box 270231, Rochester, NY 14627, United States of America

E-mail: kevin.parker@rochester.edu

Keywords: elastography, sonoelastography, biomechanics, imaging, stiffness, shear waves, review

Abstract

From the development of x-ray imaging in the late 19th century, the field of medical imaging developed an impressive array of modalities. These can measure and image a variety of physical parameters from absorption coefficients to spin–spin relaxations. However, throughout most of the 20th century, the intrinsic biomechanical properties of tissues remained hidden from conventional radiology. This changed around 1990 when it was demonstrated that medical ultrasound systems with their fast pulse repetition rate and high sensitivity to motion could create images related to the stiffness of tissues and their shear wave properties. From there, vigorous development efforts towards imaging the elastic properties of tissues were launched across different modalities. These progressed from the research phase, through implementation on clinical scanners, through extensive clinical trials of selected diagnostic tasks, to government approvals, payer approvals, international standards statements, and into routine clinical practice around the globe. This review covers highlights of some major topics of the technical and clinical developments over the last 30 years with brief pointers to some of the remaining issues for the next decade of development.

1. Introduction

Since ancient times, the palpation of tissues was used to provide diagnostic clues as to the state of accessible tissues and organs. The field of biomechanics developed a modern mathematical framework from the time of Hooke (1678) and was overviewed in the classic biomechanics textbook by Fung (1981). However, the development of modern biomechanics was largely separated from radiology throughout their development phases. Around 1990, it was demonstrated that ultrasound systems could be re-engineered to *image* the hidden elastic properties of tissues and whole organs (Lerner and Parker 1987, Lerner *et al* 1988, 1990, Yamakoshi *et al* 1990, Ophir *et al* 1991, Parker and Lerner 1992). These developments set off a robust and diverse international effort to optimize strategies for elastographic imaging and then identify key diagnostic applications.

Today, the biomechanical properties of tissues are widely considered to be important parameters for tissue characterization, as many of the pathological and physiological changes involve the alteration of tissue biomechanics (Fung 1981, Sarvazyan *et al* 1995, Parker *et al* 2011, Doyley 2012, Glaser *et al* 2012, Wang and Larin 2015). It is known that changes in tissue stiffness occur in pathologies such as cancer, fibrosis associated with liver cirrhosis, and atheroma and calcification associated with arteriosclerosis (Shiina *et al* 2015). Therefore, a careful evaluation and assessment of the changes in biomechanical properties can provide a way for early diagnosis and improved treatment of various diseases and lead to a better understanding of different physiological conditions of cells, tissues, and organs.

Generally, the biomechanics of tissue can exhibit anisotropic, viscous, and nonlinear behavior, and these properties will differ depending on the direction, extent, and rate of deformation. However, a simple first-order linear assumption of an elastic and isotropic material has been frequently applied, where stiffness can easily be expressed using a simple elastic modulus (Landau and Lifschitz 1970, Fung 1981). In the case of biological tissues, there are a variety of factors that determine stiffness including the tissue's fatty and fibrous components. Shiina *et al* (2015) mentioned that atherosclerotic plaques become stiffer with disease progression as their composition changes from lipid to fibrotic and calcified tissue. At the macroscopic level,

Table 1. Examples of reported Young's moduli of cells, tissues, and organs caused by pathological or physiological changes. In some cases such as the liver, ranges can be reported, however measurements can depend on techniques employed and experimental conditions. Adapted with permission from Wang and Larin (2015) and Shiina *et al* (2015).

Tissue type	Tissue condition	Young's modulus (kPa)	
Cornea (Wollensak *et al* 2003)	Normal	1.3×10^3	
	Collagen cross-linking	5.9×10^3	
Lens nucleus (Hollman *et al* 2007)	Middle age (40 years old)	5.2	
	Old age (63–70 years old)	10.6	
Liver Left column: (Castera *et al* 2008) Right column: (Singh *et al* 2016)	Normal	<2.5	
	Mild fibrosis	2.5–7	7.5–11.4
	Significant fibrosis	7–9.5	9.6–14.1
	Severe fibrosis	9.5–12.5	12.0–18.3
	Cirrhosis	>12.5	15.6–20.1
Breast (Samani *et al* 2007)	Normal fat	3.2	
	Normal fibroglandular tissue	3.2	
	Fibroadenoma	6.4	
	Ductal carcinoma *in situ*	16.3	
	Low-grade invasive ductal carcinoma	10.4	
	High-grade invasive ductal carcinoma	42.5	
Skin (Agache *et al* 1980)	Younger (3–30 years old)	4.2×10^2	
	Older (30–89 years old)	8.2×10^2	
Skeletal muscle (Shinohara *et al* 2010)	Relaxation	40.6	
	Contraction	258	
Aortic wall (Lee *et al* 1992)	Non-fibrous	41.2	
	Fibrous	354	
	Calcified	81.7	

the tissue in the margins around a malignant breast tumor is resistant to deformation and feels hard during palpation; therefore, tissue elasticity will differ depending on the microscopic or macroscopic observation (Shiina *et al* 2015). Fortunately, even when the elastic modulus is determined using a simple macroscopic assumption, it shows a high correlation with disease. For example, previous reviews summarized measurements in different tissues in terms of the Young's modulus E (Wang and Larin 2015, Shiina *et al* 2015), a traditional measure of stiffness of a solid. Table 1 shows the Young's modulus for different tissues, pathology, and physiology with measurement scales ranging from cell level to organ level.

A purely mechanical characterization of materials, based on uniaxial mechanical tensile and compression tests, has frequently been used as the gold standard. This type of measurement relies on the precise determination of the relationship between stress and the resultant strain (Markowski 1991, Zhang *et al* 2007). However, the testing procedure is generally destructive. The structural and functional properties of soft tissues are difficult to maintain during the measurement. As noted by Wang and Larin (2015), *in situ* assessment of biomechanical properties is generally impossible using this method.

Thus, a medical imaging approach—now generally termed elastography—was developed for objectively assessing the biomechanical properties of tissues. Roughly 30 years have elapsed since the first report of a non-invasive elasticity image using ultrasound (Lerner and Parker 1987, Lerner *et al* 1988). The next decade of research and development in many labs was followed by the commercial introduction of ultrasound elastography. This period of rapid growth has been summarized by several recent books (Zheng and Huang 2016, Hirsch *et al* 2017, Nenadic *et al* 2019, Alam and Garra 2020). This review paper's purpose is to capture some insights from the past three decades of growth and development, highlight some of the major approaches and applications, and point towards future growth and unmet needs. Thus, this review is organized as follows. Section 2 reviews the underlying principles that enable the imaging of biomechanical properties. Section 3 provides some general classification schemes for organizing the many different approaches to elastography, in order to give a sense of the major categories and application spaces. Section 4 recounts some of the historical development of the field. Next, the major clinical diagnostic targets are highlighted in section 5. Technical issues and challenges are summarized in section 6. The evolution of guidelines and consensus statements from major professional societies around the world are given in section 7. Finally, some promising technical advances likely to shape the next decade are highlighted in section 8. In appendix A, we provide a mathematical background for the techniques that comprise elastography, specifically the basic relations that govern displacement and motion of tissues. In appendix B, a compendium of acronyms is provided for convenience. These topics, taken together, are intended to provide a sense of the trajectory of this rapidly evolving field.

2. Principles of elastography

In many cases it is convenient to model tissue behavior in terms of waves propagating within an elastic or viscoelastic material. Two types of waves are supported, as shown in table 2: pressure (longitudinal) waves and shear (transverse) waves which propagate independently in the bulk material, interacting only at boundaries.

In the shear wave, the yellow arrow indicates the transverse motion and the polarization direction. In the case of ordinary ultrasound images, pressure (longitudinal) waves are used and their speed c_l is defined as:

$$c_l = \sqrt{\frac{K}{\rho}}, \tag{1}$$

where K is the bulk modulus and ρ indicates the density of the medium, which is approximately 1000 kg m^{-3} in soft tissues.

For typical biomaterials, the pressure wave speed is orders of magnitude faster than the shear wave speed (SWS). In the case of soft tissues, the pressure wave speed is typically comparable to the sound speed in water ($c_l = 1500$ m s^{-1}). Thus, there is little contrast difference in K between tissues (Shiina *et al* 2015).

On the other hand, the shear wave equation can be obtained from the basic equations of motion (see appendix A) by noting that there is no volume change as layers of material move in shear, transverse to the direction of propagation (Graff 1975), so the dilatation term $\nabla \cdot \mathbf{u} = 0$. The shear wave equation is then:

$$\nabla^2 \mathbf{u} = \frac{1}{c_s^2}\ddot{\mathrm{u}}, \tag{2}$$

where the SWS is

$$c_s = \sqrt{\frac{\mu}{\rho}}, \tag{3}$$

and μ is shear modulus. This equation can either be solved in terms of standing waves or propagating waves, depending on the particular conditions. In order to be consistent assuming $c_l = 1500$ m s^{-1}, biological tissues are nearly incompressible with Poisson's ration υ approaching the limit of $0.49 < \upsilon < 0.5$. In this regime as υ approaches 0.5, the shear modulus is related to Young's modulus E as:

$$\mu = \frac{E}{2(1+\upsilon)} \rightarrow \frac{E}{3}. \tag{4}$$

Thus, for a nearly incompressible isotropic elastic material, a measurement of the SWS $c_s = \sqrt{E/3\rho}$ can be used to obtain an estimate of the stiffness E of the material. Furthermore, in elastographic imaging experiments, the focus of attention is typically on the shear wave properties and not on longitudinal pressure wave properties, which have already been investigated extensively for ultrasound images.

Equations (1) and (3) indicate that the larger K and μ are, the stiffer the medium is, and the faster the waves will propagate. The shear waves will attenuate rapidly and disappear in the MHz ultrasound band, but when the frequency is below 1 kHz, attenuation is lower and they can propagate within organs *in vivo*. Moreover, their velocity is quite low ($c_s = 1 - 10$ m s^{-1}) compared with longitudinal waves, so μ is in the range of 1–100 kPa. Thus, there is a large difference among tissues' stiffness, which enables elastography methods to reconstruct images with high tissue contrast (Sarvazyan *et al* 1998, Sarvazyan and Hill 2004).

For methods that include shear waves, equation (12) in appendix A is also the starting point, and for the sinusoidal steady state case, this equation simplifies to equation (2) and the one-dimensional (1D) solution to transverse displacement $u_y(x)$ is sinusoidal with a characteristic wavelength λ, and where the displacement in the y direction corresponds to the shear wave displacements shown in figure 1 and table 2. Any direct estimate of wavelength yields the Young's modulus E using the limiting form of equation (4) for nearly incompressible materials, and this principle forms the basis for many imaging approaches.

3. Classification of elastography methods

Over time, several groups have proposed different approaches to measure SWS, shear modulus, Young's modulus, and other mechanical parameters to correlate them with the elastic tissue properties. Overviews of the different classes of techniques can be found in review papers such as (Greenleaf *et al* 2003, Parker *et al* 2011, Doyley 2012, Glaser *et al* 2012, Barr 2014, Wang and Larin 2015, Shiina *et al* 2015, Mulligan *et al* 2016), but the important specific details will be described in section 4. Generally speaking, all simple linear

Table 2. Pressure and shear waves. Adapted with permission from Stack Exchange Inc. (2020) and Shiina *et al* (2015).

	Direction of propagation and vibration	Sound speed	Main use (band frequency)
Pressure (longitudinal) wave	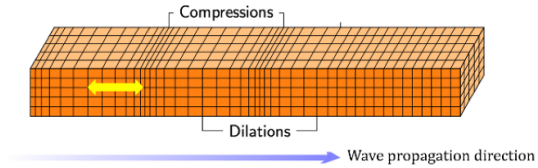	$c_l = \sqrt{\frac{K}{\rho}} K \approx 2\,\text{GPa}$Soft tissue$c_l \approx 1500\,\text{m s}^1$	Pulse-echo imaging method (MHz band)
Shear (transverse) wave	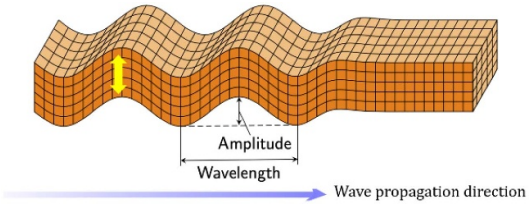	$c_s = \sqrt{\frac{\mu}{\rho}} \mu \approx 1 - 100\,\text{kPa}$Soft tissue$c_s \approx 1 - 10\,\text{m s}^{-1}$	Elastography ($\leq$1 kHz band)

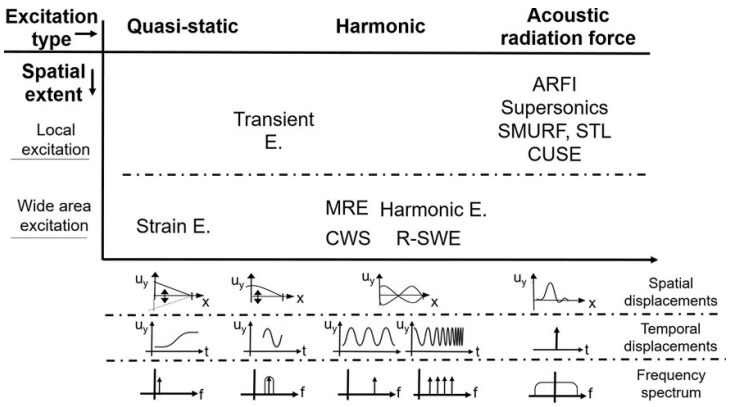

Figure 1. Spatio-temporal characteristics of mechanical loading in ultrasound elastography. This figure is a summary of excitation methods from quasi-static through dynamic vibration and tone burst; it is not meant to imply that these are the only possible approaches. The displacement field u_y is illustrated for each case. Strain E: strain elastography; Transient E: transient elastography; CWS: crawling wave sonoelastography; MRE: magnetic resonance elastography; Harmonic E: time harmonic elastography; R-SWE: reverberant shear wave elastography; ARFI: acoustic radiation force impulse; SMURF: spatially modulated ultrasound radiation force; STL: single tracking location; CUSE: comb-push ultrasound shear elastography. Adapted with permission from (Parker *et al* 2011, Mulligan *et al* 2016). Generally from left to right the shear excitations or applied forces have higher frequencies, and so the type of shear that is propagated changes shape according to the particular solutions of equations found in appendix A.

responses of tissue can be captured by equation (12) in appendix A, and this simplifies further due to special conditions such as quasi-static displacements (equation (13)) or shear wave excitation (equations (2) and (3)). In fact, the time-dependent terms can be seen as important drivers of the particular response of tissues, and this leads naturally to a continuum, or spectrum, of approaches from very slow motion to sinusoidal steady state motion, to impulsive motion as depicted in figure 1.

Elastography is generally classified by the particular imaging modality, the measured physical quantity, and the applied stimulus or load that is utilized. Considering the range of imaging modalities and their types (Wang and Larin 2015, Mulligan *et al* 2016), one way to categorize the different modalities for elastography is by their respective spatial-scale coverage and their penetration depth (see figure 2). Each imaging modality has different features and can be characterized by factors such as the spatial resolution, field-of-view limits, imaging speed, and displacement sensitivity.

Another way to categorize the more widely used approaches is by the class of applied stimulus: quasi-static, harmonic (continuous), or transient waves (see figure 3). Each one of these has unique mathematics and approaches for inverse solutions, but all rely on a continuum of biomechanical responses (Parker *et al* 2005, Doyley 2012). In the next sections, the methods that have been integrated into clinical practice are categorized by the applied excitation load into the following groups:

4. Historical development

4.1. Prior studies of tissue motion

As the field of biomechanics progressed, different techniques were used to study inherent physiological motion and the response of tissues to applied motions. Landmark research that presages the later development of elastography was done in the 1950s at Wright Patterson Air Force base. An elegant mathematical treatment of an oscillating sphere in a viscoelastic medium was published by Oestreicher (1951) as a model for slow waves (shear) and fast waves (compression) in tissues. These results had profound implications for later tissue elasticity imaging including the presence of longitudinal shear waves (Carstensen *et al* 2008, Carstensen and Parker 2015). Next, from the same group, Von Gierke *et al* used a strobe light to quantify surface waves across the human thigh, generated by a vibrating piston source in contact with the skin at 64 Hz. The surface wavelength and wave speed were estimated (von Gierke *et al* 1952), which could be related to material properties of an ideal semi-infinite medium (Graff 1975).

In later decades, the evolution of medical ultrasound systems with A-mode, M-mode, and then real time B-mode provided the means for localized *in vivo* assessment of deep tissue response to internal or external forces or compression by the ultrasound transducer (Gros *et al* 1978, Hill and Kratochwil 1981, Guyer *et al* 1986, Ueno *et al* 1988, Tristam *et al* 1988, Bamber *et al* 1988).

The study of naturally occurring motions sought to discriminate between healthy and abnormal conditions. For example, Wilson and Robinson developed a radio frequency (RF) M-mode ultrasound signal

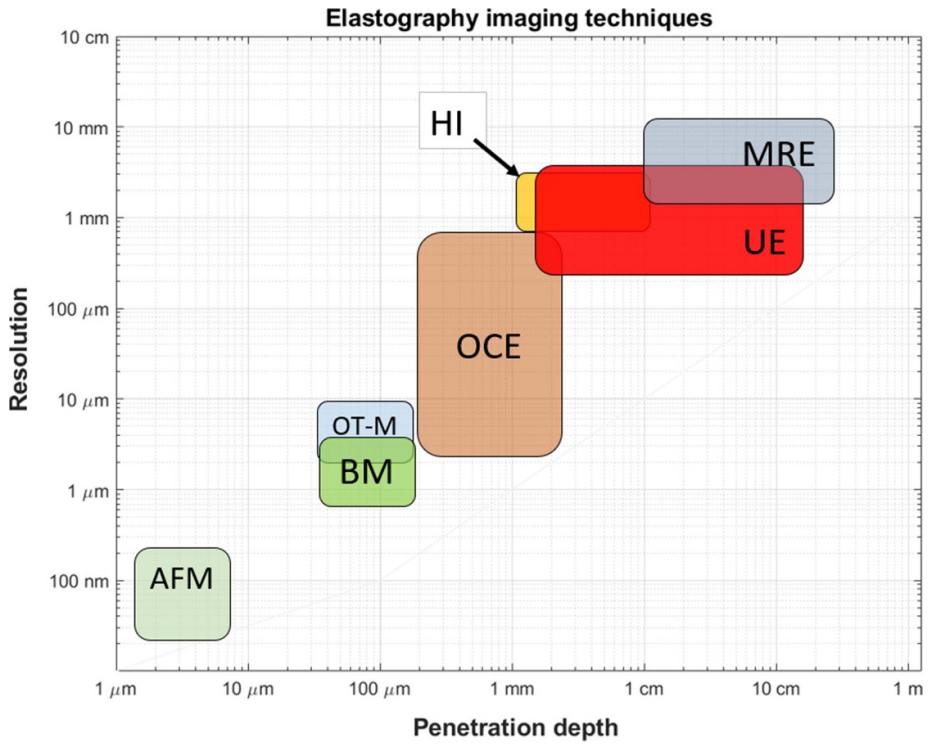

Figure 2. Comparison of different imaging modalities in elastography based on penetration depth and resolution. AFM: atomic force microscopy; BM: Brillouin microscopy; OT-M: optical tweezers-based microrheology; OCE: optical coherence elastography; HI: holographic imaging; UE: ultrasound elastography; MRE: magnetic resonance elastography. Adapted with permission from (Mulligan *et al* 2016).

processing technique to measure small displacements of liver tissue caused by the radial expansion of arteries within the liver from cardiac pulsations (Wilson and Robinson 1982). Dickinson and Hill estimated a correlation coefficient between successive A-scan lines to quantify tissue motion. Assuming small displacements, the decorrelation was modeled as being proportional to displacement (Dickinson and Hill 1982). Tristam *et al* (1986) further developed the technique to investigate the responses of normal and cancerous liver to cardiac pulsation. De Jong *et al* (1990) also used a modified correlation technique to measure tissue motion.

Fetal lung elasticity was investigated as an important parameter of fetal lung maturity by Birnholz and Farrell (1985) using ultrasound assessment of lung motion near the heart. Adler *et al* (1990) applied quantitative correlation techniques to digitized M-mode images to measure the temporally and spatially averaged systolic to diastolic deformation.

Holen *et al* (1985) characterized the Bessel-band Doppler spectrum when using Doppler ultrasound to examine unusually oscillating heart valves. Taylor (1976) proved that the Doppler spectrum from a vibrating target is mathematically analogous to a pure-tone frequency modulation (FM) process.

Cox and Rogers studied the Doppler ultrasound response of fish auditory organs to low-frequency sound. They estimated the vibration amplitude of the hearing organ from the FM theory and specifically the ratio of the carrier to the first side band of the Doppler spectrum (1987).

At much lower frequencies in human tissues, Eisensher *et al* used M-mode ultrasound to track tissue motion induced in breast and liver tissue by a 1.5 Hz vibration source. They found that the quasi-static compression response from benign lesions was more sinusoidal, whereas the response from malignant tumors tended to be more nonlinear (Eisensher *et al* 1983).

Krouskop *et al* (1987) proposed a quantitative measurement of tissue elasticity using gated pulse Doppler to detect tissue motion subjected to an external vibration. They implied that an estimate of tissue stiffness could be determined in a very small region, i.e. 0.5 × 0.5 mm, within a homogeneous medium. Collectively these studies demonstrated that ultrasound, especially M-mode and Doppler interrogations, could contain quantitative parameters that relate to the material properties of tissues, relevant to the assessment of normal vs. pathological conditions.

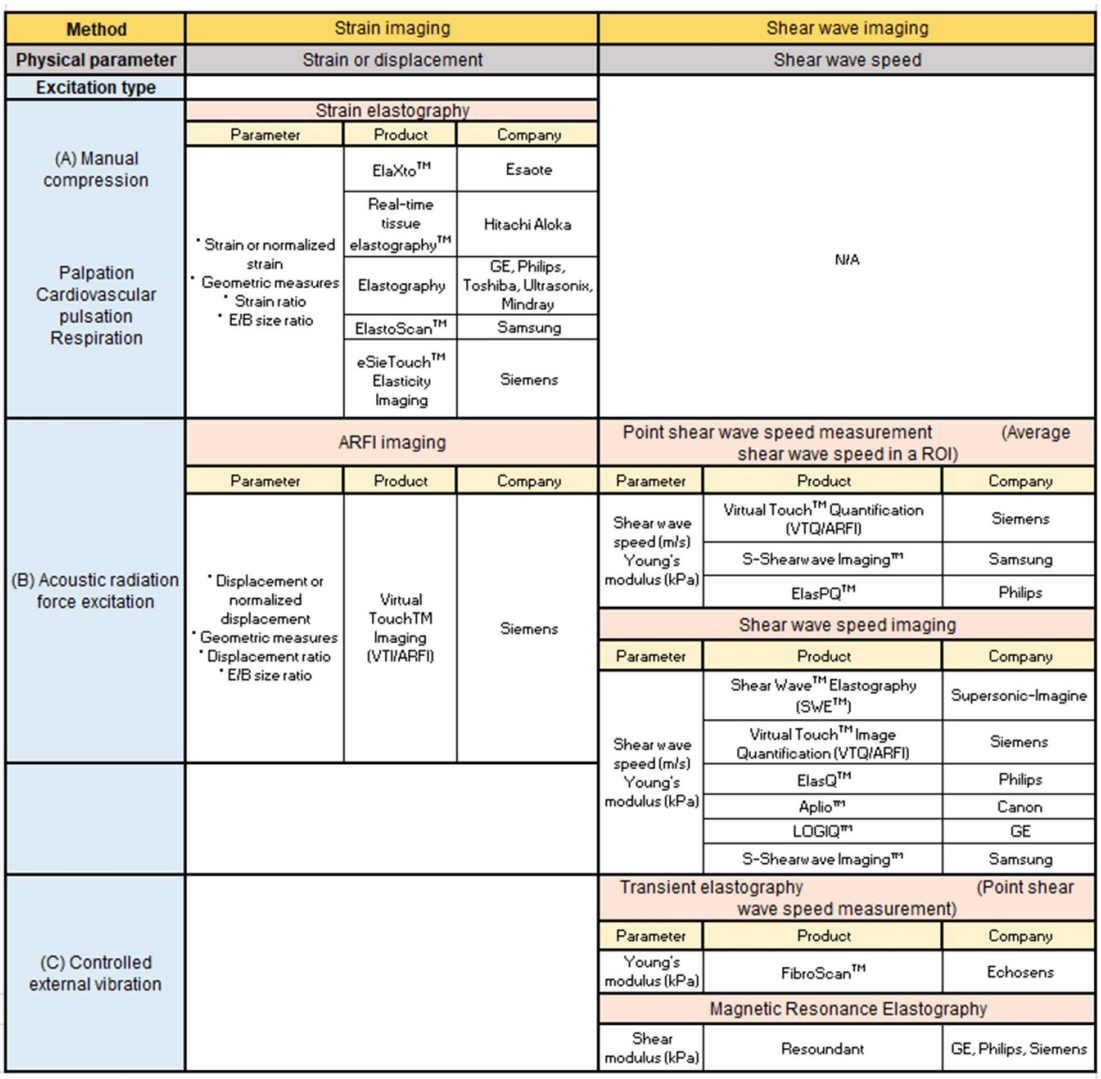

Figure 3. Elastographic methods categorized by measured physical parameter (columns) and type of excitation (rows). Approved clinical scanners employing these techniques are also represented. Adapted with permission from (Shiina *et al* 2015).

4.2. Vibration sonoelastography imaging

4.2.1. Vibration-amplitude sonoelastography

The transition to *imaging* the biomechanical properties of tissue was initiated by sonoelastography techniques, defined as the application of a continuous low-frequency vibration (between 40 and 1000 Hz) to propagate shear waves in tissues (Lerner and Parker 1987, Lerner *et al* 1988). The simplest real-time imaging version of sonoelastography utilized the color Doppler display of the amplitude of the propagating shear waves in sinusoidal steady state, and this was denoted as vibration-amplitude sonoelastography. In cases where a stiff lesion is present in soft tissues, a deficit in the normal vibration patterns can be seen in the real-time vibration images. This approach was used as a tool to display the early shear wave propagation experiments in phantoms and tissues (including modal patterns within regular boundaries). Using the information from images, the SWS of sound within an organ could also be determined (Parker and Lerner 1992).

The first vibration-amplitude sonoelastography image is shown in figure 4. This inaugural image mapped out the vibration amplitude within a sponge and saline phantom containing a hard lesion (the dark area). As the phantom was vibrated from below, range-gated Doppler was used to determine the vibration amplitude of the phantom's interior.

Researchers at the University of Rochester next employed a modified color Doppler instrument to create real-time vibration-amplitude sonoelastography images, wherein vibration above a certain level (~2 microns) produced a saturated color (figure 5).

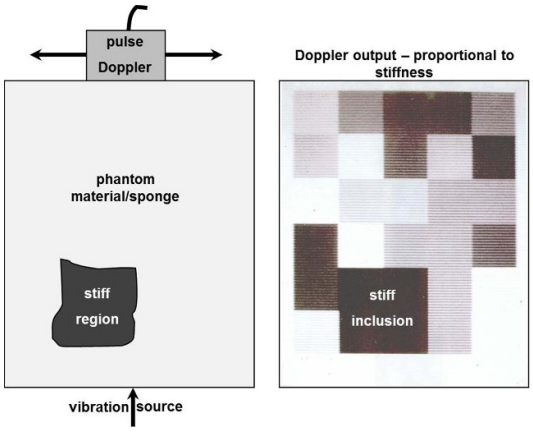

Figure 4. Original imaging data and schematic of the first known image of relative stiffness, derived from Doppler data in a phantom with applied vibration. The original image was published in 1987 and 1988 (Lerner and Parker 1987, Lerner *et al* 1988) and marks the emergence of elastographic imaging. This figure is used with permission, (Alam and Garra 2020), page 46, copyright Elsevier.

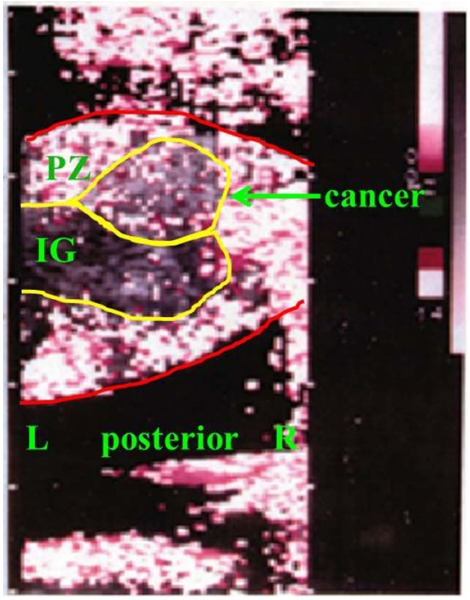

Figure 5. A representative first-generation image of vibration sonoelastography, circa 1990. Doppler spectral variance is employed as an estimator of vibration in the 2–10 μm range and displayed over the B-scan images. No color implies low vibrations below threshold. Shown is the fill-in of vibration within a whole prostate, with a growing cancerous region indicated by the deficit of color within the peripheral zone. *IG*, inner gland; *L*, left zone; *PZ* peripheral zone; *R*, right. This figure is used with permission (Alam and Garra 2020), page 47, copyright Elsevier.

4.2.2. Vibration-phase sonoelastography

Independently, researchers at the University of Tokyo developed a vibration phase gradient approach (Yamakoshi *et al* 1990). Sato's group mapped the phase and amplitude of low-frequency wave propagation in tissues. This provided quantitative estimates of wave propagation velocity and dispersion (linked to tissue elasticity and viscosity).

4.2.3. Modal pattern and eigenmodes analysis in sonoelastography

These initial imaging techniques were further reinforced by tissue elastic constant measurements, finite element modeling results, inhomogeneous phantoms, and *ex vivo* tissue sonoelastography (Lerner *et al* 1990, Parker *et al* 1990, 1993).

Thus by 1990, the nascent field of vibration sonoelastography (also called sonoelastography and sonoelasticity at this time) included real-time imaging techniques and stress–strain analysis of human tissues, such as the prostate. The accumulating evidence from tissues and finite element models

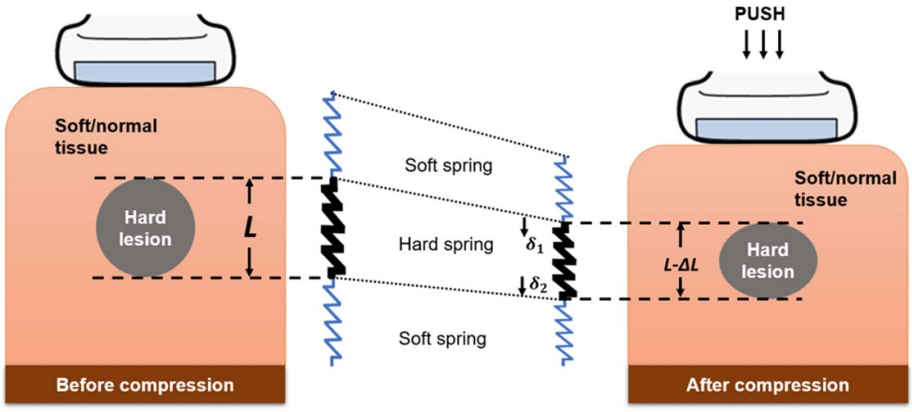

Figure 6. Schematic image to illustrate the strain images produced by early compression elastography. When a very small pressure is applied to tissue with the ultrasound probe along the axial direction, the tissue deformation can be measured using a 1D spring model. This is obtained by calculating the correlation between the RF signal acquired by the probe, before and after compression.

demonstrated convincingly that conventional ultrasound Doppler imaging scanners could image vibrations and shear wave patterns so as to detect areas with elevated Young's modulus values.

A confirming result was published in 1992 (Parker and Lerner 1992), demonstrating that vibrational eigenmodes could be created in organs, including the liver and kidneys, where surfaces create coherent reflections of sinusoidal steady-state shear waves. Stiff lesions produced a localized disturbance of the eigenmode pattern and, from the regular patterns imaged at discrete eigenfrequencies, the Young's modulus of the background could be calculated. These early demonstrations of single frequency shear waves have broadened into a wide category of harmonic shear wave approaches as will be discussed in section 4.4.3.

4.3. Strain imaging

4.3.1. Quasi-static elastography

Two-dimensional (2D) tissue strain estimates were introduced by Ophir *et al* (1991) at the University of Texas at Houston. Quasi-static or compression elastography, the first type of elastography to be incorporated into clinical scanners (Doyley 2012, Shiina *et al* 2015), utilizes a comparison of ultrasound B-scan RF information from tissue before and after a modest compression. It measures the axial strain induced within the tissue using either manual compression or cardiovascular/respiratory pulsation. A small motion is induced within the tissue (typically on the order of 2% of the axial dimension (Doyley 2012)) with a quasi-static mechanical source (usually the hand-held transducer). The axial component of the internal tissue displacement is then measured, usually by performing a cross-correlation analysis on pre- and post-deformed RF echo frames. Then, strain elastograms are produced by spatially differentiating the axial component of displacement. The concept can be explained by invoking the stress–strain relations under a simple uniaxial (1D) displacement. This was modeled by the use of springs, as depicted in figure 6.

In quasi-static elastography, soft tissues are typically modeled as a series of 1D springs that are arranged in a simple fashion as depicted in figure 6. The stiffest spring will compress the least. Thus, by calculating the strain (the derivative of displacement), areas of relative stiffness could be identified and imaged as low strain regions. For this simple mechanical model, the measured strain (ε) is related to the internal stress (σ) using Hooke's law:

$$\sigma = E\varepsilon, \tag{5}$$

where E is the Young's modulus of the tissue.

As shown in figure 6, when a very slight pressure is applied to tissue with a probe in the beam direction, displacement $\delta(z)$ at each site z is calculated by comparing the echo signal before and after compression. The strain ε is approximated as the difference in displacement between two points (δ_1, δ_2) divided by their pre-compression distance L:

$$\varepsilon = \frac{\mathrm{d}\delta}{\mathrm{d}z} \rightarrow \frac{\delta_2 - \delta_1}{L}. \tag{6}$$

In equation (5), Young's modulus E can be obtained if stress σ and strain ε are known. However, because it is difficult to actually calculate the stress distribution *in vivo*, it is typically assumed to be constant (i.e. $\sigma \approx 1$) (Doyley 2012). As a result, stiff segments with a large E will have a small strain ε; therefore, strain

images may approximate relative stiffness across an image, which may be simple to interpret. The advantage of this technique is that the hand-held ultrasound scanning transducer can be used to produce a localized compression up to the normal diagnostic depth of superficial organs such as the breast and thyroid gland. On the other hand, the disadvantages include the relative nature of the strain image, the requirement for nearly uniform strain to interpret the image, the tendency of objects to move out-of-plane during compression, and the difficulty of compressing deeper organs. The stress is not easily transmitted to deep organs such as the liver (Parker *et al* 2011, Doyley 2012, Shiina *et al* 2015).

Quasi-static elastography was originally developed as an ultrasound imaging technique (Ophir *et al* 1991, O'Donnell *et al* 1994, Bamber and Bush 1996, Sumi 2005), but other medical imaging modalities such as magnetic resonance (MR) (Fowlkes *et al* 1995, Plewes *et al* 2000) and optical coherence tomography (OCT) (Mulligan *et al* 2016) have also been used to measure the relative stiffness. Strain elastography (SE) has been commercialized and is currently being used in various fields of clinical medicine, including breast cancer diagnosis (Hall *et al* 2003, Itoh *et al* 2006, Shiina *et al* 2015).

4.3.2. Acoustic radiation force impulse (ARFI) imaging elastography

Acoustic radiation force (ARF) results from the transfer of momentum from the propagating ultrasonic wave to the tissue through which it is propagating due to absorption and scattering mechanisms. The magnitude of the applied ARF (F) can be related to the acoustic absorption (α), the speed of sound (c) in the tissue, and the temporal average intensity of the acoustic beam (I) by (Nyborg 1965, Torr 1984):

$$F = \frac{2\alpha I}{c}. \tag{7}$$

The transfer of momentum from the propagating acoustic wave to the tissue is defined by the duration of the acoustic pulse. Thus, tissue deformation can be induced using focused ARF excitation.

Although radiation force has a long history in physics and acoustics (Sarvazyan *et al* 1998, 2010), the use of ARF as a tissue characterization modality was proposed by Sugimoto *et al* (1990) as a laboratory system that applied radiation force to a tissue sample, while measuring the resulting displacement with an ultrasonic probe. The use of ARFI in an imaging system with estimates of displacements from deep internal tissue was described by Nightingale *et al* (1999, 2001) and this approach became commercially available. ARFI provides multiple parameters and strategies, for example one can map the maximum displacement as points are successively pushed, or the relaxation time following each push. Imaging pulses before and after application of focused ARF push pulses are used to monitor the tissue displacement (as a measure of deformation) within the region of the excitation. The same transducer is used to generate the push pulse as well as to monitor the resulting tissue displacement. The tissue displacement response is directly related to the magnitude of the applied force and inversely related to the tissue stiffness. Thus, images of tissue displacement that show relative differences in stiffness can be generated, with information somewhat analogous to the images generated in quasi-static elastography.

The advantages of ARFI stem from the fact that a pushing pulse of radiation force can be focused and applied to different imaging systems. ARFI does not rely on transducer compression as the quasi-static SE methods do, and thus, it has the advantage of being able to focus the 'push' within organs, where it would be difficult to generate deformation with compression from the body surface. However, ARF is a relatively weak effect, thus high intensities and heating of the system and tissue place limits on the resulting displacements (Palmeri and Nightingale 2004). In addition, as with quasi-static elastography, nonlinear tissue responses can be generated by transducer compression, so minimal compression should be applied during ARFI imaging. Moreover, the push pulses are of longer duration than standard ultrasound diagnostic pulses, and current methods typically employ relatively low frame rates to maintain acoustic output within diagnostic limits (Parker *et al* 2011, Shiina *et al* 2015). The effective depth of ARFI in current systems is limited to about 6.5 cm (RSNA/QIBA 2012).

The technique has been demonstrated in a variety of tissues including breast (Sharma *et al* 2004), prostate (Zhai *et al* 2010, 2012), and for delineation of stiff RF ablation lesions (Fahey *et al* 2004, 2005). ARFI has also been applied using optical coherence elastography (OCE) (Larin and Sampson 2017).

4.4. Shear wave imaging

Currently, the largest group of techniques in elastography employ shear wave phenomena associated with transient and harmonic approaches. A subset of transient and broadband techniques utilizes shear wave results from ARF push pulses (Sarvazyan *et al* 1998) or external push pulses (Catheline *et al* 1999a) of short-duration pulses as an initial condition, which then results in a propagating shear wave. By tracking of the propagating wave, the SWS can be estimated, and this yields the Young's modulus, or stiffness, of the material (Sarvazyan *et al* 1998). A variety of approaches employing radiation force, with diverse clinical

applications, have been developed (Fatemi and Greenleaf 1998, Nightingale *et al* 1999, Konofagou and Hynynen 2003, Bercoff *et al* 2004b, Mcaleavey and Menon 2007, Parker *et al* 2011, Hazard *et al* 2012, Hah *et al* 2012). When these techniques estimate the propagation of a broadband shear wave pulse, the results can be classified as group velocity estimates.

Another subset of techniques apply continuous harmonic shear waves. Harmonic schemes can employ sinusoidal steady-state excitations or decompose a harmonic ensemble into its frequency components. A major expansion of single-frequency sinusoidal shear wave excitations was launched with magnetic resonance elastography (MRE) approaches (Muthupillai *et al* 1995). Others included crawling waves (Wu *et al* 2006), and reverberant shear waves (Parker *et al* 2017, Ormachea *et al* 2018). When these techniques estimate shear wave propagation around a single frequency, the results can be classified as phase velocity.

Additional estimations have been developed for underwater acoustics and geomechanics using random signals (Roux *et al* 2005) and these have been extended to noise correlation measurements and time reversal solutions in soft tissues (Sabra *et al* 2007, Catheline *et al* 2008, Gallot *et al* 2011, Brum *et al* 2015, Rabin and Benech 2019).

4.4.1. Transient elastography (TE)

Although the term 'transient elastography' has been used to categorize a broader class of methods based on ARF in different reviews (Parker *et al* 2011, Doyley 2012), only the method that uses a controlled external vibrator is considered TE in this section, following the classification scheme used by Shiina *et al* (2015).

In TE, a low frequency (50 Hz) external mechanical vibrator was integrated with an ultrasound M-mode system (Catheline *et al* 1999b) in the laboratory of Professor Mathias Fink at Paris University. Later, Sandrin *et al* (2003) implemented this technique in a stand-alone clinical device which became the first commercially available ultrasonic shear wave measurement system, FibroScan^{TM} (Echosens, Paris, France). This device does not require integration into a conventional imaging system. Its integrated applicator can be applied through the ribs to excite a short vibration tone burst which propagates into the liver. The ultrasound tracking provides the particle displacement along the axial center line, and from this a global estimate of liver elasticity can be estimated (it is specifically designed for measuring liver stiffness without displaying a B-mode image.). The ultrasound transducer has a fixed focal configuration, and the SWS that is measured corresponds to the group SWS in the region of tissue along the A-line that is imaged by the transducer. The FibroScan^{TM} displays the corresponding Young's modulus, computed using equation (4) (Sandrin *et al* 2003).

4.4.2. ARF-based shear wave elastography (SWE)

Sarvazyan *et al* (1998) proposed a method that used a focused ARF beam 'push pulse' to generate local shear waves, and ultrasonic imaging was used to monitor the resulting shear wave propagation away from the radiation force push location. Since the same transducer can be used to generate the shear waves and to image their local propagation, it was possible to use B-mode image guidance during the measurement.

The different ARF-based modalities report a group SWS and/or Young's modulus ('point' SWS measurement) in a local region of interest, as well as 2D images that depict the SWS and/or Young's modulus at rates of up to a few frames per second (Shiina *et al* 2015). ARF can be applied at a single focal location or a multiple focal zone configuration in which each focal zone is interrogated in rapid succession, enabling real-time shear wave images to be formed. For the latter configuration, Bercoff *et al* (2004b) developed an ultrasound scanner with an ultra-high frame rate (i.e. 10 K frames per second) that was capable of tracking the shear waves propagating from an ARF impulse within the tissue (for illustration see figure 7). Multiple focal ARF impulses are fired at a rapid rate (compared to the relatively slow shear wave propagation). This approach has been termed 'supersonic shear imaging (SSI)' and is implemented in a SSI scanner (Bercoff *et al* 2004a, 2004b). This approach has been used to study the viscoelastic properties of breast lesions (Tanter *et al* 2008), muscles (Deffieux *et al* 2008), and liver (Muller *et al* 2009), and is now a well-established approach to ultrasonic elastography (Cosgrove *et al* 2013).

Other ARF-based methods have been reported as well. Fatemi and Greenleaf (1998) proposed a technique known as vibroacoustography which uses ARF to vibrate tissues in the kHz range, using two overlapping ultrasound beams with slightly different frequencies. The resulting tissue mechanical response is dependent on the local acoustic mechanical properties of tissue that are obtained using a hydrophone. Vibroacoustography could visualize microcalcifications with high contrast resolution (Fatemi and Greenleaf 1998). Konofagou and Hynynen (2003) devised localized harmonic imaging (HMI) using an amplitude-modulated focused beam, for the detection of localized stiffness. They tracked radiofrequency signals and estimated localized oscillatory motion produced by a harmonic radiation force using two focused ultrasound transducer elements. HMI was used for sonication and monitoring of thermal ablation in tissues (Maleke and Konofagou 2008) and to extract viscoelastic parameters (Vappou *et al* 2009). Mcaleavey *et al* (2007) devised a method termed 'spatially modulated ultrasound radiation force' (SMURF). In this technique,

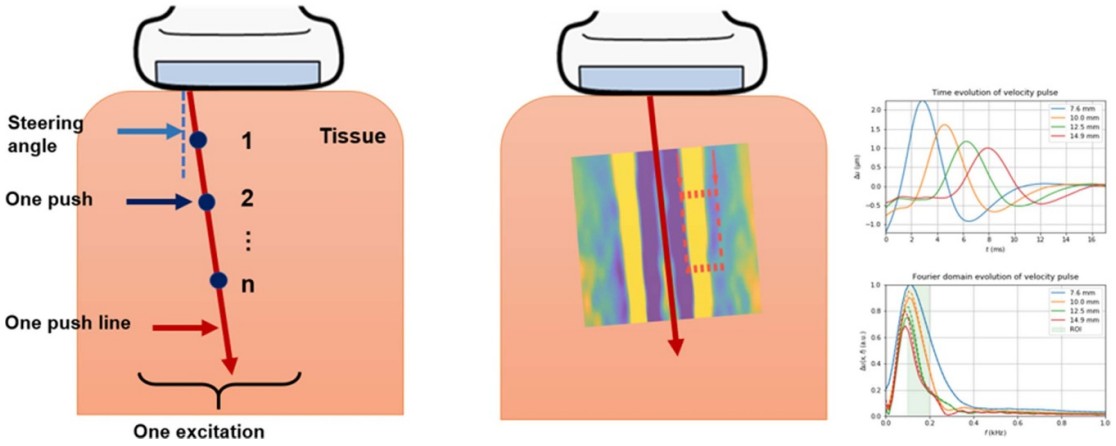

Figure 7. (left) Representation of shear wave measurements from multiple focused radiation force excitation beams, at different depths, which creates push pulses. The constructive shear wave interference forms a supersonic cone and a quasi-plane shear wave. (center) The ultrasound system then uses an ultrafast imaging mode to track the propagating shear waves through the medium. (right) Examples of particle velocity signals in time at different positions with their corresponding frequency spectrum range.

instead of utilizing a sharp focal region to deliver an ARF impulse to the tissue, a shear wave of known spatial frequency is generated, by using array beamforming techniques to produce a shear wave of a desired wavelength, and then the temporal frequency response of the vibrating tissue is measured as the wave propagates through a point. Then, Elegbe and Mcaleavey (2013), proposed a different ARF-based approach to track the induced shear waves termed 'single tracking location ARF'. In this approach, it was found that another source of error was the speckle-induced bias in phase estimation. The authors demonstrated that methods that involve tracking in a single location, as opposed to multiple locations, are less sensitive to this source of error since the measurement is differential in nature and cancels out speckle-induced phase errors (Elegbe and Mcaleavey 2013). Song *et al* (Pengfei *et al* 2012, Song *et al* 2013) applied multiple unfocused and focused ultrasound beams arranged in a comb pattern (comb-push) to generate shear waves. A directional filter is then used to isolate the left-to-right (LR) and right-to-left (RL) propagating shear waves. Then, smoother 2D SWS maps were obtained by combining the LR and RL SWS maps. Selzo and Gallippi (2013) proposed an ARF-based method called viscoelastic response (VisR) imaging. In this approach, displacement versus time profiles in response to two successive ARF excitations are fit to the mass-spring damper model. Then, relative elasticity and relative viscosity images are created to characterize the viscoelastic properties. Some applications of VisR include normal canine muscle (Selzo and Gallippi 2013), mechanical anisotropy in skeletal muscle (Moore *et al* 2017), and renal transplant status *in vivo* (Hossain *et al* 2018). Additional applications using ARF have been also reported using OCT (Mulligan *et al* 2016).

4.4.3. Harmonic SWE

Another broad category of elastography uses continuous wave external vibration sources and can be classified as harmonic elastography (HE) (Parker *et al* 2011, Doyley 2012, Shiina *et al* 2015). This approach was first explored as an ultrasound-based imaging method (Lerner and Parker 1987, Lerner *et al* 1988, Parker *et al* 1990, Yamakoshi *et al* 1990), as described in section 4.1, and has grown into a broad set of approaches across magnetic resonance imaging (MRI), OCT, and ultrasound. In general terms, HE approaches apply a low frequency (typically <2 kHz) and a spatially localized sinusoidal mechanical source. The shear waves produced by this excitation are tracked through an internal region using an ultrasound, MRI, or optical system.

In ultrasound or OCE, the phase and amplitude of the propagating shear waves are estimated by applying similar techniques to those used in color Doppler imaging (Lerner *et al* 1990, Parker *et al* 1990, Yamakoshi *et al* 1990). However, in MRI, novel phase-contrast imaging methods were developed (Muthupillai *et al* 1995, Plewes *et al* 1995, Sinkus *et al* 2000, Weaver *et al* 2001) to estimate local displacements caused by shear waves. MR elastography has a number of advantages, including the potential for large volumetric acquisition of 3D displacement vectors, albeit at the cost of longer acquisition and processing times. A rich set of mathematical approaches has been applied to derive accurate estimators of stiffness from the vector components of displacement tracked by MRE (Greenleaf *et al* 2003, Doyley 2012).

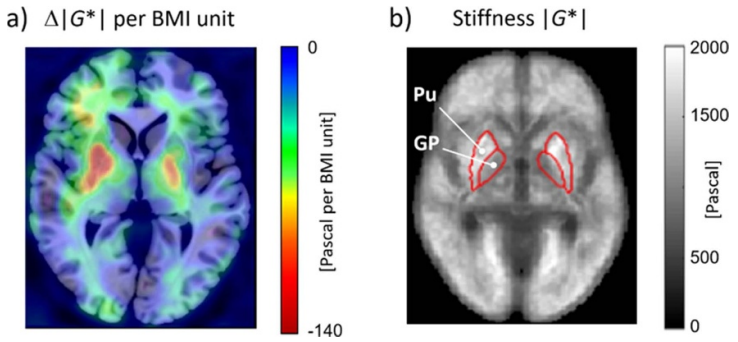

Figure 8. (a) MRE map of the (age-corrected) stiffness change per BMI unit indicating a strong link between BMI and tissue stiffness of the globus pallidus (GP) and putamen (Pu). (b) Group-averaged elastogram in an exemplary transversal slice through the brain covering the Pu and GP. Reprinted by permission from SpringerLink (Hetzer *et al* 2019).

In any imaging system, if we can assume plane shear wave behavior, an approximate local elasticity is obtained measuring the local wavelength using equation (3) and:

$$c_s = \lambda f_v, \tag{8}$$

where f_v is the instantaneous vibration frequency and λ is the local wavelength. Some examples include the techniques proposed by Manduca *et al* (2001) that used a bank of wavelet filters (Knutsson *et al* 1994) to estimate shear modulus from local estimates of instantaneous frequency.

Inverse mathematical solutions to the Helmholtz wave equation have been studied in MRE and ultrasound harmonic shear wave applications (Greenleaf *et al* 2003, Doyley 2012). For example, in MRE a multifrequency dual elastovisco inversion technique (MDEV inversion) derives the shear modulus and its associated lossy or viscous component, by a least squares error solution related to the Helmholtz equation (Hirsch *et al* 2014, Hetzer *et al* 2019). Figure 8 shows the elastography map of brain stiffness (right image), obtained from a group average across 22 males of varying body mass index (BMI), and also the change in shear modulus within the brain as a function of BMI over the study population (left image). Highlighted areas delineate neurological centers known to be associated with obesity and satiation. It is also noteworthy that this entire MRE reconstruction pipeline is publicly available under https://bioqic-apps.charite.de/Login.

Alternatively in ultrasound inversion techniques, vibro-elastography is a multi-frequency HE approach in which an external shear wave source is used to excite the tissue and a model is fit to the resulting steady state tissue motion (Turgay *et al* 2006, Eskandari *et al* 2008, Abeysekera *et al* 2015, Honarvar *et al* 2015).

Other harmonic shear wave approaches exploit unique characteristics, for example Wu *et al* (2004) devised an approach to compute shear modulus images from interference patterns, termed crawling waves, which were generated using two vibration sources operating at slightly different frequencies. Chen *et al* (2009) used a 'push' transducer that transmits a continuous amplitude modulated ultrasound beam to generate harmonic vibrations into the tissue. Then, the generated shear waves were monitored using a separate ultrasound detect beam. The phase difference of the shear waves between two locations along the propagation path was used to calculate the SWS. Tzschatzsch *et al* (2016) created 2D time-harmonic elastography (2D-THE) using external harmonic stimulation at multiple frequencies to create compound SWS maps. More recently, reverberant shear waves (Parker *et al* 2017, Ormachea *et al* 2018, 2019) have been proposed for general elastography. In this technique, a profusion of shear waves across different directions is established, aided by all reflections from boundaries and inhomogeneities. The mathematics of the limiting case of a three-dimensional (3D) distribution of shear waves leads to a simple local estimator of wave speed and stiffness covering a full field of view to 16 cm depth. Figure 9 illustrates the generation of a reverberant shear wave field (steps A to C) and 2D shear speed images obtained from simulated complex shear wave fields at 300 Hz (case D), and *in vivo* liver and kidney tissues at 100 Hz (case E).

In the context of commercially available clinical methods, one harmonic-based approach is in general use. It applies an external, MRI-compatible vibration source to induce harmonic shear waves and is incorporated into MRI scanners as indicated in figure 3. This is generally termed MRE (Muthupillai *et al* 1995). It is worth noting that MRE reports its results in terms of the shear modulus, whereas ultrasound-based shear wave methods report either SWS or Young's modulus (Glaser *et al* 2012).

Additionally, harmonic SWE in OCE is typically performed with excitation frequencies within the audio frequency range (20 Hz–20 kHz). The elastography images are generated from spatially-localized displacements, or alternatively from the properties of the mechanical wavefields within the sample. Through

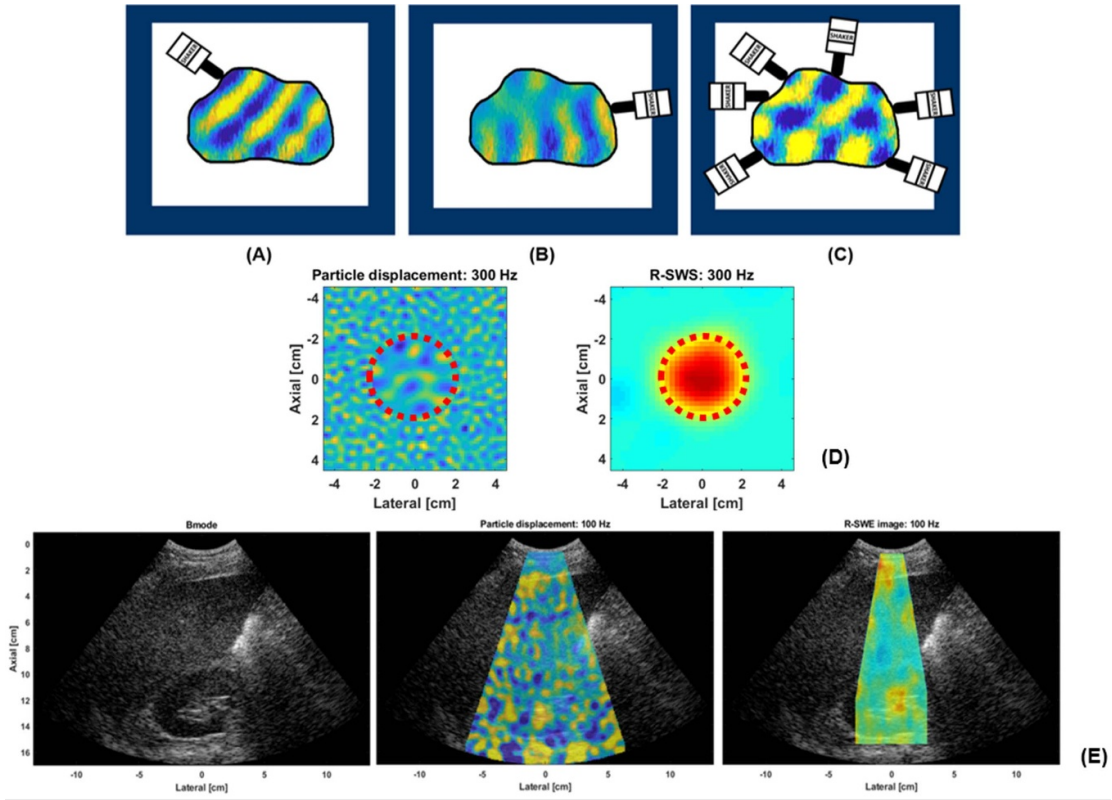

Figure 9. Generation of a reverberant shear wave field. Initially, harmonic and unidirectional shear waves propagate at specific directions depending on the external vibrator location (cases A and B). With multiple external sources (case C), and considering the presence of reflections from boundaries, shear waves propagate in many directions. These all contribute to the creation of the reverberant shear wave field. Once established, the magnitude and phase of the selected frequency component is extracted from the complex field to measure the local shear wave speed. Case D shows the particle displacement (left) from one simulated reverberant shear wave field at 300 Hz, and the 2D SWS image (right) obtained using the R-SWE approach. Case E shows an *in vivo* liver and kidney B-scan (left). The reverberant field can be observed in the particle displacement (center) image, and the obtained SWS (right) image using the R-SWE approach, both superimposed on the B-mode image.

the application of a mechanical model, the biomechanical properties are then reflected in terms of the SWS, shear modulus, or Young's modulus (Mulligan *et al* 2016).

An advantage using harmonic-based signals in elastography is that they may produce stronger shear waves at deeper tissue regions of interest (ROI), and they provide a robust means for determining additional parameters such the evolution of SWS as a function of frequency (dispersion). The dispersion result could be linked to more advanced rheological models for better tissue characterization. A disadvantage of HE is that the spatial resolution of the final elastograms is limited (Doyley 2012) and the approach requires additional hardware in the form of external vibration sources in order to produce shear waves.

To summarize this history, figure 10 illustrates the evolution of elastography since it was initiated more than 30 years ago. It shows some of the well-characterized approaches and depicts each technique based on the excitation load type used and the qualitative or quantitative parameter outputs.

5. Clinical applications using ultrasound elastography

To illustrate the importance of different elastography methods, this section describes some clinical results demonstrating the diagnostic use of ultrasound elastography. This section is not comprehensive since many thousands of papers have been published on clinical applications; we highlight only a few of the largest areas in terms of patient scans and reports. For further details, the following reviews could be used: breast tissue (Barr *et al* 2015b), liver tissue (Ferraioli *et al* 2015), thyroid tissue (Cosgrove *et al* 2017), and prostate tissue (Barr *et al* 2017), along with several applications in Nenadic *et al* (2019). Parallel results from MRE can be found in other overviews (Glaser *et al* 2012, Low *et al* 2016, Serai *et al* 2017, Bunevicius *et al* 2019)

5.1. Breast

SE and ARF-based SWE have been shown to improve characterization for some breast masses. It has been suggested that the application of both methods on a patient may improve the confidence in the results, and

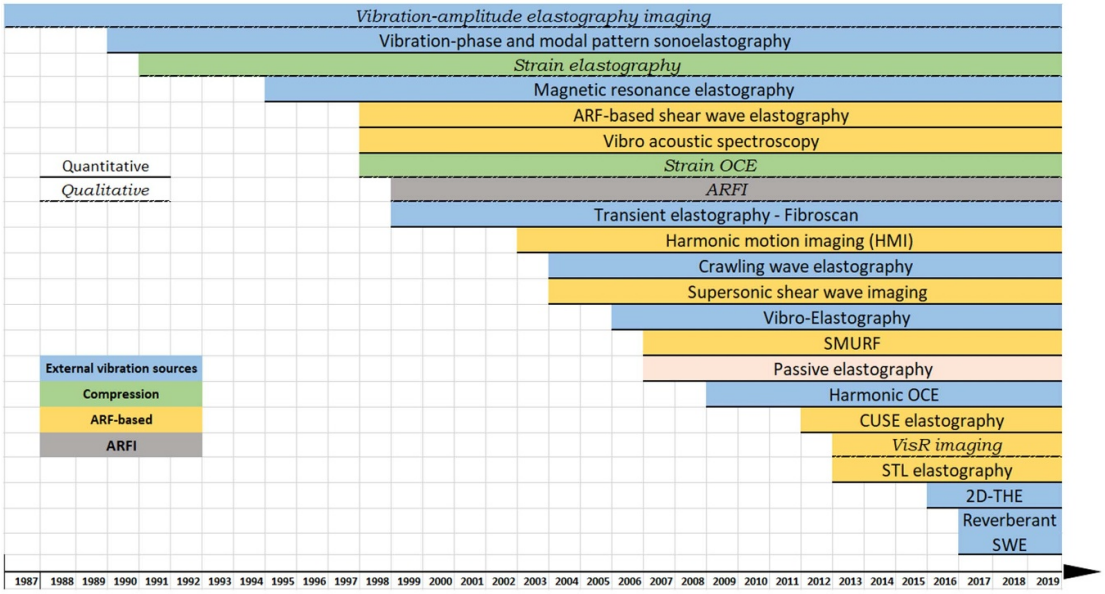

Figure 10. The 30+ year timeline of the evolution of elastography methods showing some of the main approaches. Each color represents the excitation load employed by each method. The italicized names indicate that the method produces a qualitative output, the non-italicized names indicate that the method yields a quantitative output. The methods are summarized in section 4.

that either of these methods can be used to better characterize any abnormality previously identified on a conventional B-mode image (Barr *et al* 2015b).

The utility of SE may be that it could improve the sensitivity and positive predictive value of conventional B-mode images when diagnosing BI-RADS 3 and 4 focal lesions (Chiorean *et al* 2008), and it could improve diagnostic confidence in BIRADS 2 lesions with an elasticity score of 2 or below. It may be used to re-classify BIRADS 3 lesions with an elasticity score of 2 or below as BIRADS 2 (Tan *et al* 2008). Other studies showed that SE can be a tool for evaluation of therapy and for lesions that do form a mass (Nakashima and Moriya 2013). It has been shown that SE has the ability to differentiate between benign and malignant masses using either the Tsukuba score (Itoh *et al* 2006) or the EI/B mode ratio (Barr *et al* 2015b). The EI/B mode ratio compares the lesion size obtained using elastography to the B-mode size. In (Barr *et al* 2012), a large multi-center unblinded trial evaluated 635 biopsy proven cases using Barr's criteria (an EI/B-mode ratio <1.0 as benign and ≥ 1.0 as malignant (Barr 2010)). The results indicated a sensitivity of 99% and a specificity of 87%. In addition, SE has shown that there are particular strain patterns that can characterize a lesion as cystic (Barr *et al* 2015b).

The application of ARF-based SWE improved the characterization of lesions over BI-RADS alone, with a sensitivity and specificity of 93.1% and 59.4% for BI-RADS and 92.1% and 76.4% with the addition of SWE. In another study of 158 patients, Chang *et al* (2011) found that the mean elasticity values were significantly higher in malignant masses (153 ± 58 kPa) than benign masses (46 ± 43 kPa) ($p < 0.0001$). In another series of 161 masses, including 43 malignancies, using a SWS cut-off of 3.6 m s^{-1} (38 kPa), a sensitivity of 91% and a specificity of 80.6% were achieved (Tozaki *et al* 2012). Figure 11 illustrates the advantage of using both SE and ARF-based SWE methods for better breast tissue characterization. Both elastography methods were applied in a patient and indicated the presence of a possible malignant lesion. Biopsy results confirmed that lesion corresponded to an invasive ductal carcinoma (IDC).

5.2. Liver

Liver elastography is useful for the evaluation of diffuse liver diseases with, generally, good reproducibility and improved accuracy in assessing the severity of fibrosis It has been shown that elastography is capable of distinguishing significant fibrosis (F2 or greater) from non-significant (F0–F1) fibrosis. However, more data are needed to confirm its use to distinguish between consecutive stages of early fibrosis. Some parameters such as liver inflammation, liver congestion, and biliary obstruction have been identified as confounding factors when measuring the SWS or the Young's modulus (Ferraioli *et al* 2015, Petitclerc *et al* 2017).

In TE, liver stiffness values correlated strongly with Metavir fibrosis stages. Some studies (Arena *et al* 2008, Lupsor *et al* 2008, Degos *et al* 2010, Zarski *et al* 2012) showed a substantial overlap in liver stiffness between adjacent stages of hepatic fibrosis, particularly for lower stages. In other studies, it can be seen that TE accurately discriminates cirrhosis from significant fibrosis (area under receiver operating characteristic

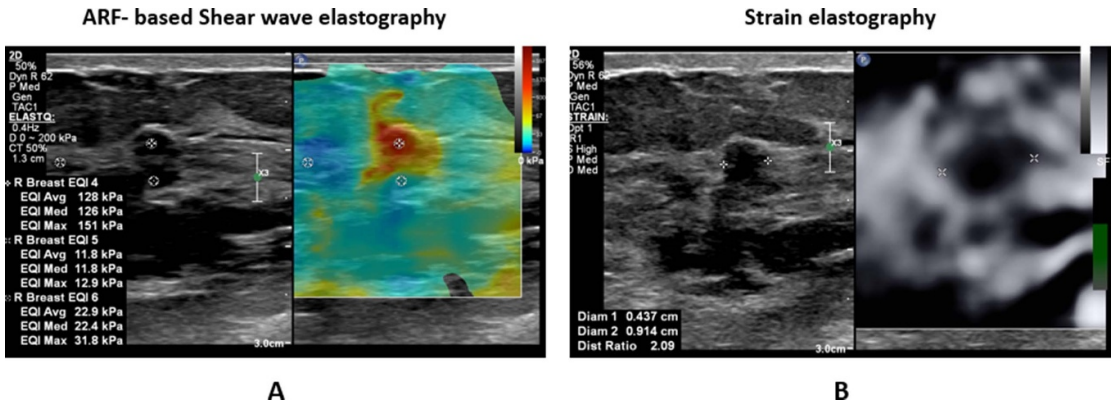

Figure 11. Elastography images for an *in vivo* breast tissue. Both elastography images were obtained from the same patient using ARF-based SWE (A) and SE (B). Biopsy results confirmed that lesion corresponds to an IDC. In (A), SWS were higher than 4.5 m s^{-1} in the lesion area. In (B), the lesion appears larger than in the corresponding B-mode. Both criteria indicate the presence of a malignant lesion (Barr *et al* 2015b). Images courtesy of Dr R G Barr.

(AUROC) 0.87–0.98; correct classification 85% to 94%) (AUROC 0.75–0.93; correct classification from 57% to 90%) (Ferraioli *et al* 2015). In patients with non-alcoholic fatty liver disease (NAFLD), TE confidently excluded severe fibrosis and cirrhosis with a high negative predictive value (approximately 90%) (Wong *et al* 2010). TE has also been evaluated in cholestatic liver diseases (Corpechot *et al* 2006, 2012), in a variety of chronic liver diseases (Foucher *et al* 2006, Ganne-Carrie *et al* 2006, Fraquelli *et al* 2007), as well as in alcoholic liver disease (Nahon *et al* 2008, Nguyen-Khac *et al* 2008).

In ARF-based SWE, stiffness estimates ranging from 2.6 to 6.2 kPa have been reported for histologically proven normal livers (Suh *et al* 2014). Bavu *et al* (2011) evaluated 113 patients with chronic hepatitis C. The results showed good agreement between fibrosis staging and elasticity assessment, and showed a higher accuracy in assessing mild and intermediate stages of fibrosis. Ferraioli *et al* (2012) used SWE to evaluate liver fibrosis in patients with chronic hepatitis C in a pilot study on 121 patients. This study applied optimal cut-off values of 7.1 kPa for significant fibrosis ($F \geq 2$), 8.7 kPa for advanced fibrosis ($F \geq 3$), and 10.4 kPa for cirrhosis ($F = 4$). AUROC curves were 0.92 ($F \geq 2$), 0.98 ($F \geq 3$), and 0.98 ($F = 4$). In addition, it has been reported that stiffness values are not correlated with liver steatosis (Ferraioli *et al* 2012, Suh *et al* 2014) or with necro-inflammation (Ferraioli *et al* 2012).

5.3. Thyroid

Ultrasound elastography, using either SE or ARF-based SWE, is a valid and useful additional tool to B-mode and color Doppler ultrasound in thyroid evaluation. Cosgrove *et al* (2017) recommended that SE be combined with conventional ultrasound to improve specificity based on the studies of (Cosgrove *et al* 2013, Cantisani *et al* 2015a, 2015b). The Tsukuba score (Itoh *et al* 2006), was used in a study of 92 patients, in which 49 patients were scored 1 and 2, all benign; 13 patients were scored 3, one carcinoma and 12 benign lesions; and 30 patients were scored 4 and 5, all carcinomas. Thus, scores 4 and 5 were highly predictive of malignancy ($p < 0.0001$), with a sensitivity of 97%, specificity of 100% (Rago *et al* 2007, Rago and Vitti 2008). Several studies have assessed the strain ratio, the ratio between the strain in adjacent thyroid tissue and strain in the nodule. A cutoff >4.22 resulted in a sensitivity of 81.8%, specificity of 82.9%, and accuracy of 88% (Ning *et al* 2012), whereas 3.79 was the best cutoff point in another study, with a sensitivity of 97.8% and specificity of 85.7% (Xing *et al* 2011).

Cosgrove *et al* (2017) showed that ARF-based elastography is useful in evaluating the thyroid stiffness nodules and differentiating between malignant and benign nodules. Based on Dong *et al* (2015), SWE has good sensitivity and specificity for identification of thyroid nodules. Most studies have evaluated SWE for the differentiation of thyroid nodules in a general population with promising results (Sebag *et al* 2010, Walsh *et al* 2012, Park *et al* 2015, Liu *et al* 2015a, 2015b, 2015c, 2015d). Park *et al* (2015) reported a mean stiffness value >85 kPa or a maximum value >94 kPa as an independent predictor of malignancy. Zhang *et al* (2012) reported SWS values for benign and malignant thyroid nodules of 2.34 ± 1.17 m s^{-1} and 4.82 ± 2.53 m s^{-1}, respectively ($p < 0.001$).

5.4. Prostate

Early work in sonoelastography indicated promising results for prostate cancer (PCA) detection with sensitivity approaching 80% or higher, far above that of B-mode ultrasound (Lee *et al* 1991, Taylor *et al* 2004,

2005). As instrumentation developed, SE became perhaps the most studied elastography method for PCA localization (Barr *et al* 2017). The addition of SE can increase the PCA detection rate (Konig *et al* 2005, Tsutsumi *et al* 2007, Pallwein *et al* 2007a, 2007b, Aigner *et al* 2010, Brock *et al* 2012, Wang *et al* 2015). Furthermore, the addition of SE can improve lesion localization for image-guided prostate biopsy (Barr *et al* 2017). In Kamoi *et al* (2008), using biopsy as the reference, the sensitivity, specificity, and accuracy of SE for prostate lesions were reported as 68%, 81%, and 76%, respectively. Zhang *et al* (2014) investigated the diagnostic performance of SE in the diagnosis of PCA in 7 studies with surgical pathology as the reference: the pooled sensitivity and specificity of SE were 72% and 76%, respectively.

Using ARF-based SWE, some studies suggested that the stiffness value of a lesion correlates with the Gleason score (Correas *et al* 2015). The addition of SWE in prostate can increase the PCA detection rate (Barr 2014, Correas *et al* 2015, Boehm *et al* 2015a, 2015b). Barr *et al* (2017), showed that SWS values were statistically significantly higher in PCAs than in benign lesions ($p < 0.002$ in all studies). For this analysis, only one system was used (Aixplorer system, SuperSonic Imagine, Aix en Provence, France). In addition, aggressive PCAs exhibited statistically significantly higher tissue stiffness ($p < 0.01$ in all studies) than indolent PCAs in several studies (Ahmad *et al* 2013, Woo *et al* 2014). Correas *et al* (2015) reported, in a 184 patient study, the sensitivity, specificity, and positive and negative predictive values of 97%, 70%, 70%, and 97%, respectively, for a 35 kPa cutoff for diagnosing PCA with Gleason scores $\geq$6.

5.5. Skeletal muscle

The study of muscle elastic properties is complicated by the active contractility of the muscle under voluntary control and by the anisotropic alignment of the muscle fibers. Nonetheless, the history of elastography in muscle parallels the development of the field, beginning with the early results from Yamakoshi and Sato (Yamakoshi *et al* 1990). Other developments include the inverse problem approach of Levinson (Levinson *et al* 1995, Yeung *et al* 1998, Fu *et al* 2000), the application of crawling waves (Hoyt *et al* 2008), shear waves (Gennisson *et al* 2003, 2010, Koo *et al* 2013, 2014, Eby *et al* 2013), indentation (Zheng and Mak 1999), the VisR imaging approach (Selzo and Gallippi 2013), and MRE techniques (Dresner *et al* 2001, Sack *et al* 2002, Jenkyn *et al* 2003, Uffmann *et al* 2004, Papazoglou *et al* 2005, Bensamoun *et al* 2006, Klatt *et al* 2010). Because muscle and tendons are comprised of highly directional fiber bundles, the propagation of waves is known to be anisotropic, and some shear wave measurements have begun to characterize the dependence of elastic properties along and across the major long axis (Jenkyn *et al* 2003, Papazoglou *et al* 2005, Gennisson *et al* 2010, Lee *et al* 2012, Song *et al* 2012, Green *et al* 2013, Wang *et al* 2013a, Qin *et al* 2014, Hossain *et al* 2017).

5.6. Cardiovascular

The stiffness of arterial walls has been a medical concern since at least the late 19th century and the mathematical treatment of the Windkessel effect (Frank 1899). A later landmark development in theoretical treatments was Womersley's solution for pulsatile flow in which a stiff arterial wall is assumed along with a periodic frequency of the heartbeat (Womersley 1955), and this was extended to the case of elastic vessel walls (Barnard *et al* 1966).

With the rapid development of elastographic imaging techniques in the 1990s, a new wave of measurements of the elastic properties of arteries, plaques, and cardiovascular tissues was enabled (Hoffmeister *et al* 1996, de Korte *et al* 1998, de Korte and van der Steen 2002, Trahey *et al* 2003, Dumont *et al* 2006, Rogowska *et al* 2006, Schmitt *et al* 2010, Couade *et al* 2011, Korukonda *et al* 2013, Shcherbakova *et al* 2014, Vos *et al* 2017, Doyley 2018). Myocardial wall stiffness is itself a particular focus of interest and has been investigated by the analysis of intrinsic motion, or alternatively with external vibration sources (Liu *et al* 2016, Song *et al* 2016, Papadacci *et al* 2017, Vos *et al* 2017, Strachinaru *et al* 2017, 2019, Arani *et al* 2017, Bunting *et al* 2018, Nenadic *et al* 2018, Sabbadini *et al* 2019, Cvijic *et al* 2020). Various pathological conditions including vulnerable plaques, regions of infarcts, and blood clots (Viola *et al* 2002, Rubin *et al* 2003, Durst *et al* 2013) are now considered to be detectable and quantifiable using elastographic techniques.

6. Current limitations and technical problems in ultrasound elastography

In this section we highlight some technical issues that are commonly confronted by clinicians when making diagnostic assessments using commercially available ultrasound scanners. Again, we focus on only a few of the more major applications.

6.1. Clinical limitations

6.1.1. Breast tissue

In SE, different studies report different cut-off values for the strain ratio; thus, a multi-center study that includes accuracy control is needed. In SWE, due to problems associated with weak shear wave propagation

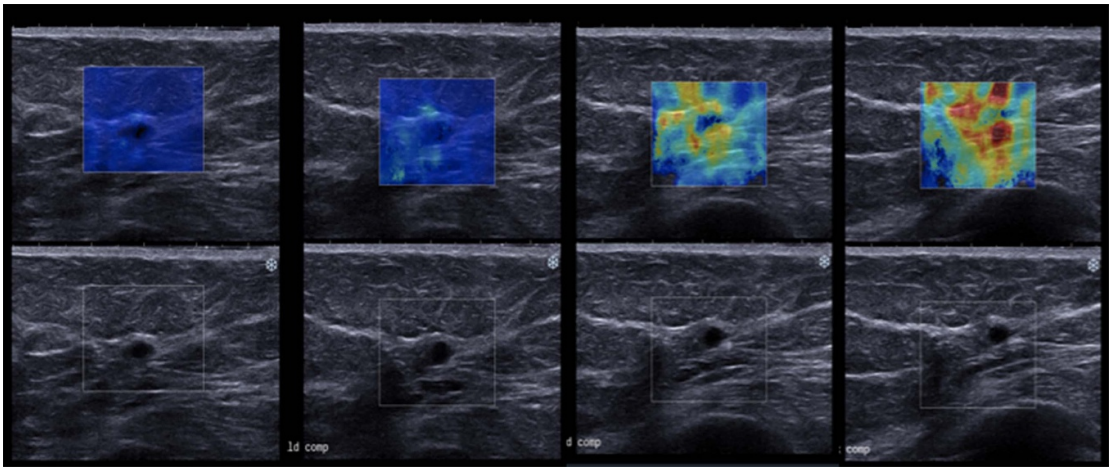

Figure 12. The effect of increasing compression on a cyst breast lesion. Simply applying more contact force on the hand held transducer (left to right images) is sufficient to compress tissue and change stiffness measurements. Note that with minimal pre-compression (left column), the cyst has no signal as shear waves do not propagate in simple cysts. As pre-compression is applied, the stiffness of the cyst and surrounding tissues significantly increases. For a moderate and marked compression (right column), the cyst lesion reports elasticity values (in kPa units) corresponding to a malignant lesion. Images courtesy of Dr R G Barr.

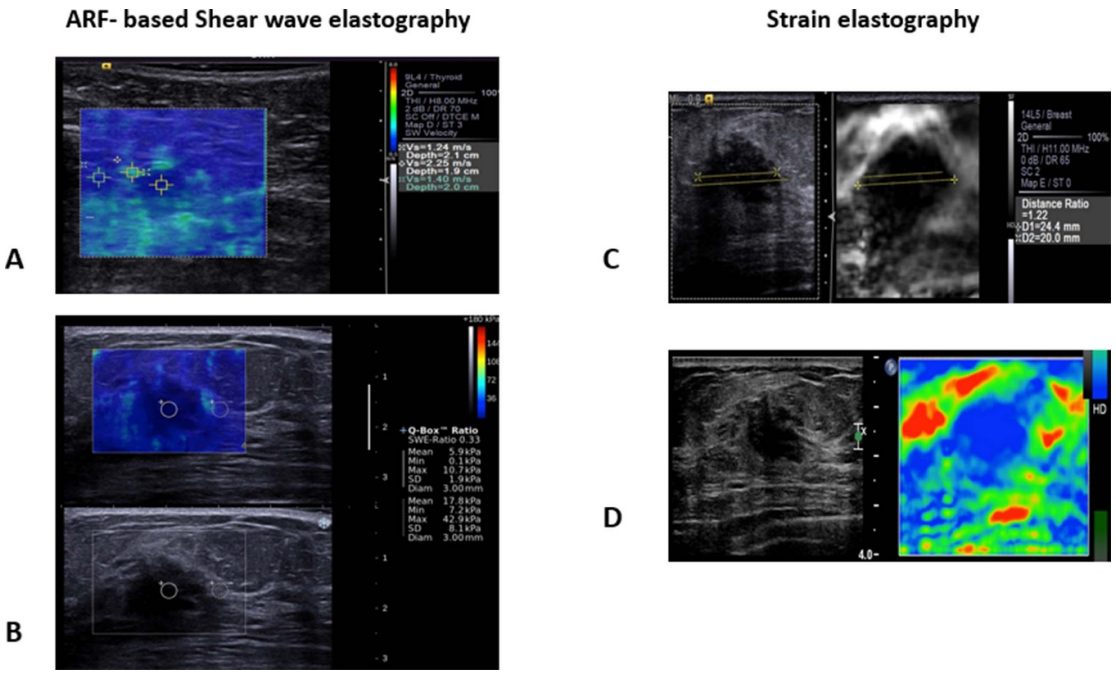

Figure 13. 37-year old patient with a mass in the right breast presenting as IDC. ARF-based SWE images from two different vendors (A) and (B) show low SWS values, suggestive of a benign lesion. SE images from two different vendors (C) and (D) both show EI/B-mode ratio greater than 1, suggestive of malignancy. Images courtesy of Dr R G Barr.

in tumors, SWS measurements can be inaccurate. Similarly, shear waves do not propagate in low viscosity liquids; therefore, simple cysts will not be assessed (Barr *et al* 2015b). Additionally, the stiffness of the breast can be increased significantly by compression caused by the hand-held transducer, this can be a potential source of operator-dependent variability. This phenomenon is linked to the general nonlinear behavior of tissues, as discussed in section 8.1. A clinical example is shown in figure 12.

Figure 13 illustrates the different elastography results using strain and ARF-based elastography methods from different vendors on an *in vivo* breast examination with confirmed IDC. It has been reported that some IDC cases show a low SWS value using ARF-based SWE, but high EI/B ratio using SE methods (Barr *et al* 2012). The causes of these differences are not fully resolved.

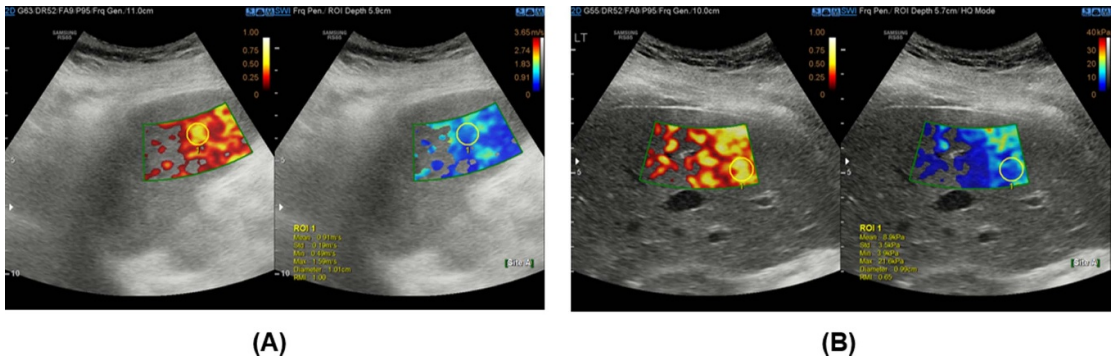

Figure 14. Illustration of some limitations in elastography in *in vivo* scans in a highly attenuated media. In each case, the left image indicates the goodness of data as a color; the right image shows the SWS parameter. Both liver tissue elastograms were acquired using an ARF-based SWE method implemented in a RS85 Samsung ultrasound system. (A) Patient with a F2 and S2 stages of fibrosis and steatosis, respectively. (B) Patient with a F0 and S3 stages of fibrosis and steatosis, respectively.

6.1.2. Liver tissue

TE cannot technically be performed in patients with ascites. On the other hand, SE can be applied in patients with ascites and narrow intercostal spaces, but it is difficult to generate clear SE images in severely obese patients. In ARF-based SWE, the majority of the studies have been performed in patients with chronic hepatitis C, therefore the chosen cutoffs may not be applicable to other viral etiologies or to NAFLD. Generally, obesity is a common limitation of all ultrasound-based elastography methods. Maximum acquisition depth with current technology is 6.5 cm. Other limitations are narrow intercostal spaces. Most methods show higher stiffness values when the levels of aminotransferases are elevated (Ferraioli *et al* 2015). Figure 14 shows an example in two *in vivo* liver cases where SWE was used. As shown, no complete or high quality images were obtained in these high viscosity liver tissues, as they correspond to high levels of steatosis. Strategies to overcome this limitation include the use of lower ultrasound frequencies, or the substitution of alternative methods such as reverberant SWE as shown in figure 9.

6.1.3. Thyroid tissue

In SE, transverse scans are more susceptible to interference from carotid artery pulsations. Several factors can affect the results of elastography, including calcifications and cystic components, the experience of the operator, and motion artifacts from respiration and carotid pulsations. In ARF-based SWE, pressure applied by the probe increases the tissue stiffness and large and deeply-seated nodules cannot be properly assessed (Cosgrove *et al* 2017).

6.1.4. Prostate tissue

The major limitations of SE are the lack of uniform compression over the entire gland and penetration in large prostate glands; these result in poor SE image quality. In ARF-based SWE, only a limited ROI can be measured and shear waves cannot be generated in deep regions (reliable ARF pulses from transrectal ultrasound sources typically penetrate only 3–4 cm). In the presence of macrocalcifications, the stiffness values are overestimated. In case of a large prostate, SWE cannot measure the anterior zone (Barr *et al* 2017).

6.2. Ultrasound SWS imaging system problems

Data suggests that there are still some systematic errors and variances attributed to the different systems at the various sites. Hall *et al* (2013) reported that there is a statistically significant difference in SWS estimates in different and almost pure elastic phantoms. The inter-system variability ranges from 6% to 12%, with nominal SWS between 1.0 and 2.0 m s^{-1}. This study suggests that there is strong evidence of a depth-dependent bias in SWS among different systems and phantoms.

A subsequent study reported that the SWS measurement variance increases as a function of higher stiffness and focal depth (Palmeri *et al* 2015). The results obtained agreed with the limitations of finite SW spatial and temporal sampling, and the decreased signal-to-noise ratio (SNR) associated with increasing stiffness and depth reported in (Shiina *et al* 2015). Another source of inter-system variability, which was not characterized in (Hall *et al* 2013), was the impact of viscosity, which can lead to shear wave dispersion (SWD) and affect group velocity estimates generated by imaging systems. The objective in (Palmeri *et al* 2015) was to compare different ultrasound imaging systems and measure SWS in different tissue-mimicking viscoelastic phantoms that represent normal and fibrotic liver. Because different systems report different elastic modulus/SWS metrics, all metrics were reported in terms of SWS, the parameter that all systems inherently

measure. All the tested phantoms were characterized by the phase velocity at 200 Hz, and the linear dispersion slope (dc/df) from 100 to 400 Hz. Since some methods measure the phase velocity and others the group velocity, it is important to have an understanding of how both of these parameters can be compared in order to achieve better agreement for the clinical results among all the elastography methods.

Palmeri *et al* (2015), also reported that SWS measurements were more consistent at shallower depths (3.0 and 4.5 cm); the greater inter-system variability at the deepest focal depth (7.0 cm) may be due to poor SNR deeper in the phantoms. Despite the fact that current generation ultrasound SWS imaging systems can estimate elastic properties, there is room for improvement to reduce inter-system variability and allow reported SWS to be directly compared to other systems. Moreover, more advanced biomechanical parameters such as SWS dispersion and shear wave attenuation (SWA) could be measured in order to perform a better viscoelastic tissue characterization as will be discussed in section 8.

7. International guidelines and consensus

Perhaps the earliest effort to bring together the nascent international research community in elastography was the inaugural International Conference on the Ultrasonic Measurement and Imaging of Tissue Elasticity in Niagara Falls, Ontario, Canada, in October of 2002, sponsored by the University of Texas and the University of Rochester (ITEC 2002). By this point in the early 21st century, the availability of clinical scanners capable of elastography techniques was beginning to expand, providing more clinicians and specialists with the tools for making images and measurements related to stiffness. This resulted in a proliferation of papers and conference presentations related to studies of normal and diseased tissue stiffness. As these accumulated, the variability in results across observers, across patients, and across measurement techniques and platforms could be assessed. A number of organizations began the important work of identifying best clinical practices and identifying the role of co-factors that influence biomechanical measurements, while minimizing variability. Major efforts include the guidelines from the European Federation (Cosgrove *et al* 2013) and Japan (Kudo *et al* 2013, Nakashima *et al* 2013, Shiina 2013). Next, the Society of Radiologists in Ultrasound published a consensus statement on elastography (Barr *et al* 2015a). The World Federation for Ultrasound in Medicine and Biology published an extensive set of guidelines (Ferraioli *et al* 2015, 2018), and other societies continued to develop specific guidelines (EASL and ALEH 2015, Kemp *et al* 2015, Lim *et al* 2017, Shiha *et al* 2017). A more detailed review of the particular recommendations of these groups is found in Ferraioli (2019).

In addition to these clinically oriented efforts, the Radiological Society of North America (RSNA) had independently developed a framework for cooperation between the medical imaging industry, academics, and clinicians to establish reliable quantitative biomarkers across different modalities and different clinical tasks. Ideally, a measurement of a particular tissue parameter should provide the same result on any platform in any clinic, anywhere in the world. The Quantitative Imaging Biomarkers Alliance (QIBA) created a task force on stiffness measurements which began to address elastography techniques (Hall *et al* 2013, Chen *et al* 2017), with the important goal of cross-platform agreement.

Another related issue pertains to the rheological models used in elastography. Even within the simplified world of linear, isotropic, and viscoelastic materials, there are many traditional rheological (stress–strain) models to choose from (Fung 1981). Each of these has specific time domain and frequency domain behaviors and the particular choice of model can influence or bias the estimation of viscoelastic parameters. In the worst case, two different systems using two different rheological models could report incompatible parameters. There is no widespread agreement on standardization here, but a recent publication has made the case for reaching a consensus around fractional derivative models which have strong experimental and theoretical support (Parker *et al* 2019).

8. Promising directions for the next decade

The robust development of elastographic techniques and applications continues to gather momentum. Growing clinical applications include every deformable tissue and organ, from skin layers and corneal layers to the lungs and brain. In this section we focus more on technical improvements that will add to the overall capabilities and parameter sets provided by elastography in the near future.

8.1. Nonlinear parameters

In solid mechanics and biomechanics, linear stress strain relationships are commonly understood to be only a simplification of more general nonlinear behavior, and in fact most tissues exhibit a progressive stiffening when extended beyond a few percent of strain (Fung 1981), called ‘strain hardening’ as illustrated in figure 12. Many types of mathematical models exist for nonlinear behavior in rheology, acoustics, and shear

wave propagation. Of interest in imaging the elastic properties of tissues is the possibility that nonlinear parameters for normal tissues may differ from pathological cases, including cancers. Presumably the structural and composition differences between tissues create a range of nonlinear parameters that can be used as a diagnostic tool (Varghese *et al* 2000, Samani and Plewes 2004, O'Hagan and Samani 2009).

There has been encouraging development of systems and estimators for nonlinear parameters (Catheline *et al* 2003, Erkamp *et al* 2004, Gennisson *et al* 2007, Mehrabian *et al* 2010, Koo *et al* 2011, Goenezen *et al* 2012, Guzina *et al* 2015, Bernal *et al* 2016, Nazari and Barbone 2018, Napoli *et al* 2018, Dord *et al* 2019, Rosen and Jiang 2019, Osapoetra *et al* 2019, Goswami *et al* 2019a, 2019b, Wang *et al* 2019b). Generally, these require a progression of stress–strain states to be completed within the ROI of the imaging system, and within a fairly limited timespan. Creating imaging strategies for estimating nonlinear parameters in a user-independent, accurate, ergonomic, and high resolution platform remains an important goal with many promising clinical application.

8.2. Viscoelastic parameters

The lossy nature of shear wave propagation can be related to pathological conditions. For example, chronic liver disease can be caused by many different etiologies (i.e. hepatitis B and C, NAFLD, NASH (non-alcoholic steatohepatitis)) (Ferraioli *et al* 2015, Parker *et al* 2015, Barr 2018). In order to assess chronic liver disease, it is necessary to differentiate between the presence of fibrosis, inflammation, and steatosis. Currently, the gold standard for quantitative measurement of these conditions are liver biopsy, which is invasive with concomitant patient risk (Barr 2018). Elastography has had success in measuring liver stiffness which is correlated with higher grades of liver fibrosis. However, there are confounding factors that affect the SWS measurement such as inflammation, increased portal venous flow, extrahepatic cholestasis, and steatosis (Barr 2018). For the latter condition, the assessment of the degree of steatosis is critical also for the diagnosis of NAFLD. Thus, there is need for a non-invasive and ultrasound readily available method to quantify these other factors and assess the tissue changes with treatment.

Different approaches to measure the viscoelastic properties of the liver are becoming available to clinicians, many involving shear waves. The additional parameters that can now be measured with SWE are SWD and SWA. Using ARF-based methods, SWD can be calculated by measuring the linear dispersion slope of the phase velocity over a frequency range. The phase velocity is extracted from the phase shift or difference of the shear waves over the propagated distance (Chen *et al* 2004, Deffieux *et al* 2009). Another approach obtains the phase velocity by calculating the 2D Fourier transform from the particle velocity signals, finding the maximum spatial frequency $k(\omega)$ at each discrete temporal frequency (Nenadic *et al* 2013, Nightingale *et al* 2015, Kumar *et al* 2018). Using harmonic waves, SWD is obtained from the phase velocity at different vibration frequencies. Then, a linear dispersion slope over a specific frequency range is calculated (Barry *et al* 2014, Tzschatzsch *et al* 2015, Ormachea *et al* 2019). Additional literature about dispersion includes the comparison of ARF and harmonic based methods to evaluate SWS and SWD using ultrasound (Ormachea *et al* 2016) and SWD estimation using MRE (Tzschatzsch *et al* 2015, Urban *et al* 2017).

Some emerging clinical studies that include SWD results are now summarized. Trout *et al* (2020), evaluated SWD in 128 children and 32 adults with no liver disease. In this study, it was found that SWD was associated with viscosity and was lower in adults compared with children (11.4 m s^{-1} kHz^{-1} and 10.24 m s^{-1} kHz^{-1} in children and adults, respectively). Yoo *et al* (2019), studied two different patient groups to evaluate the inter- and intra-variability of SWD in liver tissue. They found a SWD around 11.3 m s^{-1} kHz^{-1} in patients and 10 m s^{-1} kHz^{-1} in healthy people. Ormachea *et al* (2019) obtained deep 2D SWS and SWD images in normal and obese liver volunteers. Whereas the SWS did not show a clear difference between these cases, the SWD results showed a better differentiation (0.28 m s^{-1}100 Hz and 0.54 m s^{-1}100 Hz for the normal and obese case, respectively). Lee *et al* (2019) evaluated the role of SWD in detecting allograft damage after liver transplant by using SWD to monitor necroinflammation. They found a SWD of 12 m s^{-1} kHz^{-1} for patients without necroinflammation, and a SWD of 9.8 m s^{-1} kHz^{-1} in patients with necroinflammation (de Araujo Neto 2020). Sugimoto *et al* (2018b) studied 24 patients and found that lobular inflammation in liver is correlated with SWD (12.5–15.5 m s^{-1} kHz^{-1}). Later, in a review article, Sugimoto *et al* (2020) indicated that this preliminary clinical study, together with preclinical research (Sugimoto *et al* 2018a), showed that SWS closely correlates with the degree of fibrosis, but SWD better predicts the degree of necroinflammation. Mould *et al* (2019) evaluated one case with HELLP syndrome (haemolysis, elevated liver enzyme levels, and low platelets) over an extended period, indicating that SWD could assess the changes and progress during treatments. They reported that a SWD value less than 11 m s^{-1} kHz^{-1} was normal in liver.

SWD can also be used, together with SWS, to predict the shear and viscosity moduli using a rheological model (i.e. Voigt, Kelvin-Voigt, or power law models). Deffieux *et al* (2014), evaluated 120 liver cases, they measured SWD and employed a Voigt model to estimate viscosity and concluded that viscosity is a poor

predictor for steatosis staging. It was found that viscosity correlates with liver fibrosis, but not with steatosis. However, Sugimoto *et al* (2020) indicated that this discrepancy, compared with other clinical results, may be due to the different population characteristics and etiologies in patients studied by Deffieux *et al* (2014). Another study reported by Chen *et al* (2013) estimated viscosity in 35 patients and showed that viscosity was a less predictive value for liver stiffness and fibrosis staging. This study did not include an analysis of viscosity and its usefulness for steatosis evaluation. Moreover, some studies reported viscosity values based on a rheological model rather than the raw linear dispersion slope. In this case, it is worth emphasizing again the importance of finding a consensus on which rheological model best characterizes the viscoelastic properties of tissues (Parker *et al* 2019).

SWD has also been measured in other applications. Ormachea *et al* (2019) measured SWD in two patients with fibroadenomas and one with dense breast tissue using the reverberant shear wave elastography (R-SWE) approach. Tanter *et al* (2008) measured SWD in breast tissue to illustrate the difference in SWS results obtained by ARF-based method as compared with MRE. Kumar *et al* (2018) reported that shear viscosity, obtained from SWD, was significantly different between malignant and benign breast masses. Deffieux *et al* (2009) measured SWD in biceps brachii muscle, demonstrating tissue anisotropy. Simon *et al* (2018) analyzed SWD in *ex vivo* normal placentas and found that SWD may be able to distinguish placental structures. Callé *et al* (2018) evaluated SWD in 20 *ex vivo* normal placentas and later applied a rheological model based on a power law function. The study reported that the power law coefficient was tissue-dependent. Although it was not the main purpose of the study, SWD was also used to measure Achilles tendon viscosity in the orientation perpendicular to the tendon fiber by fitting the leaky Lamb wave equation and assuming a Voigt model by Brum *et al* (2014).

Figure 15 summarizes the results for SWD, as a function of frequency range, on human liver experiments. The SWD results were obtained using ARF and harmonic based elastography methods using ultrasound and MRI. Each clinical study reported the SWD at different frequency ranges and the range of SWD estimates is illustrated by the vertical shade bars representing standard deviation around the horizontal mean SWD values. However, some of these studies did not report the frequency range (i.e. Studies A to G in figure 15). Thus, we selected 100 Hz to 400 Hz as a reference frequency range for all of these cases mainly for two reasons: the studies used the same ultrasound equipment (i.e. Aplio *i*800, Canon Medical Systems), and all are based on ARF-based SWE, a method where the propagating shear wave frequency range (Deffieux *et al* 2009) is typically in the low hundred(s) Hz.

In a clinical study of liver SWA, Sharma *et al* (2019) focused on the hypothesis that steatosis adds a viscous (lossy) component to the liver, which increases SWA. In this research, SWA was measured in 20 patients. The results were compared with pathology scores obtained from liver biopsies. They found that SWA increases with higher stages of steatosis, ∼7, ∼8, ∼13, and ∼18 dB cm^{-1}150 Hz for S0, S1, S2, and S3 steatosis scores, respectively. This supports their hypothesis and indicates the possible utility of the measurements for non-invasive and quantitative assessment of steatosis. Nenadic *et al* (2017) used a spatial frequency broadening measure of attenuation, and concluded that liver transplant rejection cases had a lower SWA than normal livers. Budelli *et al* (2017) measured the SWA in phantoms and *in vivo* liver with good correlation using two different techniques, SSI and TE. Alternatively, some methods measure ultrasound attenuation based on longitudinal waves. Trout *et al* (2020) measured ultrasound attenuation in 32 adult livers and found that attenuation values ranged from 0.31 to 0.75 dB cm^{-1} MHz^{-1} in healthy adults. Sugimoto *et al* (2018b) reported ultrasound attenuation values of 0.65, 0.8, and 0.92 dB cm^{-1} MHz^{-1} for S1, S2, and S3 steatosis stages, and considered that attenuation was correlated with steatosis, whereas SWD did not show a tendency with steatosis. Additionally, Sasso *et al* (2010) first reported the controlled attenuation parameter (CAP), a dedicated and proprietary technology to measure ultrasound attenuation in order to assess the degree of liver steatosis. CAP is measured at the central frequency of 3.5 MHz using the FibroScan^{TM} scanner and is expressed in dB/m. Yen *et al* (2017) measured CAP in 1554 chronic liver disease patients and found a correlation with steatosis grades.

As observed, there are promising preliminary clinical results based on adding new viscoelastic tissue parameters. However, some questions remain to be answered. For instance, Fujii *et al* (2019) has worked with hepatic viscoelastic models and shown that the frequency range used to calculate the SWD is important for interpreting results. The low frequency range (25–100 Hz) worked better to classify fibrous tissue, whereas the high frequency (200–500 Hz) range was superior for viscosity characterization among the simulated materials. The biomechanical theories of steatosis clearly emphasize the importance of shear wave frequency for interpreting results (Parker *et al* 2018a).

Figure 15 clearly shows the discrepancies among different methods due to the different frequencies they used to measure the SWD. These discrepancies become more important to reconcile as some of the studies do not report the frequency range used to obtain the SWD results. In that sense, what is the appropriate

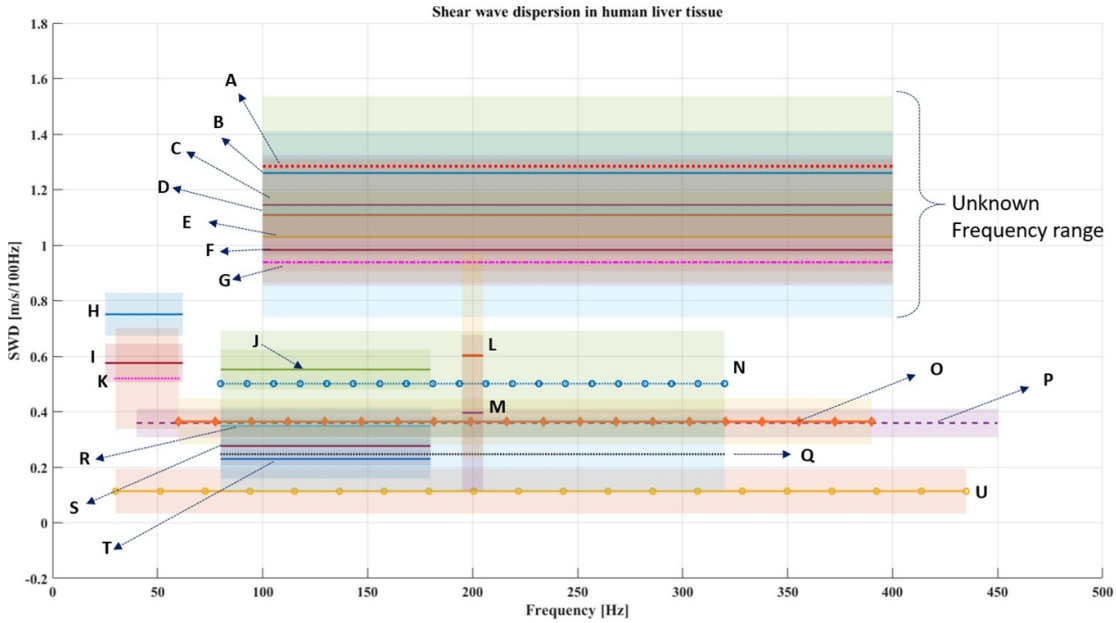

Figure 15. The range of shear wave dispersion estimates reported from human liver studies. The *y*-axis represents the mean reported dispersion in m s^{-1}100 Hz. The shaded vertical bars represent the standard deviation values reported in each study. The *x*-axis represents the frequency range used to measure the SWD. (A) Lobular inflammation, grade II (Sugimoto *et al* 2018b); (B) With necroinflammation (Lee *et al* 2019); (C) Healthy liver in children (Trout *et al* 2020); (D) Healthy liver in adults (Yoo *et al* 2019); (E) Healthy liver in adults (Trout *et al* 2020); (F) Without necroinflammation (Lee *et al* 2019); (G) Lobular inflammation, grade I (Sugimoto *et al* 2018b); (H) Healthy liver (Klatt *et al* 2007); (I) Healthy liver (Asbach *et al* 2008); (J) Ex vivo human liver, 10% fat + cirrhosis, (Barry *et al* 2012); (K) Volunteers (Tzschatzsch *et al* 2015); (L) NAFLD >F3 stage (Nightingale *et al* 2015); (M) NFLD <F2 stage (Nightingale *et al* 2015); (N) Obese patient (Ormachea *et al* 2019); (O) Healthy liver (Muller *et al* 2009); (P) Healthy liver (Deffieux *et al* 2009); (Q) Thin patient (Ormachea *et al* 2019); (R) *Ex vivo* human liver, 10% fat + fibrosis, (Barry *et al* 2012); (S) *Ex vivo* human liver, 10% fat, (Barry *et al* 2012); (T) *Ex vivo* normal human liver (Barry *et al* 2012); (U) Liver fibrosis F1 (Bavu *et al* 2011).

frequency range to measure dispersion? Should the frequency range be the same for all the clinical applications? Is SWD able to measure steatosis?

A similar reasoning may be applied to SWA, some studies have reported results at one specific frequency: 100 Hz (Parker *et al* 2018a, 2018c), 150 Hz (Sharma *et al* 2019). Other studies reported results at different frequencies: 140 Hz to 220 Hz (Budelli *et al* 2017), 100 Hz to 300 Hz (Nenadic *et al* 2017). Furthermore, other studies reported the ultrasound (longitudinal) wave attenuation. Which attenuation parameter, shear or longitudinal, should be measured, and what units and viscoelastic models should be commonly reported?

It is germane to point out that some of these clinical studies and others (Chen and Holm 2003, Zhang *et al* 2007, Urban *et al* 2017, Parker *et al* 2018b) have shown that many normal tissues exhibit a SWS with a power law behavior. The SWD is linked to SWA via the Kramers–Kronig relations (Szabo 1995, Chen and Holm 2003, Parker 2014). Thus, dispersion of phase velocity in an individual liver should be linked to the lossy, attenuating nature of the tissue (Parker *et al* 2015). In that context, it may be reasonable to measure the power law coefficient, which is directly related to the SWD and SWA and has the advantage of being frequency-independent (Parker *et al* 2018b). Of course, further studies will be needed to better understand the consistency between these three parameters. We believe these considerations should be included in future consensus efforts to standardize the additional parameters.

8.3. Anisotropy and guided waves

In the fields of optics, acoustics, and mechanics, there are well developed theories and measurement techniques for capturing the directional properties of stress–strain relations and wave propagation. Similarly in biomechanics, the directional orientation of muscle fibers and tendons has long been recognized (Fung 1981). A number of investigators in elastography have made measurements related to the anisotropic nature of muscle and other structures, as mentioned in section 5.5. In simplest terms, stress–strain behavior and SWS will vary with direction in anisotropic materials (Levinson 1987, Royer *et al* 2011). The limitations of conventional ultrasound 1D array systems are a disadvantage here since only one image plane is acquired with high motion sensitivity in only the axial direction. Thus in a complicated 3D biomechanical model, only one vector component of motion is available in only one 2D slice. This situation is improved with volumetric scanning in advanced ultrasound systems (Correia *et al* 2018) and in MRI, computed tomography (CT), and

OCT volumetric scans. The issue of anisotropy becomes more important as more anisotropic tissues come under routine study, including the cornea, tendons, nerves, and the brain (Zvietcovich 2020).

A variety of different types of waves can be formed in structures such as cylinders (arteries) or rods (tendons), for example see chapters 1–4 of Graff (1975). These types of guided waves are dependent on the elastic properties of the material, but also the size and shape and boundary conditions including the properties of the surrounding tissues. Surface waves are similar in their dependence on boundary conditions, including Lamb, Rayleigh, Scholte, and Stoneley waves (Mercado *et al* 2015, Langdon *et al* 2017). In these cases the measured speed of the shear wave disturbance and the dispersion can be a complicated function of the geometry and conditions. Nonetheless, the application of wave theories has been incorporated into elastographic studies of biological structures including arteries (Bernal *et al* 2011, Urban *et al* 2015), skin layers (Kirkpatrick 2003, Urban *et al* 2015), tendons (Jenkyn *et al* 2003, Drakonaki *et al* 2009, Brum *et al* 2014, Helfenstein-Didier *et al* 2016), cardiac muscle (Konofagou *et al* 2002, Kanai 2005, Nenadic *et al* 2011), and corneal layers (Tanter *et al* 2009). These types of studies have wide potential in expanding elastography outside of radiology, to routine use in ophthalmology, cardiology, sports medicine, and many other specializations.

8.4. Optical elastography

OCT elastography, now commonly referred to as OCE (Mulligan *et al* 2016), was introduced by (Schmitt 1998). This article was published roughly a decade after the introduction of ultrasound elastography (Lerner and Parker 1987), and a few years after the introduction of MRE (Muthupillai *et al* 1995).

The spatial scales of US elastography and MRE for elasticity imaging remain at the macroscopic level with an organ-size field of view and the typical resolution of hundreds of micrometers to several millimeters. On the other hand, OCE offers unique capabilities such as higher spatial resolution (between organ and cellular levels) and rapid 3D acquisition (Wang and Larin 2015, Mulligan *et al* 2016, Larin and Sampson 2017). These features allow OCE to fill the gap of the imaging scales (between ultrasound, magnetic resonance, and cellular level imaging) as observed in figure 2, and thus it has the potential to make great impacts on the biomechanical characterization of tissues (Wang and Larin 2015, Mulligan *et al* 2016, Larin and Sampson 2017).

Ultrasound and OCT have many similarities and therefore share several approaches to estimate the biomechanical properties of tissue. Thus, OCE uses quasi-static, transient, and harmonic excitations that are analogous to those used in ultrasound elastography (Mulligan *et al* 2016, Larin and Sampson 2017).

After the first publication, and especially since 2008, OCE expanded rapidly with several research groups reporting promising results and progress (Larin and Sampson 2017). Undoubtedly, the field will continue to grow as there are multiple opportunities and applications where OCE has great potential (Mulligan *et al* 2016, Larin and Sampson 2017). In that context, some studies have already evaluated the performance of OCE across different methods with different excitation forces (Zvietcovich *et al* 2016a, 2017). Furthermore, due to the different excitation loads, special emphasis has been taken to characterize the different waves propagating in the scanned media (i.e. longitudinal shear, shear, surface, lamb waves) (Zvietcovich *et al* 2016b, 2019a, 2019b, Han *et al* 2017).

Several applications have been reported using OCE, including non-contact mechanical stimulation (Huang *et al* 2009, Ambrozinski *et al* 2016). The main applications are found in cornea (Ford *et al* 2011, Li *et al* 2013, 2014, Ambrozinski *et al* 2016, Zvietcovich *et al* 2019b), soft-tissue tumor (Liang *et al* 2008, 2010, Adie and Boppart 2010, Kennedy *et al* 2012, Wang *et al* 2012), arterial wall (Qi *et al* 2012, 2013, 2014), muscle (Chin *et al* 2014, Wang and Larin 2014, Wang *et al* 2014), skin (Adie *et al* 2009, Kennedy *et al* 2011, Li *et al* 2012), single cells (Crecea *et al* 2013), crystalline lens (Wang *et al* 2013b, Wu *et al* 2015), tendon (Guan *et al* 2013), and *ex vivo* mouse brain (Ge *et al* 2019). Figure 16 shows the application of OCE in *ex vivo* porcine cornea using the reverberant SWE approach (Zvietcovich *et al* 2019b). The cornea is excited by a piezoelectric actuator attached to an eight-pronged ring. This configuration helps to generate a reverberant field, a limiting condition of shear waves propagating at multiple directions, to extract the elasticity information at different layers of the cornea tissue.

As observed, OCE's advantages include the ability generate elastograms with high resolution, promising an optimal tool for fine-scale clinical applications. More importantly, as emphasized by Mulligan *et al* (2016), OCE and ultrasound elastography may be integrated to generate a multimodal approach where each can add important information from the micro and macro level structure of the tissues.

8.5. Computational and technological advances

One important framework for approaching elastography is through the formulation of mathematical inverse problems (Barbone and Gokhale 2004, Barbone and Oberai 2007, Baghani *et al* 2009). Measured quantities from the imaging system include the motion vectors, and possibly boundary conditions, whereas the

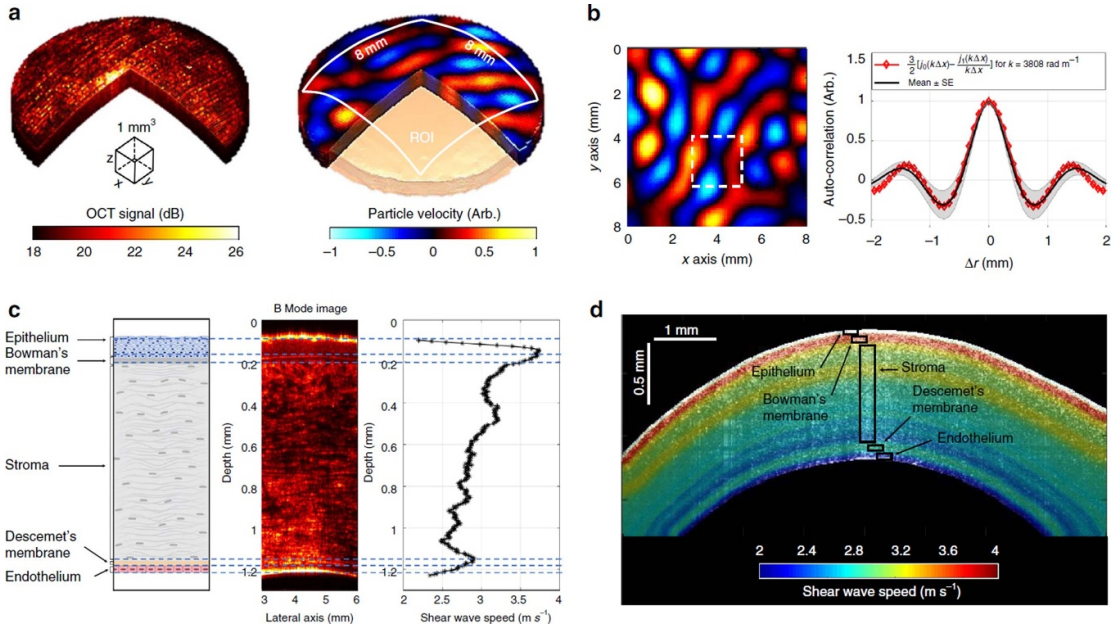

Figure 16. OCE/R-SWE in *ex vivo* porcine cornea for elasticity characterization of layers, Reprinted by permission from Springer Nature from Zvietcovich *et al* (2019b). Reverberant shear waves were acquired applying a 2 kHz vibration signal and a spectral domain phase sensitive OCT system. (A) Acquired B-mode 3D volume (left side), and particle velocity reverberant volume of cornea (right side). (B—left side), a particle velocity frame is extracted at the cornea epithelium from (A). (B—right side), average autocorrelation curve ($N = 360$ curves) taken along radial cuts of the 2D auto-correlation plot (2×2 mm^2 window size). Then, estimations of local wavenumber (k), and, therefore, shear wave speed (c_s) using $c_s = 2\pi f/k$, were calculated for all depths from the top (epithelium) to bottom (endothelium) layers of cornea. (C) Average depth-dependent SWS profile of the *ex vivo* cornea and how it correlates with (1) structural information from the B-mode intensity image of the same cornea sample, and (2) the anatomical description of some of the corneal layers. (D) 2D shear wave speed map superimposed on a B-mode structural image of the cornea.

unknowns include the biomechanical properties within the ROI. The unknown quantities can be as simple as a single unknown (linear, isotropic) stiffness assumed to be nearly constant across an ROI within a tissue, or as complicated as a set of viscoelastic parameters in a highly directional, anisotropic material, with significant spatial variation in 3D. A review of inverse problems in elastography has been published by Doyley (2012) covering quasi-static, transient, and sinusoidal steady state conditions. The issue of regularization of inverse problems continues to be a robust area of research (Honarvar *et al* 2012), and it is possible that new developments will have an impact on the data sets and solutions that are encountered in elastography.

Related to this is the emergence of artificial intelligence, machine learning, and deep learning algorithms in medical imaging. While many of these pertain to classification tasks, some are able to incorporate physical models (Li 2018, Dramsch *et al* 2019), or serve as alternative computational paths to inverse problems (Hoerig *et al* 2017, 2019). Some machine learning approaches require careful curation of large data sets for initial training of the neural nets. The impact of these on different categories of elastography will be determined over the next decade.

Another general area of technological improvement that will impact elastography is the advance of higher resolution 3D and four-dimensional (4D) image sets across a number of modalities. In ultrasound, the progress in 2D transmit/receive arrays and ultrafast plane wave transmit schemes is creating novel platforms with higher temporal and spatial resolutions (Provost *et al* 2014, Gennisson *et al* 2015, Huang and Zeng 2017). In MRI, CT, and OCT a variety of technical advances are pushing the volumetric data sets to higher spatial and/or temporal resolution (Malczewski 2020).

Since elastography inherently relies on the detection of stress and strain in three spatial dimensions over time, all the accumulating advances in the basic imaging platforms can potentially add to our ability to extract viscoelastic parameters at high spatial resolution. Temporal resolution in elastography, meaning the ability to track rapid changes in the stiffness of tissues, may also increase in importance as dynamic effects become more widely explored (Mcaleavey *et al* 2016, Parker 2017, Patz *et al* 2019, Kreft *et al* 2020).

Finally, the pressing need for a fundamental, multi-scale, biological explanation for the imaging results seen in elastography should be addressed in the coming years. The entire field can be viewed as an inverted pyramid, where millions of images of stiff lesions and tissues have accumulated yet in many cases the details of the underlying biological, structural, and compositional causes are poorly understood. For example, some cancers present as very stiff lesions and this can be superficially attributed to causes such as desmoplastic

reaction. However, a detailed multiscale explanation, bridging from the microscopic structural changes to the macroscopic observations from medical imaging scanners that incorporate elastography, are required. Some recent investigations are making progress in this direction (Wang *et al* 2019a, Vincent *et al* 2020).

9. Conclusion

Some 2500 years ago, the Greek philosopher Heraclitus of Ephesus proposed a sweeping theory of philosophy and rheology: ***panta rhei*** (πάντα ρεῖ, 'everything flows') (Beris and Giacomin 2014). After a delay of two and a half millennia, we have finally been able to noninvasively visualize and quantify the rheology of tissues and internal organs, *in vivo*, with adequate spatial and temporal resolution. This proves to be of great value in detecting and diagnosing pathological conditions, or staging diseases. While tremendous strides have been made over the last 30 years, the field of 'imaging the elastic properties of tissues' is still expanding rapidly in terms of clinical applications, commercial platforms, modalities, approaches, and the drive towards ever improving accuracy and spatial and temporal resolution. Every deformable tissue, organ, and structure is now a potential application of elastography imaging. According to Heraclitus, that is indeed a very extensive set of targets for future developments.

Acknowledgments

The authors wish to honor great contributors to the field who have recently died. These include J Abeysekera, Y Fung, D Cosgrove, E Carstensen, and J Ophir, whose insights illuminated many paths that are yet moving forward. The authors regret they could highlight only a limited number of major topics due to space constraints and wish to acknowledge many clinical applications and specialized techniques that are innovative and inspiring but were not able to be included in this article. We also thank Dr R Barr and Professor I Sack for sharing their insights and clinical examples, and the continuing advice from our colleagues Professor M Doyley and Dr D Rubens.

Appendix A. Governing equations for elastography

The conservation of linear momentum, a fundamental accounting of forces, deformations, and acceleration, is derived for a deformable medium using the methods of continuum mechanics, and in integral form applied to some volume:

$$\frac{\mathrm{d}}{\mathrm{d}t}\iiint_V \rho\dot{\mathbf{u}}\mathrm{d}V = \iint_S \mathbf{T}^{(\mathbf{n})}\mathrm{d}S + \iiint_V \rho\mathbf{b}\mathrm{d}V, \tag{9}$$

where ρ is the density, $\dot{\mathbf{u}}$ is the displacement vector (with the superposed dot indicating a time derivative), $\mathbf{b}$ is the body force per unit mass vector, and $\mathbf{T}^{(\mathbf{n})}$ is the traction vector on the surface S (with outward unit normal $\mathbf{n}$) of volume V. This equation states that the rate of change of linear momentum is equal to the resultant applied surface and body forces.

Writing the traction vector in terms of the stress tensor σ as $\mathbf{T}^{(\mathbf{n})} = \sigma \cdot \mathbf{n}$, neglecting the body forces (such as gravity) because their effects can be subtracted from the measured response, and considering the deformation small enough that it can be expressed in terms of the infinitesimal strain tensor (ε_{ij}):

$$\varepsilon_{ij} = \frac{1}{2}\left(\frac{\partial u_i}{\partial x_j} + \frac{\partial u_j}{\partial x_i}\right). \tag{10}$$

Then, the constitutive relation relating stress (σ) and strain for a linearly elastic, isotropic medium can be written as:

$$\sigma_{ij} = 2\mu\varepsilon_{ij} + \lambda\varepsilon_{kk}\delta_{ij} = \frac{E}{1+\upsilon}\left(\varepsilon_{ij} + \frac{\upsilon}{1-2\upsilon}\varepsilon_{kk}\delta_{ij}\right), \tag{11}$$

where μ and λ are called the Lamé constants, μ is also called the shear modulus, E is the elastic, or Young's, modulus, υ is the Poisson's ratio, and δ_{ij} is the Kronecker delta (equal to 1 if $i = j$, and 0 otherwise).

In homogeneous regions, where λ and μ are constant, a differential equation is obtained in terms of the displacement vector:

$$(\lambda+\mu)\frac{\partial u_j}{\partial x_j \partial x_i} + \mu\frac{\partial^2 u_i}{\partial x_j \partial x_j} = \rho\ddot{u}_i \quad \text{or} \quad (\lambda+\mu)\nabla(\nabla\cdot\mathbf{u}) + \mu\nabla^2\mathbf{u} = \rho\ddot{\mathbf{u}}, \tag{12}$$

where the body forces, such as gravity, have been assumed to be negligible. Given the initial and boundary conditions, and the force or displacement excitation, equation (12) governs the general dynamic response of a homogeneous, isotropic, linearly elastic material. If excitation loads are applied slowly (quasi-statically) or if the displacement response is measured after all the motion has stopped, then the right-hand side of this equation is negligible and set equal to zero. Therefore, this equation governs the static, quasi-static and dynamic (transient and harmonic wave propagation) responses that can occur in response to applied loads. It should be noted that equation (12) and its simplifications pertain to an elastic material, however in lossy or viscous materials, additional terms are included to account for the dissipation. A standard treatment would be to include an imaginary (or out-of-phase) term to the elastic and shear moduli, and this creates an attenuation term in the wave equation. A short derivation of these equations can be found in 'appendix A: Shear wave speed and attenuation' of Parker *et al* (2019).

At low frequencies or slow applied compressions, equation (12) could be simplified for the consideration of quasi-static elastography experiments. In static displacement or very low frequency cyclic motion, the time derivative terms are negligibly small, and for nearly incompressible biomaterials, the divergence (or dilatation) $\nabla \cdot u \approx 0$, so equation (12) reduces to Laplace's equation:

$$\nabla^2 \mathbf{u} = 0. \tag{13}$$

For simple 1D geometry, the solution for displacement $u_x(x)$ is linear with x, and therefore the strain (the derivative of displacement) is uniform, a fact that is assumed to be true in the quasi-static elastography imaging approach for homogeneous materials. Local changes from the assumed constant strain are indications of internal structures that are harder or softer, forming the basis of imaging in compression-based elastographic methods.

In summary, equation (12) and its simplifications can predict most of the tissue responses to excitations or forces used in elastography techniques. For different approaches, the relative weight of the terms changes and affects the type of response seen, as indicated in figure 1, especially the row titled 'temporal characteristics' which directly influence the acceleration terms of equation (12) (the right hand side). This distribution of responses is examined in more detail in Parker *et al* (2005).

Appendix B. Glossary of acronyms

AFM	atomic force microscopy
ALEH	Asociación Latinoamericana para el Estudio del Hígado
ARF	acoustic radiation force
ARFI	acoustic radiation force impulse
BI-RADS	breast imaging reporting and database system
BM	Brillouin microscopy
BMI	body mass index
CAP	controlled attenuation parameter
CT	computed tomography
CUSE	comb-push ultrasound shear elastography
CWS	crawling wave sonoelastography
EASL	European Association for the Study of the Liver
EI/B	elastography image/B-mode
FM	frequency modulation
HELLP	haemolysis, elevated liver enzyme levels, low platelets
HI	holographic imaging
HMI	harmonic imaging
IDC	invasive ductal carcinoma
MDEV	multifrequency dual elastovisco
MRE	magnetic resonance elastography
MRI	magnetic resonance imaging
NAFLD	non-alcoholic fatty liver disease
NASH	non-alcoholic steatohepatitis
OCE	optical coherence elastography
OCT	optical coherence tomography
OT-M	optical tweezers-based microrheology
PCA	prostate cancer
QIBA	Quantitative Imaging Biomarkers Alliance

RF	radio frequency
ROI	region of interest
RSNA	Radiological Society of North America
R-SWE	reverberant shear wave elastography
SE	strain elastography
SMURF	spatially modulated ultrasound radiation force
SNR	signal-to-noise ratio
SSI	supersonic shear imaging
STL	single tracking location
SWA	shear wave attenuation
SWD	shear wave dispersion
SWE	shear wave elastography
SWS	shear wave speed
TE	transient elastography
THE	time harmonic elastography
UE	ultrasound elastography
VisR	viscoelastic response

ORCID iDs

J Ormachea https://orcid.org/0000-0003-2481-8133
K J Parker https://orcid.org/0000-0002-6313-6605

References

Abeysekera J, Rohling R and Salcudean S 2015 Vibro-elastography: absolute elasticity from motorized 3D ultrasound measurements of harmonic motion vectors *2015 IEEE Int. Ultrasonics Symp. (IUS)* pp 1–4
Adie S G and Boppart S A 2010 Optical coherence tomography for cancer detection *Optical Imaging of Cancer*, ed E Rosenthal and K Zinn (Berlin: Springer) pp 209–50
Adie S G, Kennedy B F, Armstrong J J, Alexandrov S A and Sampson D D 2009 Audio frequency *in vivo* optical coherence elastography *Phys. Med. Biol.* **54** 3129–39
Adler R S, Rubin J M, Bland P H and Carson P L 1990 Quantitative tissue motion analysis of digitized M-mode images: gestational differences of fetal lung *Ultrasound Med. Biol.* **16** 561–9
Agache P G, Monneur C, Leveque J L and De Rigal J 1980 Mechanical properties and Young's modulus of human skin *in vivo Arch. Dermatol. Res.* **269** 221–32
Ahmad S, Cao R, Varghese T, Bidaut L and Nabi G 2013 Transrectal quantitative shear wave elastography in the detection and characterisation of prostate cancer *Surg. Endosc.* **27** 3280–7
Aigner F, Pallwein L, Junker D, Schafer G, Mikuz G, Pedross F, Mitterberger M J, Jaschke W, Halpern E J and Frauscher F 2010 Value of real-time elastography targeted biopsy for prostate cancer detection in men with prostate specific antigen 1.25 ng ml^{-1} or greater and 4.00 ng ml^{-1} or less *J. Urol.* **184** 913–7
Alam S K and Garra B S 2020 *Tissue Elasticity Imaging. Volume 1, Theory and Methods* (Amsterdam: Elsevier)
Ambrozinski L, Song S, Yoon S J, Pelivanov I, Li D, Gao L, Shen T T, Wang R K and O'Donnell M 2016 Acoustic micro-tapping for non-contact 4D imaging of tissue elasticity *Sci. Rep.* **6** 38967
Arani A *et al* 2017 Cardiac MR elastography for quantitative assessment of elevated myocardial stiffness in cardiac amyloidosis *J. Magn. Reson. Imaging* **46** 1361–7
Arena U *et al* 2008 Reliability of transient elastography for the diagnosis of advanced fibrosis in chronic hepatitis C *Gut* **57** 1288–93
Asbach P, Klatt D, Hamhaber U, Braun J, Somasundaram R, Hamm B and Sack I 2008 Assessment of liver viscoelasticity using multifrequency MR elastography *Magn. Reson Med.* **60** 373–9
Baghani A, Salcudean S and Rohling R 2009 Theoretical limitations of the elastic wave equation inversion for tissue elastography *J. Acoust. Soc. Am.* **126** 1541
Bamber J C and Bush N L 1996 Freehand elasticity imaging using speckle decorrelation rate *Acoust. Imaging* **22** 285–92
Bamber J C, De Gonzalez L, Cosgrove D O, Simmons P, Davey J and Mckinna J A 1988 Quantitative evaluation of real-time ultrasound features of the breast *Ultrasound Med. Biol.* **14** 81–87
Barbone P E and Gokhale N H 2004 Elastic modulus imaging: on the uniqueness and nonuniqueness of the elastography inverse problem in two dimensions *Inverse Probl.* **20** 283–96
Barbone P E and Oberai A A 2007 Elastic modulus imaging: some exact solutions of the compressible elastography inverse problem *Phys. Med. Biol.* **52** 1577–93
Barnard A C, Hunt W A, Timlake W P and Varley E 1966 A theory of fluid flow in compliant tubes *Biophys. J.* **6** 717–24
Barr R G 2010 Real-time ultrasound elasticity of the breast: initial clinical results *Ultrasound Q.* **26** 61–66
Barr R G 2014 Elastography in clinical practice *Radiol. Clin. North Am.* **52** 1145–62
Barr R G 2018 Shear wave liver elastography *Abdominal Radiol.* **43** 800–7
Barr R G, Cosgrove D, Brock M, Cantisani V, Correas J M, Postema A W, Salomon G, Tsutsumi M, Xu H X and Dietrich C F 2017 WFUMB guidelines and recommendations on the clinical use of ultrasound elastography: part 5. Prostate *Ultrasound Med. Biol.* **43** 27–48
Barr R G, Destounis S, Lackey L B 2nd , Svensson W E, Balleyguier C and Smith C 2012 Evaluation of breast lesions using sonographic elasticity imaging: a multicenter trial *J. Ultrasound Med.* **31** 281–7
Barr R G *et al* 2015a Elastography assessment of liver fibrosis: Society of Radiologists in Ultrasound consensus conference statement *Radiology* **276** 845–61
Barr R G *et al* 2015b WFUMB guidelines and recommendations for clinical use of ultrasound elastography: part 2: breast *Ultrasound Med. Biol.* **41** 1148–60

Barry C T, Hah Z, Partin A, Mooney R A, Chuang K-H, Augustine A, Almudevar A, Cao W, Rubens D J and Parker K J 2014 Mouse liver dispersion for the diagnosis of early-stage fatty liver disease: a 70-sample study *Ultrasound Med. Biol.* **40** 704–13
Barry C T, Mills B, Hah Z, Mooney R A, Ryan C K, Rubens D J and Parker K J 2012 Shear wave dispersion measures liver steatosis *Ultrasound Med. Biol.* **38** 175–82
Bavu E *et al* 2011 Noninvasive *in vivo* liver fibrosis evaluation using supersonic shear imaging: a clinical study on 113 hepatitis C virus patients *Ultrasound Med. Biol.* **37** 1361–73
Bensamoun S F, Ringleb S I, Littrell L, Chen Q, Brennan M, Ehman R L and An K N 2006 Determination of thigh muscle stiffness using magnetic resonance elastography *J. Magn. Reson. Imaging* **23** 242–7
Bercoff J, Pernot M, Tanter M and Fink M 2004a Monitoring thermally-induced lesions with supersonic shear imaging *Ultrason. Imaging* **26** 71–84
Bercoff J, Tanter M and Fink M 2004b Supersonic shear imaging: a new technique for soft tissue elasticity mapping *IEEE Trans. Ultrason. Ferroelectr. Freq. Control* **51** 396–409
Beris A and Giacomin J 2014 πάντα ρεῖ: everything flows *Appl. Rheol.* **24** 52918
Bernal M, Chamming's F, Couade M, Bercoff J, Tanter M and Gennisson J L 2016 *In vivo* quantification of the nonlinear elastic shear modulus in breast lesions: feasibility study *IEEE Trans. Ultrason. Ferroelectr. Freq. Control* **63** 101–9
Bernal M, Nenadic I, Urban M W and Greenleaf J F 2011 Material property estimation for tubes and arteries using ultrasound radiation force and analysis of propagating modes *J. Acoust. Soc. Am.* **129** 1344–54
Birnholz J C and Farrell E E 1985 Fetal lung development: compressibility as a measure of maturity *Radiology* **157** 495–8
Boehm K, Budaus L, Tennstedt P, Beyer B, Schiffmann J, Larcher A, Simonis K, Graefen M, Beyersdorff D and Salomon G 2015a Prediction of significant prostate cancer at prostate biopsy and per core detection rate of targeted and systematic biopsies using real-time shear wave elastography *Urol. Int.* **95** 189–96
Boehm K, Salomon G, Beyer B, Schiffmann J, Simonis K, Graefen M and Budaeus L 2015b Shear wave elastography for localization of prostate cancer lesions and assessment of elasticity thresholds: implications for targeted biopsies and active surveillance protocols *J. Urol.* **193** 794–800
Brock M, von Bodman C, Palisaar R J, Loppenberg B, Sommerer F, Deix T, Noldus J and Eggert T 2012 The impact of real-time elastography guiding a systematic prostate biopsy to improve cancer detection rate: a prospective study of 353 patients *J. Urol.* **187** 2039–43
Brum J, Bernal M, Gennisson J L and Tanter M 2014 *in vivo* evaluation of the elastic anisotropy of the human Achilles tendon using shear wave dispersion analysis *Phys. Med. Biol.* **59** 505–23
Brum J, Catheline S, Benech N and Negreira C 2015 Quantitative shear elasticity imaging from a complex elastic wavefield in soft solids with application to passive elastography *IEEE Trans. Ultrason. Ferroelectr. Freq. Control* **62** 673–85
Budelli E, Brum J, Bernal M, Deffieux T, Tanter M, Lema P, Negreira C and Gennisson J L 2017 A diffraction correction for storage and loss moduli imaging using radiation force based elastography *Phys. Med. Biol.* **62** 91–106
Bunevicius A, Schregel K, Sinkus R, Golby A and Patz S 2019 MR elastography of brain tumors *Neuroimage Clin.* **25** 102109
Bunting E, Papadacci C, Wan E, Sayseng V, Grondin J and Konofagou E E 2018 Cardiac lesion mapping *in vivo* using intracardiac myocardial elastography *IEEE Trans. Ultrason. Ferroelectr. Freq. Control* **65** 14–20
Callé S, Simon E, Dumoux M C, Perrotin F and Remenieras J P 2018 Shear wave velocity dispersion analysis in placenta using 2D transient elastography *J. Appl. Phys.* **123** 234902
Cantisani V *et al* 2015a Strain US elastography for the characterization of thyroid nodules: advantages and limitation *Int. J. Endocrinol.* **2015** 908575
Cantisani V *et al* 2015b Diagnostic accuracy and interobserver agreement of quasistatic ultrasound elastography in the diagnosis of thyroid nodules *Ultraschall Med.* **36** 162–7
Carstensen E L and Parker K J 2015 Oestreicher and elastography *J. Acoust. Soc. Am.* **138** 2317–25
Carstensen E L, Parker K J and Lerner R M 2008 Elastography in the management of liver disease *Ultrasound Med. Biol.* **34** 1535–46
Castera L, Forns X and Alberti A 2008 Non-invasive evaluation of liver fibrosis using transient elastography *J. Hepatol.* **48** 835–47
Catheline S, Benech N, Brum J and Negreira C 2008 Time reversal of elastic waves in soft solids *Phys. Rev. Lett.* **100** 064301
Catheline S, Gennisson J L and Fink M 2003 Measurement of elastic nonlinearity of soft solid with transient elastography *J. Acoust. Soc. Am.* **114** 3087–91
Catheline S, Thomas J L, Wu F and Fink M A 1999a Diffraction field of a low frequency vibrator in soft tissues using transient elastography *IEEE Trans. Ultrason. Ferroelectr. Freq. Control* **46** 1013–9
Catheline S, Wu F and Fink M 1999b A solution to diffraction biases in sonoelasticity: the acoustic impulse technique *J. Acoust. Soc. Am.* **105** 2941–50
Chang J M, Moon W K, Cho N, Yi A, Koo H R, Han W, Noh D Y, Moon H G and Kim S J 2011 Clinical application of shear wave elastography (SWE) in the diagnosis of benign and malignant breast diseases *Breast Cancer Res. Treat.* **129** 89–97
Chen S, Dhyani M, Garra B, Hall T and Palmeri M 2017 QIBA ltrasound shear wave speed biomarker update *Ultrasound Med. Biol.* **43** S149
Chen S, Fatemi M and Greenleaf J F 2004 Quantifying elasticity and viscosity from measurement of shear wave speed dispersion *J. Acoust. Soc. Am.* **115** 2781–5
Chen S, Urban M W, Pislaru C, Kinnick R, Zheng Y, Yao A and Greenleaf J F 2009 Shearwave dispersion ultrasound vibrometry (SDUV) for measuring tissue elasticity and viscosity *IEEE Trans. Ultrason. Ferroelectr. Freq. Control* **56** 55–62
Chen S G *et al* 2013 Assessment of liver viscoelasticity by using shear waves induced by ultrasound radiation force *Radiology* **266** 964–70
Chen W and Holm S 2003 Modified Szabo's wave equation models for lossy media obeying frequency power law *J. Acoust. Soc. Am.* **114** 2570–4
Chin L, Kennedy B F, Kennedy K M, Wijesinghe P, Pinniger G J, Terrill J R, Mclaughlin R A and Sampson D D 2014 Three-dimensional optical coherence micro-elastography of skeletal muscle tissue *Biomed. Opt. Express* **5** 3090–102
Chiorean A, Duma M M, Dudea S M, Iancu A, Dumitriu D, Roman R and Sfringeu S 2008 Real-time ultrasound elastography of the breast: state of the art *Med. Ultrason.* **10** 73–82
Corpechot C, Carrat F, Poujol-Robert A, Gaouar F, Wendum D, Chazouilleres O and Poupon R 2012 Noninvasive elastography-based assessment of liver fibrosis progression and prognosis in primary biliary cirrhosis *Hepatology* **56** 198–208
Corpechot C *et al* 2006 Assessment of biliary fibrosis by transient elastography in patients with PBC and PSC *Hepatology* **43** 1118–24
Correas J M, Tissier A M, Khairoune A, Vassiliu V, Mejean A, Helenon O, Memo R and Barr R G 2015 Prostate cancer: diagnostic performance of real-time shear-wave elastography *Radiology* **275** 280–9

Correia M, Deffieux T, Chatelin S, Provost J, Tanter M and Pernot M 2018 3D elastic tensor imaging in weakly transversely isotropic soft tissues *Phys. Med. Biol.* **63** 155005
Cosgrove D, Barr R, Bojunga J, Cantisani V, Chammas M C, Dighe M, Vinayak S, Xu J M and Dietrich C F 2017 WFUMB guidelines and recommendations on the clinical use of ultrasound elastography: part 4. Thyroid *Ultrasound Med. Biol.* **43** 4–26
Cosgrove D *et al* 2013 EFSUMB guidelines and recommendations on the clinical use of ultrasound elastography. Part 2: clinical applications *Ultraschall Med.* **34** 238–53
Couade M, Pernot M, Messas E, Bel A, Ba M, Hagege A, Fink M and Tanter M 2011 *in vivo* quantitative mapping of myocardial stiffening and transmural anisotropy during the cardiac cycle *IEEE Trans. Med. Imaging* **30** 295–305
Cox M and Rogers P H 1987 Automated noninvasive motion measurement of auditory organs in fish using ultrasound *J. Vib. Acoust.* **109** 55–59
Crecea V, Ahmad A and Boppart S A 2013 Magnetomotive optical coherence elastography for microrheology of biological tissues *J. Biomed. Opt.* **18** 121504
Cvijic M *et al* 2020 Can myocardial stiffness measurements distinguish the underlying pathology in hearts with thick walls? A shear wave imaging study using ultra-high frame rate echocardiography *Eur. Heart J-Cardiovasc. Imaging* **21** 417
de Araujo Neto J M 2020 Shear-wave dispersion slope: do we have the tool for detecting necroinflammation? *Radiology* **294** 483–4
De Jong P G M, Arts T, Hoeks A P G and Reneman R S 1990 Determination of tissue motion velocity by correlation interpolation of pulsed ultrasonic echo signals *Ultrason. Imaging* **12** 84–98
de Korte C L and van der Steen A F W 2002 Intravascular ultrasound elastography: an overview *Ultrasonics* **40** 859–65
de Korte C L, van der Steen A F W, Céspedes E I and Pasterkamp G 1998 Intravascular ultrasound elastography in human arteries: initial experience in vitro *Ultrasound Med. Biol.* **24** 401–8
Deffieux T, Gennisson J L, Bousquet L, Corouge M S C, Amroun D, Tripon S, Terris B, Mallet V, Tanter M and Pol S 2014 Investigating liver stiffness and viscosity for fibrosis, steatosis and activity staging using shear wave elastography *J. Hepatol.* **62** 317–24
Deffieux T, Gennisson J L, Tanter M and Fink M 2008 Assessment of the mechanical properties of the musculoskeletal system using 2D and 3D very high frame rate ultrasound *IEEE Trans. Ultrason. Ferroelectr. Freq. Control* **55** 2177–90
Deffieux T, Montaldo G, Tanter M and Fink M 2009 Shear wave spectroscopy for *in vivo* quantification of human soft tissues visco-elasticity *IEEE Trans. Med. Imaging* **28** 313–22
Degos F, Perez P, Roche B, Mahmoudi A, Asselineau J, Voitot H, Bedossa P and group F s 2010 Diagnostic accuracy of FibroScan and comparison to liver fibrosis biomarkers in chronic viral hepatitis: a multicenter prospective study (the FIBROSTIC study) *J. Hepatol.* **53** 1013–21
Dickinson R J and Hill C R 1982 Measurement of soft tissue motion using correlation between A-scans *Ultrasound Med. Biol.* **8** 263–71
Dong F J, Li M, Jiao Y, Xu J F, Xiong Y, Zhang L, Luo H and Ding Z M 2015 Acoustic radiation force impulse imaging for detecting thyroid nodules: a systematic review and pooled meta-analysis *Med. Ultrason.* **17** 192–9
Dord J F, Goenezen S, Oberai A A, Barbone P E, Jiang J, Hall T J and Pavan T 2019 Validation of quantitative linear and nonlinear compression elastography *Ultrasound Elastography for Biomedical Applications and Medicine*, ed I Z Nenadic *et al.* (Hoboken: John Wiley and Sons Ltd) ch 10, pp 131–42
Doyley M M 2012 Model-based elastography: a survey of approaches to the inverse elasticity problem *Phys. Med. Biol.* **57** R35-R73
Doyley M M 2018 Vascular and intravascular elastography *Ultrasound Elastography for Biomedical Applications and Medicine*, ed I Nenadic *et al.* (New York: Wiley) ch 12, pp 161–70
Drakonaki E E, Allen G M and Wilson D J 2009 Real-time ultrasound elastography of the normal Achilles tendon: reproducibility and pattern description *Clin. Radiol.* **64** 1196–202
Dramsch J S, Corte G, Amini H, Macbeth C and Lüthje M 2019 Including physics in eeep learning—an example from 4D seismic pressure saturation inversion *Conf. Proc., 81st EAGE Conf. and Exhibition 2019 Workshop Programme* (https://doi.org/10.3997/2214-4609.201901967)
Dresner M A, Rose G H, Rossman P J, Muthupillai R, Manduca A and Ehman R L 2001 Magnetic resonance elastography of skeletal muscle *J. Magn. Reson. Imaging* **13** 269–76
Dumont D, Behler R H, Nichols T C, Merricks E P and Gallippi C M 2006 ARFI imaging for noninvasive material characterization of atherosclerosis *Ultrasound Med. Biol.* **32** 1703–11
Durst C *et al* 2013 Optimal imaging of in vitro clot sonothrombolysis by MR-guided focused ultrasound *J. Neuroimaging* **23** 187–91
EASL and ALEH 2015 EASL-ALEH Clinical practice guidelines: non-invasive tests for evaluation of liver disease severity and prognosis *J. Hepatol.* **63** 237–64
Eby S F, Song P, Chen S, Chen Q, Greenleaf J F and An K N 2013 Validation of shear wave elastography in skeletal muscle *J. Biomech.* **46** 2381–7
Eisensher A, Schweg-Toffer E, Pelletier G and Jacquemard G 1983 La palpation echographique rythmee-echosismographie *J. Radiol.* **64** 225–61
Elegbe E C and Mcaleavey S A 2013 Single tracking location methods suppress speckle noise in shear wave velocity estimation *Ultrason. Imaging* **35** 109–25
Erkamp R Q, Emelianov S Y, Skovoroda A R and O'Donnell M 2004 Nonlinear elasticity imaging: theory and phantom study *IEEE Trans. Ultrason. Ferroelectr. Freq. Control* **51** 532–9
Eskandari H, Salcudean S E and Rohling R 2008 Viscoelastic parameter estimation based on spectral analysis *IEEE Trans. Ultrason. Ferroelectr. Freq. Control* **55** 1611–25
Fahey B J, Nightingale K R, Mcaleavey S A, Palmeri M L, Wolf P D and Trahey G E 2005 Acoustic radiation force impulse imaging of myocardial radiofrequency ablation: initial *in vivo* results *IEEE Trans. Ultrason. Ferroelectr.* **52** 631–41
Fahey B J, Nightingale K R, Stutz D L and Trahey G E 2004 Acoustic radiation force impulse imaging of thermally- and chemically-induced lesions in soft tissues: preliminary ex vivo results *Ultrasound Med. Biol.* **30** 321–8
Fatemi M and Greenleaf J F 1998 Ultrasound-stimulated vibro-acoustic spectrography *Science* **280** 82–85
Ferraioli G 2019 Review of liver elastography guidelines *J. Ultrasound Med.* **38** 9–14
Ferraioli G *et al* 2015 WFUMB guidelines and recommendations for clinical use of ultrasound elastography: part 3: liver *Ultrasound Med. Biol.* **41** 1161–79
Ferraioli G, Tinelli C, Dal Bello B, Zicchetti M, Filice G, Filice C and Liver Fibrosis Study G 2012 Accuracy of real-time shear wave elastography for assessing liver fibrosis in chronic hepatitis C: a pilot study *Hepatology* **56** 2125–33
Ferraioli G, Wong V W, Castera L, Berzigotti A, Sporea I, Dietrich C F, Choi B I, Wilson S R, Kudo M and Barr R G 2018 Liver ultrasound elastography: an update to the WFUMB guidelines and recommendations *Ultrasound Med. Biol.* **44** 2419–40

Ford M R, Dupps W J Jr. , Rollins A M, Sinha R A and Hu Z 2011 Method for optical coherence elastography of the cornea *J. Biomed. Opt.* **16** 016005
Foucher J, Chanteloup E, Vergniol J, Castera L, Le Bail B, Adhoute X, Bertet J, Couzigou P and de Ledinghen V 2006 Diagnosis of cirrhosis by transient elastography (FibroScan): a prospective study *Gut* **55** 403–8
Fowlkes J B, Emelianov S Y, Pipe J G, Skovoroda A R, Carson P L, Adler R S and Sarvazyan A P 1995 Magnetic-resonance imaging techniques for detection of elasticity variation *Med. Phys.* **22** 1771–8
Frank O 1899 Die grundform des arteriellen pulses *Zeitschrift Für Biologie* **37** 483–526
Fraquelli M, Rigamonti C, Casazza G, Conte D, Donato M F, Ronchi G and Colombo M 2007 Reproducibility of transient elastography in the evaluation of liver fibrosis in patients with chronic liver disease *Gut* **56** 968–73
Fu D, Levinson S F, Graceswki S M and Parker K J 2000 Non-invasive quantitative reconstruction of tissue elasticity using an iterative forward approach *Phys. Med. Biol.* **45** 1495–509
Fujii S, Yamakawa M, Kondo K, Namita T and Shiina T 2019 Evaluation of shear wave dispersion in hepatic viscoelastic models including fibrous structure *Japan. J. Appl Phys.* **58** SGGE07
Fung Y C 1981 *Biomechanics: Mechanical Properties of Living Tissues* (Berlin: Springer)
Gallot T, Catheline S, Roux P, Brum J, Benech N and Negreira C 2011 Passive elastography: shear-wave tomography from physiological-noise correlation in soft tissues *IEEE Trans. Ultrason. Ferroelectr. Freq. Control* **58** 1122–6
Ganne-Carrie N, Ziol M, de Ledinghen V, Douvin C, Marcellin P, Castera L, Dhumeaux D, Trinchet J C and Beaugrand M 2006 Accuracy of liver stiffness measurement for the diagnosis of cirrhosis in patients with chronic liver diseases *Hepatology* **44** 1511–7
Ge G R, Zvietcovich F, Rolland J P, Mestre H, Giannetto M, Nedergaard M and Parker K J 2019 A preliminary study on using reverberant shear wave fields in optical coherence elastography to examine mice brain ex vivo *SPIE BiOS* (SPIE) (https://doi.org/10.1117/12.2516039)
Gennisson J L, Catheline S, Chaffai S and Fink M 2003 Transient elastography in anisotropic medium: application to the measurement of slow and fast shear wave speeds in muscles *J. Acoust. Soc. Am.* **114** 536–41
Gennisson J L, Deffieux T, Mace E, Montaldo G, Fink M and Tanter M 2010 Viscoelastic and anisotropic mechanical properties of *in vivo* muscle tissue assessed by supersonic shear imaging *Ultrasound Med. Biol.* **36** 789–801
Gennisson J L, Provost J, Deffieux T, Papadacci C, Imbault M, Pernot M and Tanter M 2015 4D ultrafast shear-wave imaging *IEEE Trans. Ultrason. Ferroelectr. Freq. Control* **62** 1059–65
Gennisson J L, Renier M, Catheline S, Barriere C, Bercoff J, Tanter M and Fink M 2007 Acoustoelasticity in soft solids: assessment of the nonlinear shear modulus with the acoustic radiation force *J. Acoust. Soc. Am.* **122** 3211–9
Glaser K J, Manduca A and Ehman R L 2012 Review of MR elastography applications and recent developments *J. Magn. Reson. Imaging* **36** 757–74
Goenezen S, Dord J F, Sink Z, Barbone P E, Jiang J, Hall T J and Oberai A A 2012 Linear and nonlinear elastic modulus imaging: an application to breast cancer diagnosis *IEEE Trans. Med. Imaging* **31** 1628–37
Goswami S, Ahmed R, Doyley M M and Mcaleavey S A 2019a Nonlinear shear modulus estimation with bi-axial motion registered local strain *IEEE Trans. Ultrason. Ferroelectr. Freq. Control* **66** 1292–303
Goswami S, Khan S, Ahmed R, Doyley M M and Mcaleavey S A 2019b Deformation independent non-linearity estimation: studies and implementation in ultrasound shear wave elastography *2019 IEEE Int. Ultrasonics Symp. (IUS)* pp 217–20
Graff K F 1975 *Wave Motion in Elastic Solids* (Oxford: Clarendon)
Green M A, Geng G, Qin E, Sinkus R, Gandevia S C and Bilston L E 2013 Measuring anisotropic muscle stiffness properties using elastography *NMR Biomed.* **26** 1387–94
Greenleaf J F, Fatemi M and Insana M 2003 Selected methods for imaging elastic properties of biological tissues *Annu. Rev. Biomed. Eng.* **5** 57–78
Gros C M, Dale G and Gairand B 1978 Breast echography: criteria of malignancy and results *Recent Advances in Ultrasound Diagnosis*, ed A Kurjak (Amsterdam: Excerpta Medica) pp 292–8
Guan G, Li C, Ling Y, Yang Y, Vorstius J B, Keatch R P, Wang R K and Huang Z 2013 Quantitative evaluation of degenerated tendon model using combined optical coherence elastography and acoustic radiation force method *J. Biomed. Opt.* **18** 111417
Guyer P B, Dewbury K C, Warwick D, Smallwood J and Taylor I 1986 Direct contact B-scan ultrasound in the diagnosis of solid breast masses *Clin. Radiol.* **37** 451–8
Guzina B B, Dontsov E V, Urban M W and Fatemi M 2015 The 'sixth sense' of ultrasound: probing nonlinear elasticity with acoustic radiation force *Phys. Med. Biol.* **60** 3775–94
Hah Z, Hazard C, Mills B, Barry C, Rubens D and Parker K 2012 Integration of crawling waves in an ultrasound imaging system. Part 2: signal processing and applications *Ultrasound Med. Biol.* **38** 312–23
Hall T J *et al.* 2013 RSNA/QIBA: shear wave speed as a biomarker for liver fibrosis staging *2013 IEEE Int. Ultrasonics Symp. (IUS)* pp 397–400
Hall T J, Zhu Y and Spalding C S 2003 *in vivo* real-time freehand palpation imaging *Ultrasound Med. Biol.* **29** 427–35
Han Z, Li J, Singh M, Wu C, Liu C H, Raghunathan R, Aglyamov S R, Vantipalli S, Twa M D and Larin K V 2017 Optical coherence elastography assessment of corneal viscoelasticity with a modified Rayleigh-Lamb wave model *J. Mech. Behav. Biomed. Mater.* **66** 87–94
Hazard C, Hah Z, Rubens D and Parker K 2012 Integration of crawling waves in an ultrasound imaging system Part 1: system and design considerations *Ultrasound Med. Biol.* **38** 296–311
Helfenstein-Didier C, Andrade R J, Brum J, Hug F, Tanter M, Nordez A and Gennisson J L 2016 *in vivo* quantification of the shear modulus of the human Achilles tendon during passive loading using shear wave dispersion analysis *Phys. Med. Biol.* **61** 2485–96
Hetzer S, Hirsch S, Braun J, Sack I and Weygandt M 2019 Viscoelasticity of striatal brain areas reflects variations in body mass index of lean to overweight male adults *Brain Imaging Behav.* **14** 2477–87
Hill C R, Kratochwil A, Biology E.F. o S f U i M a and Corporation P 1981 *Medical ultrasonic images: formation, display, recording, and perception: based on papers presented at a European symposium held in Brussels*, (January 31-February 1, 1981) (Amsterdam Excerpta Medica) vol 541 pp 292–8
Hirsch S, Braun J and Sack I 2017 *Magnetic Resonance Elastography: Physical Background and Medical Applications* (Weinheim: Wiley-VCH)
Hirsch S, Guo J, Reiter R, Papazoglou S, Kroencke T, Braun J and Sack I 2014 MR elastography of the liver and the spleen using a piezoelectric driver, single-shot wave-field acquisition, and multifrequency dual parameter reconstruction *Magn. Reson Med.* **71** 267–77

Hoerig C, Ghaboussi J and Insana M F 2017 An information-based machine learning approach to elasticity imaging *Biomech. Model Mechanobiol.* **16** 805–22
Hoerig C, Ghaboussi J and Insana M F 2019 Data-driven elasticity imaging using cartesian neural network constitutive models and the autoprogressive method *IEEE Trans. Med. Imaging* **38** 1150–60
Hoffmeister B K, Handley S M, Wickline S A and Miller J G 1996 Ultrasonic determination of the anisotropy of Young's modulus of fixed tendon and fixed myocardium *J. Acoust. Soc. Am.* **100** 3933–40
Holen J, Waag R C and Gramiak R 1985 Representations of rapidly oscillating structures on the Doppler display *Ultrasound Med. Biol.* **11** 267–72
Hollman K W, O'Donnell M and Erpelding T N 2007 Mapping elasticity in human lenses using bubble-based acoustic radiation force *Exp. Eye Res.* **85** 890–3
Honarvar M, Lobo J, Mohareri O, Salcudean S E and Rohling R 2015 Direct vibro-elastography FEM inversion in Cartesian and cylindrical coordinate systems without the local homogeneity assumption *Phys. Med. Biol.* **60** 3847–68
Honarvar M, Sahebjavaher R S, Salcudean S E and Rohling R 2012 Sparsity regularization in dynamic elastography *Phys. Med. Biol.* **57** 5909–27
Hooke R 1678 *Lectures De Potentia Restitutiva (Trans: Of Spring: Explaining the Power of Springing Bodies: To Which are Added Some Collections)* (London: John Martyn)
Hossain M M, Moore C J and Gallippi C M 2017 Acoustic radiation force impulse (ARFI)-induced peak displacements reflect degree of anisotropy in transversely isotropic elastic materials *IEEE Trans. Ultrason. Ferroelectr. Freq. Control* **64** 989–1001
Hossain M M *et al* 2018 Evaluating renal transplant status using viscoelastic response (VisR) ultrasound *Ultrasound Med. Biol.* **44** 1573–84
Hoyt K, Kneezel T, Castaneda B and Parker K J 2008 Quantitative sonoelastography for the *in vivo* assessment of skeletal muscle viscoelasticity *Phys. Med. Biol.* **53** 4063–80
Huang Q and Zeng Z 2017 A review on real-time 3D ultrasound imaging technology *Biomed. Res. Int.* **2017** 6027029
Huang Y P, Zheng Y P, Wang S Z, Chen Z P, Huang Q H and He Y H 2009 An optical coherence tomography (OCT)-based air jet indentation system for measuring the mechanical properties of soft tissues *Meas. Sci. Technol.* **20** 1–11
ITEC 2002 *Proc. of the First Int. Conf. on the Measurement and Imaging of Tissue Elasticity* (available at: www.elasticityconference.org/prior_conf/2002/2002Proceedings.pdf)
Itoh A, Ueno E, Tohno E, Kamma H, Takahashi H, Shiina T, Yamakawa M and Matsumura T 2006 Breast disease: clinical application of US elastography for diagnosis *Radiology* **239** 341–50
Jenkyn T R, Ehman R L and An K N 2003 Noninvasive muscle tension measurement using the novel technique of magnetic resonance elastography (MRE) *J. Biomech.* **36** 1917–21
Kamoi K, Okihara K, Ochiai A, Ukimura O, Mizutani Y, Kawauchi A and Miki T 2008 The utility of transrectal real-time elastography in the diagnosis of prostate cancer *Ultrasound Med. Biol.* **34** 1025–32
Kanai H 2005 Propagation of spontaneously actuated pulsive vibration in human heart wall and *in vivo* viscoelasticity estimation *IEEE Trans. Ultrason. Ferroelectr. Freq. Control* **52** 1931–42
Kemp W, Levy M, Weltman M, Lubel J and Australian Liver A 2015 Australian Liver Association (ALA) expert consensus recommendations for the use of transient elastography in chronic viral hepatitis *J. Gastroenterol. Hepatol.* **30** 453–62
Kennedy B F, Liang X, Adie S G, Gerstmann D K, Quirk B C, Boppart S A and Sampson D D 2011 *in vivo* three-dimensional optical coherence elastography *Opt. Express* **19** 6623–34
Kennedy K M, Kennedy B F, Mclaughlin R A and Sampson D D 2012 Needle optical coherence elastography for tissue boundary detection *Opt. Lett.* **37** 2310–2
Kirkpatrick S J 2003 Optical assessment of tissue mechanics: acousto-optical elastography of skin *Saratov Fall Meeting 2002: Optical Technologies in Biophysics and Medicine IV Proc. SPIE* 5068 (Accessed: 13 October 2003) (https://doi.org/10.1117/12.518636)
Klatt D, Hamhaber U, Asbach P, Braun J and Sack I 2007 Noninvasive assessment of the rheological behavior of human organs using multifrequency MR elastography: a study of brain and liver viscoelasticity *Phys. Med. Biol.* **52** 7281–94
Klatt D, Papazoglou S, Braun J and Sack I 2010 Viscoelasticity-based MR elastography of skeletal muscle *Phys. Med. Biol.* **55** 6445–59
Knutsson H, Westin C and Granlund G 1994 Local multiscale frequency and bandwidth estimation *Proc. of 1st Int. Conf. on Image Processing* vol 1 pp 36–40
Konig K, Scheipers U, Pesavento A, Lorenz A, Ermert H and Senge T 2005 Initial experiences with real-time elastography guided biopsies of the prostate *J. Urol.* **174** 115–7
Konofagou E E, D'Hooge J and Ophir J 2002 Myocardial elastography–a feasibility study *in vivo Ultrasound Med. Biol.* **28** 475–82
Konofagou E E and Hynynen K 2003 Localized harmonic motion imaging: theory, simulations and experiments *Ultrasound Med. Biol.* **29** 1405–13
Koo T K, Cohen J H and Zheng Y 2011 A mechano-acoustic indentor system for *in vivo* measurement of nonlinear elastic properties of soft tissue *J. Manipulative Physiol. Ther.* **34** 584–93
Koo T K, Guo J Y, Cohen J H and Parker K J 2013 Relationship between shear elastic modulus and passive muscle force: an ex-vivo study *J. Biomech.* **46** 2053–9
Koo T K, Guo J Y, Cohen J H and Parker K J 2014 Quantifying the passive stretching response of human tibialis anterior muscle using shear wave elastography *Clin. Biomech.* **29** 33–39
Korukonda S, Nayak R, Carson N, Schifitto G, Dogra V and Doyley M M 2013 Noninvasive vascular elastography using plane-wave and sparse-array imaging *IEEE Trans. Ultrason. Ferroelectr. Freq. Control* **60** 332–42
Kreft B, Tzschatzsch H, Schrank F, Bergs J, Streitberger K J, Waldchen S, Hetzer S, Braun J and Sack I 2020 Time-resolved response of cerebral stiffness to hypercapnia in humans *Ultrasound Med. Biol.* **46** 936–43
Krouskop T A, Dougherty D R and Vinson F S 1987 A pulsed Doppler ultrasonic system for making noninvasive measurements of the mechanical properties of soft tissue *J. Rehabil. Res. Dev.* **24** 1–8
Kudo M *et al* 2013 JSUM ultrasound elastography practice guidelines: liver *J. Med. Ultrason* **40** 325–57
Kumar V, Denis M, Gregory A, Bayat M, Mehrmohammadi M, Fazzio R, Fatemi M and Alizad A 2018 Viscoelastic parameters as discriminators of breast masses: initial human study results *PloS One* **13** e0205717
Landau L D and Lifschitz E M 1970 *Theory of Elasticity* Vol. 7 (Oxford: Pergamon)
Langdon J H, Elegbe E, Gonzalez R S, Osapoetra L, Ford T and Mcaleavey S A 2017 Measurement of liver stiffness using shear wave elastography in a rat model: factors impacting stiffness measurement with multiple- and single-tracking-location techniques *Ultrasound Med. Biol.* **43** 2629–39

Larin K V and Sampson D D 2017 Optical coherence elastography—OCT at work in tissue biomechanics [Invited] *Biomed. Opt. Express* **8** 1172–202
Lee D H, Lee J Y, Bae J S, Yi N J, Lee K W, Suh K S, Kim H, Lee K B and Han J K 2019 Shear-wave dispersion slope from US shear-wave elastography: detection of allograft damage after liver transplantation *Radiology* **293** 327–33
Lee F Jr. , Bronson J P, Lerner R M, Parker K J, Huang S R and Roach D J 1991 Sonoelasticity imaging: results in in vitro tissue specimens *Radiology* **181** 237–9
Lee R T, Richardson S G, Loree H M, Grodzinsky A J, Gharib S A, Schoen F J and Pandian N 1992 Prediction of mechanical properties of human atherosclerotic tissue by high-frequency intravascular ultrasound imaging. An in vitro study *Arterioscler. Thromb.* **12** 1–5
Lee W N, Larrat B, Pernot M and Tanter M 2012 Ultrasound elastic tensor imaging: comparison with MR diffusion tensor imaging in the myocardium *Phys. Med. Biol.* **57** 5075–95
Lerner R M, Huang S R and Parker K J 1990 'Sonoelasticity' images derived from ultrasound signals in mechanically vibrated tissues *Ultrasound Med. Biol.* **16** 231–9
Lerner R M and Parker K J 1987 Sonoelasticity images derived from ultrasound signals in mechanically vibrated targets *Seventh European Communities Workshop*, ed J Tjissen (Nijmegen: The Netherlands)
Lerner R M, Parker K J, Holen J, Gramiak R and Waag R C 1988 Sonoelasticity: medical elasticity images derived from ultrasound signals in mechanically vibrated targets *Acoust. Imaging* **16** 317–27
Levinson S F 1987 Ultrasound propagation in anisotropic soft tissues: the application of linear elastic theory *J. Biomech.* **20** 251–60
Levinson S F, Shinagawa M and Sato T 1995 Sonoelastic determination of human skeletal-muscle elasticity *J. Biomech.* **28** 1145–54
Li C, Guan G, Reif R, Huang Z and Wang R K 2012 Determining elastic properties of skin by measuring surface waves from an impulse mechanical stimulus using phase-sensitive optical coherence tomography *J. R. Soc. Interface* **9** 831–41
Li J, Wang S, Manapuram R K, Singh M, Menodiado F M, Aglyamov S, Emelianov S, Twa M D and Larin K V 2013 Dynamic optical coherence tomography measurements of elastic wave propagation in tissue-mimicking phantoms and mouse cornea *in vivo* *J. Biomed. Opt.* **18** 121503
Li J, Wang S, Singh M, Aglyamov S, Emelianov S, Twa M D and Larin K V 2014 Air-pulse OCE for assessment of age-related changes in mouse cornea*in vivo Laser Phys. Lett.* **11** 065601
Li W 2018 Machine learning in acoustic applications with wave physics models, a tutorial *J. Acoust. Soc. Am.* **144** 1683
Liang X, Adie S G, John R and Boppart S A 2010 Dynamic spectral-domain optical coherence elastography for tissue characterization *Opt. Express* **18** 14183–90
Liang X, Oldenburg A L, Crecea V, Chaney E J and Boppart S A 2008 Optical micro-scale mapping of dynamic biomechanical tissue properties *Opt. Express* **16** 11052–65
Lim J K, Flamm S L, Singh S, Falck-Ytter Y T and Clinical Guidelines Committee of the American Gastroenterological A 2017 American Gastroenterological Association Institute guideline on the role of elastography in the dvaluation of liver fibrosis *Gastroenterology* **152** 1536–43
Liu B, Liang J, Zheng Y, Xie X, Huang G, Zhou L, Wang W and Lu M 2015a Two-dimensional shear wave elastography as promising diagnostic tool for predicting malignant thyroid nodules: a prospective single-centre experience *Eur. Radiol.* **25** 624–34
Liu B, Liang J, Zhou L, Lu Y, Zheng Y, Tian W and Xie X 2015b Shear wave elastography in the diagnosis of thyroid nodules with coexistent chronic autoimmune Hashimoto's thyroiditis *Otolaryngol. Head Neck Surg.: Off J. Am. Acad. Otolaryngol. Head Neck Surg.* **153** 779–85
Liu B J *et al* 2015c Quantitative shear wave velocity measurement on acoustic radiation force impulse elastography for differential diagnosis between benign and malignant thyroid nodules: a meta-analysis *Ultrasound Med. Biol.* **41** 3035–43
Liu B J, Xu H X, Zhang Y F, Xu J M, Li D D, Bo X W, Li X L, Guo L H, Xu X H and Qu S 2015d Acoustic radiation force impulse elastography for differentiation of benign and malignant thyroid nodules with concurrent Hashimoto's thyroiditis *Med. Oncol.* **32** 50
Liu Y, Royston T J, Klatt D and Lewandowski E D 2016 Cardiac MR elastography of the mouse: initial results *Magn. Reson Med.* **76** 1879–86
Low G, Kruse S A and Lomas D J 2016 General review of magnetic resonance elastography *World J. Radiol.* **8** 59–72
Lupsor M, Badea R, Stefanescu H, Grigorescu M, Sparchez Z, Serban A, Branda H, Iancu S and Maniu A 2008 Analysis of histopathological changes that influence liver stiffness in chronic hepatitis C. Results from a cohort of 324 patients *J. Gastrointestinal Liver Dis.* **17** 155–63
Malczewski K 2020 Rapid diffusion weighted imaging with enhanced resolution *Appl. Magn. Reson.* **51** 221–39
Maleke C and Konofagou E E 2008 Harmonic motion imaging for focused ultrasound (HMIFU): a fully integrated technique for sonication and monitoring of thermal ablation in tissues *Phys. Med. Biol.* **53** 1773–93
Manduca A, Oliphant T E, Dresner M A, Mahowald J L, Kruse S A, Amromin E, Felmlee J P, Greenleaf J F and Ehman R L 2001 Magnetic resonance elastography: non-invasive mapping of tissue elasticity *Med. Image Anal.* **5** 237–54
Markowski W 1991 *Machine and method for uniaxial mechanical material testing* patent number 5005424, USPTO
Mcaleavey S and Menon M 2007 7B-3 Direct estimation of shear modulus using spatially modulated acoustic radiation force impulses *Ultrasonics Symp. 2007 IEEE* pp 558–61
Mcaleavey S A, Menon M and Orszulak J 2007 Shear-modulus estimation by application of spatially-modulated impulsive acoustic radiation force *Ultrason. Imaging* **29** 87–104
Mcaleavey S A, Parker K J, Ormachea J, Wood R W, Stodgell C J, Katzman P J, Pressman E K and Miller R K 2016 Shear wave elastography in the living, perfused, post-delivery placenta *Ultrasound Med. Biol.* **42** 1282–8
Mehrabian H, Campbell G and Samani A 2010 A constrained reconstruction technique of hyperelasticity parameters for breast cancer assessment *Phys. Med. Biol.* **55** 7489–508
Mercado K P, Langdon J, Helguera M, Mcaleavey S A, Hocking D C and Dalecki D 2015 Scholte wave generation during single tracking location shear wave elasticity imaging of engineered tissues *J. Acoust. Soc. Am.* **138** EL138-EL44
Moore C J, Hossain M D M and Gallippi C M 2017 2D ARFI and viscoelastic response (VisR) anisotropy imaging in skeletal muscle. *2017 IEEE Int. Ultrasonics Symp. (IUS)* pp 1–4
Mould A, Abbott S and Welman C J 2019 HELLP syndrome: an ultrasound case of geographically altered liver parenchymal echogenicity with shear wave elastography, shear wave dispersion and attenuation imaging correlation *Australas. J. Ultrasound Med.* **23** 149–55
Muller M, Gennisson J L, Deffieux T, Tanter M and Fink M 2009 Quantitative viscoelasticity mapping of human liver using supersonic shear imaging: preliminary *in vivo* feasibility study *Ultrasound Med. Biol.* **35** 219–29
Mulligan J A, Untracht G R, Chandrasekaran S N, Brown C N and Adie S G 2016 Emerging approaches for high-resolution imaging of tissue biomechanics with optical coherence elastography *IEEE J. Sel. Top. Quant.* **22** 246–65

Muthupillai R, Lomas D J, Rossman P J, Greenleaf J F, Manduca A and Ehman R L 1995 Magnetic-resonance elastography by direct visualization of propagating acoustic strain waves *Science* **269** 1854–7
Nahon P, Kettaneh A, Tengher-Barna I, Ziol M, de Ledinghen V, Douvin C, Marcellin P, Ganne-Carrie N, Trinchet J C and Beaugrand M 2008 Assessment of liver fibrosis using transient elastography in patients with alcoholic liver disease *J. Hepatol.* **49** 1062–8
Nakashima K and Moriya T 2013 Comprehensive ultrasound diagnosis for intraductal spread of primary breast cancer *Breast Cancer* **20** 3–12
Nakashima K, Shiina T, Sakurai M, Enokido K, Endo T, Tsunoda H, Takada E, Umemoto T and Ueno E 2013 JSUM ultrasound elastography practice guidelines: breast *J. Med. Ultrason* **40** 359–91
Napoli M E, Freitas C, Goswami S, Mcaleavey S, Doyley M and Howard T M 2018 Hybrid rorce/velocity control with compliance estimation via strain elastography for robot assisted ultrasound screening *2018 7th IEEE Int. Conf. on Biomedical Robotics and Biomechatronics (Biorob)* pp 1266–73
Nazari N and Barbone P 2018 Shear wave speed in pressurized soft tissue *J. Mech. Phys. Solids* **119** 60–72
Nenadic I, Urban M W, Qiang B, Chen S and Greenleaf J 2013 Model-free quantification of shear wave velocity and attenuation in tissues and its *in vivo* application *J. Acoust. Soc. Am.* **134** 4011
Nenadic I Z, Qiang B, Urban M W, Zhao H, Sanchez W, Greenleaf J F and Chen S 2017 Attenuation measuring ultrasound shearwave elastography and *in vivo* application in post-transplant liver patients *Phys. Med. Biol.* **62** 484
Nenadic I Z, Urban M, Gennisson J, Bernal M, Tanter M and Greenleaf J 2019 *Ultrasound Elastography for Biomedical Applications and Medicine* (Hoboken: John Wiley and Sons Ltd.)
Nenadic I Z, Urban M W, Mitchell S A and Greenleaf J F 2011 Lamb wave dispersion ultrasound vibrometry (LDUV) method for quantifying mechanical properties of viscoelastic solids *Phys. Med. Biol.* **56** 2245–64
Nenadic I Z, Urban M W, Pislaru C, Escobar D, Vasconcelos L and Greenleaf J F 2018 *in vivo* open- and closed-chest measurements of left-ventricular myocardial viscoelasticity using lamb wave dispersion ultrasound vibrometry (LDUV): a feasibility Study *Biomed. Phys. Eng. Express* **4** 047001
Nguyen-Khac E *et al* 2008 Assessment of asymptomatic liver fibrosis in alcoholic patients using fibroscan: prospective comparison with seven non-invasive laboratory tests *Aliment. Pharmacol. Ther.* **28** 1188–98
Nightingale K, Nightingale R, Palmeri M and Trahey G 1999 Finite element analysis of radiation force induced tissue motion with experimental validation. In: *Ultrasonics Symp., 1999 Proc. 1999 IEEE* vol 2 pp 1319–23
Nightingale K R, Palmeri M L, Nightingale R W and Trahey G E 2001 On the feasibility of remote palpation using acoustic radiation force *J. Acoust. Soc. Am.* **110** 625–34
Nightingale K R, Rouze N C, Rosenzweig S J, Wang M H, Abdelmalek M F, Guy C D and Palmeri M L 2015 Derivation and analysis of viscoelastic properties in human liver: impact of frequency on fibrosis and steatosis staging *IEEE Trans. Ultrason. Ferroelectr. Freq. Control* **62** 165–75
Ning C P, Jiang S Q, Zhang T, Sun L T, Liu Y J and Tian J W 2012 The value of strain ratio in differential diagnosis of thyroid solid nodules *Eur. J. Radiol.* **81** 286–91
Nyborg W L M 1965 11—Acoustic Streaming *Physical Acoustics*, ed W P Mason (New York: Academic) pp 265–331
O'Donnell M, Skovoroda A R, Shapo B M and Emelianov S Y 1994 Internal displacement and strain imaging using ultrasonic speckle tracking *IEEE Trans. Ultrason. Ferroelectr.* **41** 314–25
O'Hagan J J and Samani A 2009 Measurement of the hyperelastic properties of 44 pathological ex vivo breast tissue samples *Phys. Med. Biol.* **54** 2557–69
Oestreicher H L 1951 Field and impedance of an oscillating sphere in a viscoelastic medium with an application to biophysics *J. Acoust. Soc. Am.* **23** 707–14
Ophir J, Cespedes I, Ponnekanti H, Yazdi Y and Li X 1991 Elastography: a quantitative method for imaging the elasticity of biological tissues *Ultrason. Imaging* **13** 111–34
Ormachea J, Castaneda B and Parker K J 2018 Shear wave speed estimation using reverberant shear wave fields: implementation and feasibility studies *Ultrasound Med. Biol.* **44** 963–77
Ormachea J, Lavarello R J, Mcaleavey S A, Parker K J and Castaneda B 2016 Shear wave speed measurements using crawling wave sonoelastography and single tracking location shear wave elasticity imaging for tissue characterization *IEEE Trans. Ultrason. Ferroelectr. Freq. Control* **63** 1351–60
Ormachea J, Parker K J and Barr R G 2019 An initial study of complete 2D shear wave dispersion images using a reverberant shear wave field *Phys. Med. Biol.* **64** 145009
Osapoetra L O, Watson D M and Mcaleavey S A 2019 Intraocular pressure-dependent corneal elasticity measurement using high-frequency ultrasound *Ultrason. Imaging* **41** 251–70
Pallwein L, Mitterberger M, Struve P, Horninger W, Aigner F, Bartsch G, Gradl J, Schurich M, Pedross F and Frauscher F 2007a Comparison of sonoelastography guided biopsy with systematic biopsy: impact on prostate cancer detection *Eur. Radiol.* **17** 2278–85
Pallwein L, Mitterberger M, Struve P, Pinggera G, Horninger W, Bartsch G, Aigner F, Lorenz A, Pedross F and Frauscher F 2007b Real-time elastography for detecting prostate cancer: preliminary experience *BJU Int.* **100** 42–46
Palmeri M *et al* 2015 RSNA QIBA ultrasound shear wave speed Phase II phantom study in viscoelastic media *Ultrasonics Symp. (IUS), 2015 IEEE Int.* pp 1–4
Palmeri M L and Nightingale K R 2004 On the thermal effects associated with radiation force imaging of soft tissue *IEEE Trans. Ultrason. Ferroelectr. Freq. Control* **51** 551–65
Papadacci C, Bunting E A, Wan E Y, Nauleau P and Konofagou E E 2017 3D myocardial elastography *in vivo IEEE Trans. Med. Imaging* **36** 618–27
Papazoglou S, Braun J, Hamhaber U and Sack I 2005 Two-dimensional waveform analysis in MR elastography of skeletal muscles *Phys. Med. Biol.* **50** 1313–25
Park A Y, Son E J, Han K, Youk J H, Kim J A and Park C S 2015 Shear wave elastography of thyroid nodules for the prediction of malignancy in a large scale study *Eur. J. Radiol.* **84** 407–12
Parker K J 2014 Real and causal hysteresis elements *J. Acoust. Soc. Am.* **135** 3381–9
Parker K J 2017 Are rapid changes in brain elasticity possible? *Phys. Med. Biol.* **62** 7425–39
Parker K J, Doyley M M and Rubens D J 2011 Imaging the elastic properties of tissue: the 20 year perspective *Phys. Med. Biol.* **56** R1–R29
Parker K J, Huang S R, Lerner R M, Lee F Jr. , Rubens D and Roach D 1993 Elastic and ultrasonic properties of the prostate *Ultrasonics Symp., 1993 Proc., IEEE 1993* vol 2 pp 1035–8

Parker K J, Huang S R, Musulin R A and Lerner R M 1990 Tissue response to mechanical vibrations for 'sonoelasticity imaging' *Ultrasound Med. Biol.* **16** 241–6
Parker K J and Lerner R M 1992 Sonoelasticity of organs: shear waves ring a bell *J. Ultrasound Med.* **11** 387–92
Parker K J, Ormachea J, Drage M G, Kim H and Hah Z 2018a The biomechanics of simple steatosis and steatohepatitis *Phys. Med. Biol.* **63** 105013
Parker K J, Ormachea J and Hah Z 2018b Group versus phase velocity of shear waves in soft tissues *Ultrason. Imaging* **40** 343–56
Parker K J, Ormachea J, Will S and Hah Z 2018c Analysis of transient shear wave in lossy media *Ultrasound Med. Biol.* **44** 1504–15
Parker K J, Ormachea J, Zvietcovich F and Castaneda B 2017 Reverberant shear wave fields and estimation of tissue properties *Phys. Med. Biol.* **62** 1046–61
Parker K J, Partin A and Rubens D J 2015 What do we know about shear wave dispersion in normal and steatotic livers? *Ultrasound Med. Biol.* **41** 1481–7
Parker K J, Szabo T and Holm S 2019 Towards a consensus on rheological models for elastography in soft tissues *Phys. Med. Biol.* **64** 215012
Parker K J, Taylor L S, Gracewski S and Rubens D J 2005 A unified view of imaging the elastic properties of tissue *J. Acoust. Soc. Am.* **117** 2705–12
Patz S *et al* 2019 Imaging localized neuronal activity at fast time scales through biomechanics *Sci. Adv.* **5** eaav3816
Pengfei S, Heng Z, Manduca A, Urban M W, Greenleaf J F and Shigao C 2012 Comb-push ultrasound shear elastography (CUSE): a novel method for two-dimensional shear elasticity imaging of soft tissues *IEEE Trans. Med. Imaging* **31** 1821–32
Petitclerc L, Sebastiani G, Gilbert G, Cloutier G and Tang A 2017 Liver fibrosis: review of current imaging and MRI quantification techniques *J. Magn. Reson. Imaging* **45** 1276–95
Plewes D B, Betty I, Urchuk S N and Soutar I 1995 Visualizing tissue compliance with MR imaging *J. Magn. Reson. Imaging* **5** 733–8
Plewes D B, Bishop J, Samani A and Sciarretta J 2000 Visualization and quantification of breast cancer biomechanical properties with magnetic resonance elastography *Phys. Med. Biol.* **45** 1591–610
Provost J, Papadacci C, Arango J E, Imbault M, Fink M, Gennisson J L, Tanter M and Pernot M 2014 3D ultrafast ultrasound imaging *in vivo Phys. Med. Biol.* **59** L1–L13
Qi W, Chen R, Chou L, Liu G, Zhang J, Zhou Q and Chen Z 2012 Phase-resolved acoustic radiation force optical coherence elastography *J. Biomed. Opt.* **17** 110505
Qi W, Li R, Ma T, Kirk Shung K, Zhou Q and Chen Z 2014 Confocal acoustic radiation force optical coherence elastography using a ring ultrasonic transducer *Appl. Phys. Lett.* **104** 123702
Qi W, Li R, Ma T, Li J, Kirk Shung K, Zhou Q and Chen Z 2013 Resonant acoustic radiation force optical coherence elastography *Appl. Phys. Lett.* **103** 103704
Qin E C, Juge L, Lambert S A, Paradis V, Sinkus R and Bilston L E 2014 *in vivo* anisotropic mechanical properties of dystrophic skeletal muscles measured by anisotropic MR elastographic imaging: the mdx mouse model of muscular dystrophy *Radiology* **273** 726–35
Rabin C and Benech N 2019 Quantitative breast elastography from B-mode images *Med. Phys.* **46** 3001–12
Rago T *et al* 2007 Combined clinical, thyroid ultrasound and cytological features help to predict thyroid malignancy in follicular and Hupsilonrthle cell thyroid lesions: results from a series of 505 consecutive patients *Clin. Endocrinol.* **66** 13–20
Rago T and Vitti P 2008 Role of thyroid ultrasound in the diagnostic evaluation of thyroid nodules *Best Pract. Res. Clin. Endocrinol. Metab.* **22** 913–28
Rogowska J, Patel N, Plummer S and Brezinski M E 2006 Quantitative optical coherence tomographic elastography: method for assessing arterial mechanical properties *Br. J. Radiol.* **79** 707–11
Rosen D P and Jiang J 2019 A comparison of hyperelastic constitutive models applicable to shear wave elastography (SWE) data in tissue-mimicking materials *Phys. Med. Biol.* **64** 055014
Roux P, Sabra K G, Kuperman W A and Roux A 2005 Ambient noise cross correlation in free space: theoretical approach *J. Acoust. Soc. Am.* **117** 79–84
Royer D, Gennisson J L, Deffieux T and Tanter M 2011 On the elasticity of transverse isotropic soft tissues (L) *J. Acoust. Soc. Am.* **129** 2757–60
RSNA/QIBA 2012 Ultrasound SWS Biomarker CTTE (available at: http://qibawiki.rsna.org/index.php/Ultrasound_SWS_Biomarker_Ctte)
Rubin J M, Aglyamov S R, Wakefield T W, O'Donnell M and Emelianov S Y 2003 Clinical application of sonographic elasticity imaging for aging of deep venous thrombosis: preliminary findings *J. Ultrasound Med.* **22** 443–8
Sabbadini A, Caenen A, Vos H J, de Jong N and Verweij M D 2019 Modelling Lamb waves in the septal wall of the heart *J. Acoust. Soc. Am.* **146** 3070
Sabra K G, Conti S, Roux P and Kuperman W A 2007 Passive *in vivo* elastography from skeletal muscle noise *Appl. Phys. Lett.* **90** 194101
Sack I, Bernarding J and Braun J 2002 Analysis of wave patterns in MR elastography of skeletal muscle using coupled harmonic oscillator simulations *Magn. Reson Imaging* **20** 95–104
Samani A and Plewes D 2004 A method to measure the hyperelastic parameters of ex vivo breast tissue samples *Phys. Med. Biol.* **49** 4395–405
Samani A, Zubovits J and Plewes D 2007 Elastic moduli of normal and pathological human breast tissues: an inversion-technique-based investigation of 169 samples *Phys. Med. Biol.* **52** 1565–76
Sandrin L *et al* 2003 Transient elastography: a new noninvasive method for assessment of hepatic fibrosis *Ultrasound Med. Biol.* **29** 1705–13
Sarvazyan A and Hill C R 2004 *Physical Chemistry of the Ultrasound–tissue Interaction* (New York: Wiley)
Sarvazyan A P, Rudenko O V and Nyborg W L 2010 Biomedical applications of radiation force of ultrasound: historical roots and physical basis *Ultrasound Med. Biol.* **36** 1379–94
Sarvazyan A P, Rudenko O V, Swanson S D, Fowlkes J B and Emelianov S Y 1998 Shear wave elasticity imaging: a new ultrasonic technology of medical diagnostics *Ultrasound Med. Biol.* **24** 1419–35
Sarvazyan A P, Skovoroda A R, Emelianov S Y, Fowlkes J B, Pipe J G, Adler R S, Buxton R B and Carson P L 1995 Biophysical bases of elasticity imaging *Acoust. Imaging* **21** 223–40
Sasso M, Beaugrand M, de Ledinghen V, Douvin C, Marcellin P, Poupon R, Sandrin L and Miette V 2010 Controlled attenuation parameter (CAP): a novel VCTE guided ultrasonic attenuation measurement for the evaluation of hepatic steatosis: preliminary study and validation in a cohort of patients with chronic liver disease from various causes *Ultrasound Med. Biol.* **36** 1825–35
Schmitt C, Hadj Henni A and Cloutier G 2010 Ultrasound dynamic micro-elastography applied to the viscoelastic characterization of soft tissues and arterial walls *Ultrasound Med. Biol.* **36** 1492–503

Schmitt J 1998 OCT elastography: imaging microscopic deformation and strain of tissue *Opt. Express* **3** 199–211
Sebag F, Vaillant-Lombard J, Berbis J, Griset V, Henry J F, Petit P and Oliver C 2010 Shear wave elastography: a new ultrasound imaging mode for the differential diagnosis of benign and malignant thyroid nodules *J. Clin. Endocrinol. Metab.* **95** 5281–8
Selzo M R and Gallippi C M 2013 Viscoelastic response (VisR) imaging for assessment of viscoelasticity in Voigt materials *IEEE Trans. Ultrason. Ferroelectr. Freq. Control* **60** 2488–500
Serai S D, Obuchowski N A, Venkatesh S K, Sirlin C B, Miller F H, Ashton E, Cole P E and Ehman R L 2017 Repeatability of MR elastography of liver: a meta-analysis *Radiology* **285** 92–100
Sharma A C, Soo M S, Trahey G E and Nightingale K R 2004 Acoustic radiation force impulse imaging of *in vivo* breast masses *Ultrasonics Symp., 2004 IEEE* vol.1 pp 728–31
Sharma A K, Reis J, Oppenheimer D C, Rubens D J, Ormachea J, Hah Z and Parker K J 2019 Attenuation of shear waves in normal and steatotic livers *Ultrasound Med. Biol.* **45** 895–901
Shcherbakova D A *et al* 2014 Supersonic shear wave imaging to assess arterial nonlinear behavior and anisotropy: proof of principle via ex vivo testing of the horse aorta *Adv. Mech. Eng.* **6** 272586
Shiha G *et al* 2017 Asian-Pacific association for the study of the liver (APASL) consensus guidelines on invasive and non-invasive assessment of hepatic fibrosis: a. 2016. update *Hepatol Int.* **11** 1–30
Shiina T 2013 JSUM ultrasound elastography practice guidelines: basics and terminology *J. Med. Ultrason* **40** 309–23
Shiina T *et al* 2015 WFUMB guidelines and recommendations for clinical use of ultrasound elastography: part 1: basic principles and terminology *Ultrasound Med. Biol.* **41** 1126–47
Shinohara M, Sabra K, Gennisson J L, Fink M and Tanter M 2010 Real-time visualization of muscle stiffness distribution with ultrasound shear wave imaging during muscle contraction *Muscle Nerve* **42** 438–41
Simon E G, Calle S, Perrotin F and Remenieras J P 2018 Measurement of shear wave speed dispersion in the placenta by transient elastography: A preliminary *ex vivo* study *PloS One* **13** e0194309
Singh S *et al* 2016 Magnetic resonance elastography for staging liver fibrosis in non-alcoholic fatty liver disease: a diagnostic accuracy systematic review and individual participant data pooled analysis *Eur. Radiol.* **26** 1431–40
Sinkus R, Lorenzen J, Schrader D, Lorenzen M, Dargatz M and Holz D 2000 High-resolution tensor MR elastography for breast tumour detection *Phys. Med. Biol.* **45** 1649–64
Song J, Kwon O I and Seo J K 2012 Anisotropic elastic moduli reconstruction in transversely isotropic model using MRE *Inverse Probl.* **28** 115003
Song P, Bi X, Mellema D C, Manduca A, Urban M W, Greenleaf J F and Chen S 2016 Quantitative assessment of left ventricular diastolic stiffness using cardiac shear wave elastography: a pilot study *J. Ultrasound Med.* **35** 1419–27
Song P, Urban M W, Manduca A, Zhao H, Greenleaf J F and Chen S 2013 Comb-push ultrasound shear elastography (CUSE) with various ultrasound push beams *IEEE Trans. Med. Imaging* **32** 1435–47
Stack Exchange Inc 2020 TeX—LaTeX Stack Exchange (available at: https://tex.stackexchange.com/questions/528579/draw-p-and-s-waves-illustration)
Strachinaru M, Bosch J G, van Dalen B M, van Gils L, van der Steen A F W, de Jong N, Geleijnse M L and Vos H J 2017 Cardiac shear wave elastography using a clinical ultrasound system *Ultrasound Med. Biol.* **43** 1596–606
Strachinaru M, Bosch J G, van Gils L, van Dalen B M, Schinkel A F L, van der Steen A F W, de Jong N, Michels M, Vos H J and Geleijnse M L 2019 Naturally occurring shear waves in healthy volunteers and hypertrophic cardiomyopathy patients *Ultrasound Med. Biol.* **45** 1977–86
Sugimoto K, Moriyasu F, Oshiro H, Takeuchi H, Yoshimasu Y, Kasai Y, Furuichi Y and Itoi T 2018a Viscoelasticity measurement in rat livers using shear-wave US elastography *Ultrasound Med. Biol.* **44** 2018–24
Sugimoto K, Moriyasu F, Oshiro H, Takeuchi H, Yoshimasu Y, Kasai Y and Itoi T 2020 Clinical utilization of shear wave dispersion imaging in diffuse liver disease *Ultrasonography* **39** 3–10
Sugimoto K, Moriyasu F, Oshiro H, Yoshimasu Y, Takeuchi H, Kasai Y, Furuichi Y and Itoi T 2018b Value of viscosity and viscoelasticity measurement in patients with NAFLD using shear wave ultrasound elastography *Kanzo* **59** 370–3
Sugimoto T, Ueha S and Itoh K 1990 Tissue hardness measurement using the radiation force of focused ultrasound *Ultrasonics Symp., 1990. Proc.., IEEE 1990* vol 3 pp 1377–80
Suh C H, Kim S Y, Kim K W, Lim Y S, Lee S J, Lee M G, Lee J, Lee S G and Yu E 2014 Determination of normal hepatic elasticity by using real-time shear-wave elastography *Radiology* **271** 895–900
Sumi C 2005 Usefulness of ultrasonic strain measurement-based shear modulus reconstruction for diagnosis and thermal treatment *IEEE Trans. Ultrason. Ferroelectr. Freq. Control* **52** 1670–89
Szabo T L 1995 Causal theories and data for acoustic attenuation obeying a frequency power-law *J. Acoust. Soc. Am.* **97** 14–24
Tan S M, Teh H S, Mancer J F and Poh W T 2008 Improving B mode ultrasound evaluation of breast lesions with real-time ultrasound elastography–a clinical approach *Breast* **17** 252–7
Tanter M, Bercoff J, Athanasiou A, Deffieux T, Gennisson J L, Montaldo G, Muller M, Tardivon A and Fink M 2008 Quantitative assessment of breast lesion viscoelasticity: initial clinical results using supersonic shear imaging *Ultrasound Med. Biol.* **34** 1373–86
Tanter M, Touboul D, Gennisson J L, Bercoff J and Fink M 2009 High-resolution quantitative imaging of cornea elasticity using supersonic shear imaging *IEEE Trans. Med. Imaging* **28** 1881–93
Taylor K J 1976 Absolute measurement of acoustic particle velocity *J. Acoust. Soc. Am.* **59** 691–4
Taylor L S, Porter B C, Nadasdy G, Di Sant'Agnese P A, Pasternack D, Wu Z, Baggs R B, Rubens D J and Parker K J 2004 Three-dimensional registration of prostate images from histology and ultrasound *Ultrasound Med. Biol.* **30** 161–8
Taylor L S *et al* 2005 Prostate cancer: three-dimensional sonoelastography for in vitro detection *Radiology* **237** 981–5
Torr G R 1984 The acoustic radiation force *Am. J. Phys.* **52** 402–8
Tozaki M, Isobe S and Sakamoto M 2012 Combination of elastography and tissue quantification using the acoustic radiation force impulse (ARFI) technology for differential diagnosis of breast masses *Japan. J. Radiol.* **30** 659–70
Trahey G E, Dahl J J, Mcaleavey S A, Gallippi C M and Nightingale K R 2003 Arterial stiffness measurements with acoustic radiation force impulse imaging *Proc. SPIE* **5068** 235–41
Tristam M, Barbosa D C, Cosgrove D O, Bamber J C and Hill C R 1988 Application of Fourier analysis to clinical study of patterns of tissue movement *Ultrasound Med. Biol.* **14** 695–707
Tristam M, Barbosa D C, Cosgrove D O, Nassiri D K, Bamber J C and Hill C R 1986 Ultrasonic study of *in vivo* kinetic characteristics of human tissues *Ultrasound Med. Biol.* **12** 927–37
Trout A T, Xanthakos S A, Bennett P S and Dillman J R 2020 Liver shear wave speed and other quantitative ultrasound measures of liver parenchyma: prospective evaluation in healthy children and adults *AJR Am. J. Roentgenol.* **214** 557–65

Tsutsumi M, Miyagawa T, Matsumura T, Kawazoe N, Ishikawa S, Shimokama T, Shiina T, Miyanaga N and Akaza H 2007 The impact of real-time tissue elasticity imaging (elastography) on the detection of prostate cancer: clinicopathological analysis *Int. J. Clin. Oncol.* **12** 250–5

Turgay E, Salcudean S and Rohling R 2006 Identifying the mechanical properties of tissue by ultrasound strain imaging *Ultrasound Med. Biol.* **32** 221–35

Tzschatzsch H, Ipek-Ugay S, Trong M N, Guo J, Eggers J, Gentz E, Fischer T, Schultz M, Braun J and Sack I 2015 Multifrequency time-harmonic elastography for the measurement of liver viscoelasticity in large tissue windows *Ultrasound Med. Biol.* **41** 724–33

Tzschatzsch H, Nguyen Trong M, Scheuermann T, Ipek-Ugay S, Fischer T, Schultz M, Braun J and Sack I 2016 Two-dimensional time-harmonic elastography of the human liver and spleen *Ultrasound Med. Biol.* **42** 2562–71

Ueno E, Tohno E, Soeda S, Asaoka Y, Itoh K, Bamber J C, Blaszqzyk M, Davey J and Mckinna J A 1988 Dynamic tests in real-time breast echography *Ultrasound Med. Biol.* **14** 53–57

Uffmann K, Maderwald S, Ajaj W, Galban C G, Mateiescu S, Quick H H and Ladd M E 2004 *in vivo* elasticity measurements of extremity skeletal muscle with MR elastography *NMR Biomed.* **17** 181–90

Urban M W, Chen J and Ehman R L 2017 Comparison of shear velocity dispersion in viscoelastic phantoms measured by ultrasound-based shear wave elastography and magnetic resonance elastography *2017 IEEE Int. Ultrasonics Symp. (IUS)* pp 1–4

Urban M W, Nenadic I Z, Qiang B, Bernal M, Chen S and Greenleaf J F 2015 Characterization of material properties of soft solid thin layers with acoustic radiation force and wave propagation *J. Acoust. Soc. Am.* **138** 2499–507

Vappou J, Maleke C and Konofagou E E 2009 Quantitative viscoelastic parameters measured by harmonic motion imaging *Phys. Med. Biol.* **54** 3579–94

Varghese T, Ophir J and Krouskop T A 2000 Nonlinear stress-strain relationships in tissue and their effect on the contrast-to-noise ratio in elastograms *Ultrasound Med. Biol.* **26** 839–51

Vincent P, Pogue B, Wang H, Nieskoski M, Gunn J R, Marra K, Hoopes J, Samkoe K S, Doyley M and Hasan T 2020 High-resolution ex vivo elastography to characterize tumor stromal heterogeneity *in situ* in pancreatic adenocarcinoma *IEEE Trans. Biomed. Eng.* **67** 2490–96

Viola F, Longo D, Lawrence M and Walker W 2002 Analysis of clot formation with acoustic radiation force *Proceedings, SPIE Medical Imaging Ultrasonic Imaging and Signal Processing* (SPIE) pp 235–42

von Gierke H E, Oestreicher H L, Franke E K, Parrack H O and Wittern W W 1952 Physics of vibrations in living tissues *J. Appl. Physiol.* **4** 886–900

Vos H J, van Dalen B M, Heinonen I, Bosch J G, Sorop O, Duncker D J, van der Steen A F and de Jong N 2017 Cardiac shear wave velocity detection in the porcine heart *Ultrasound Med. Biol.* **43** 753–64

Walsh J, An L, Mills B, Hah Z, Moalem J, Miller M, Giampoli E, Parker K and Rubens D 2012 Quantitative crawling wave sonoelastography of benign and malignant thyroid nodules *Otolaryngol. Head Neck Surg.: Off J. Am. Acad. Otolaryngol. Head Neck Surg.* **147** 233–8

Wang H, Mislati R, Ahmed R, Vincent P, Nwabunwanne S F, Gunn J R, Pogue B W and Doyley M M 2019a Elastography can map the local inverse relationship between shear modulus and drug delivery within the pancreatic ductal adenocarcinoma microenvironment *Clin. Cancer Res.* **25** 2136–43

Wang M, Byram B, Palmeri M, Rouze N and Nightingale K 2013a Imaging transverse isotropic properties of muscle by monitoring acoustic radiation force induced shear waves using a 2D matrix ultrasound array *IEEE Trans. Med. Imaging* **32** 1671–84

Wang R, Chen J J and Hu B 2015 Transrectal real-time elastography-guided transperineal prostate biopsy as an improved tool for prostate cancer diagnosis *Int. J. Clin. Exp. Med.* **8** 6522–9

Wang S, Aglyamov S, Karpiouk A, Li J, Emelianov S, Manns F and Larin K V 2013b Assessing the mechanical properties of tissue-mimicking phantoms at different depths as an approach to measure biomechanical gradient of crystalline lens *Biomed. Opt. Express* **4** 2769–80

Wang S and Larin K V 2014 Shear wave imaging optical coherence tomography (SWI-OCT) for ocular tissue biomechanics *Opt. Lett.* **39** 41–44

Wang S and Larin K V 2015 Optical coherence elastography for tissue characterization: a review *J. Biophotonics* **8** 279–302

Wang S, Li J, Manapuram R K, Menodiado F M, Ingram D R, Twa M D, Lazar A J, Lev D C, Pollock R E and Larin K V 2012 Noncontact measurement of elasticity for the detection of soft-tissue tumors using phase-sensitive optical coherence tomography combined with a focused air-puff system *Opt. Lett.* **37** 5184–6

Wang S, Lopez A L 3rd , Morikawa Y, Tao G, Li J, Larina I V, Martin J F and Larin K V 2014 Noncontact quantitative biomechanical characterization of cardiac muscle using shear wave imaging optical coherence tomography *Biomed. Opt. Express* **5** 1980–92

Wang Y, Bayer M, Jiang J and Hall T J 2019b Large-strain 3D *in vivo* breast ultrasound strain elastography using a multi-compression strategy and a whole-breast scanning system *Ultrasound Med. Biol.* **45** 3145–59

Weaver J B, Van Houten E E, Miga M I, Kennedy F E and Paulsen K D 2001 Magnetic resonance elastography using 3D gradient echo measurements of steady-state motion *Med. Phys.* **28** 1620–8

Wilson L S and Robinson D E 1982 Ultrasonic measurement of small displacements and deformations of tissue *Ultrason. Imaging* **4** 71–82

Wollensak G, Spoerl E and Seiler T 2003 Stress-strain measurements of human and porcine corneas after riboflavin-ultraviolet-A-induced cross-linking *J. Cataract Refract Surg.* **29** 1780–5

Womersley J R 1955 Method for the calculation of velocity, rate of flow and viscous drag in arteries when the pressure gradient is known *J. Physiol.* **127** 553–63

Wong V W *et al* 2010 Diagnosis of fibrosis and cirrhosis using liver stiffness measurement in nonalcoholic fatty liver disease *Hepatology* **51** 454–62

Woo S, Kim S Y, Cho J Y and Kim S H 2014 Shear wave elastography for detection of prostate cancer: a preliminary study *Korean J. Radiol.* **15** 346–55

Wu C, Han Z, Wang S, Li J, Singh M, Liu C H, Aglyamov S, Emelianov S, Manns F and Larin K V 2015 Assessing age-related changes in the biomechanical properties of rabbit lens using a coaligned ultrasound and optical coherence elastography system *Invest. Ophthalmol. Vis. Sci.* **56** 1292–300

Wu Z, Hoyt K, Rubens D J and Parker K J 2006 Sonoelastographic imaging of interference patterns for estimation of shear velocity distribution in biomaterials *J. Acoust. Soc. Am.* **120** 535–45

Wu Z, Taylor L S, Rubens D J and Parker K J 2004 Sonoelastographic imaging of interference patterns for estimation of the shear velocity of homogeneous biomaterials *Phys. Med. Biol.* **49** 911–22

Xing P, Wu L, Zhang C, Li S, Liu C and Wu C 2011 Differentiation of benign from malignant thyroid lesions: calculation of the strain ratio on thyroid sonoelastography *J. Ultrasound Med.* **30** 663–9

Yamakoshi Y, Sato J and Sato T 1990 Ultrasonic imaging of internal vibration of soft tissue under forced vibration *IEEE Trans. Ultrason. Ferroelectr. Freq. Control* **37** 45–53

Yen Y H, Chen J F, Wu C K, Lin M T, Chang K C, Tseng P L, Tsai M C, Lin J T and Hu T H 2017 The correlation of controlled attenuation parameter results with ultrasound-identified steatosis in real-world clinical practice *J. Formosan Med. Assoc.* **116** 852–61

Yeung F, Levinson S F and Parker K J 1998 Multilevel and motion model-based ultrasonic speckle tracking algorithms *Ultrasound Med. Biol.* **24** 427–41

Yoo J, Lee J M, Joo I, Lee D H, Yoon J H, Kang H J and Ahn S J 2019 Prospective validation of repeatability of shear wave dispersion imaging for evaluation of non-alcoholic fatty liver disease *Ultrasound Med. Biol.* **45** 2688–96

Zarski J P *et al* 2012 Comparison of nine blood tests and transient elastography for liver fibrosis in chronic hepatitis C: the ANRS HCEP-23 study *J. Hepatol.* **56** 55–62

Zhai L, Madden J, Foo W C, Palmeri M L, Mouraviev V, Polascik T J and Nightingale K R 2010 Acoustic radiation force impulse imaging of human prostates ex vivo *Ultrasound Med. Biol.* **36** 576–88

Zhai L, Polascik T J, Foo W C, Rosenzweig S, Palmeri M L, Madden J and Nightingale K R 2012 Acoustic radiation force impulse imaging of human prostates: initial *in vivo* demonstration *Ultrasound Med. Biol.* **38** 50–61

Zhang B, Ma X, Zhan W, Zhu F, Li M, Huang J, Li Y, Xue L, Liu L and Wei Y 2014 Real-time elastography in the diagnosis of patients suspected of having prostate cancer: a meta-analysis *Ultrasound Med. Biol.* **40** 1400–7

Zhang M, Castaneda B, Wu Z, Nigwekar P, Joseph J V, Rubens D J and Parker K J 2007 Congruence of imaging estimators and mechanical measurements of viscoelastic properties of soft tissues *Ultrasound Med. Biol.* **33** 1617–31

Zhang Y F, Xu H X, He Y, Liu C, Guo L H, Liu L N and Xu J M 2012 Virtual touch tissue quantification of acoustic radiation force impulse: a new ultrasound elastic imaging in the diagnosis of thyroid nodules *PloS One* **7** e49094

Zheng Y P and Huang Y P 2016 *Measurement of Soft Tissue Elasticity in vivo: Techniques and Applications* (Boca Raton: CRC Press/Taylor & Francis Group)

Zheng Y P and Mak A F 1999 Extraction of quasi-linear viscoelastic parameters for lower limb soft tissues from manual indentation experiment *J. Biomech. Eng.* **121** 330–9

Zvietcovich F 2020 Dynamic optical coherence elastography *Electrical and Computer Engineering* (Rochester, NY: University of Rochester)

Zvietcovich F, Ge G R, Mestre H, Giannetto M, Nedergaard M, Rolland J P and Parker K J 2019a Longitudinal shear waves for elastic characterization of tissues in optical coherence elastography *Biomed. Opt. Express* **10** 3699–718

Zvietcovich F, Pongchalee P, Meemon P, Rolland J P and Parker K J 2019b Reverberant 3D optical coherence elastography maps the elasticity of individual corneal layers *Nat. Commun.* **10** 4895–1-13

Zvietcovich F, Rolland J P, Yao J, Meemon P and Parker K J 2017 Comparative study of shear wave-based elastography techniques in optical coherence tomography *J. Biomed. Opt.* **22** 1–17

Zvietcovich F, Yao J, Chu Y-J, Meemon P, Rolland J P and Parker K J 2016a A comparative study of shear wave speed estimation techniques in optical coherence elastography applications *Proc. SPIE 9710 Photonics West, Optical Elastography and Tissue Biomechanics III, 97100Y* (San Francisco, CA: USA) (https://doi.org/10.1117/12.2211174)

Zvietcovich F, Yao J, Rolland J P and Parker K J 2016b Optical coherence elastography of the cornea by tracking the propagation of surface acoustic waves, *Proceedings, Frontiers in Optics 2016* (Rochester, New York: Optical Society of America JTh2A.131) (https://doi.org/10.1364/FIO.2016.JTh2A.131)